RC COUPLING BEAMS WITH HIGH-STRENGTH STEEL BARS: SUMMARY OF TEST RESULTS

By

Alexander S. Weber-Kamin

Rémy D. Lequesne

Andrés Lepage

A Report on Research Sponsored by

Charles Pankow Foundation
ACI Foundation's Concrete Research Council
Concrete Reinforcing Steel Institute

Structural Engineering and Engineering Materials
SL Report 19-1
January 2019
(Fourth Printing)

THE UNIVERSITY OF KANSAS CENTER FOR RESEARCH, INC.
2385 Irving Hill Road, Lawrence, Kansas 66045-7563

RC COUPLING BEAMS WITH HIGH-STRENGTH STEEL BARS: SUMMARY OF TEST RESULTS

By

Alexander S. Weber-Kamin

Rémy D. Lequesne

Andrés Lepage

Structural Engineering and Engineering Materials
SL Report 19-1
THE UNIVERSITY OF KANSAS CENTER FOR RESEARCH INC.
LAWRENCE, KANSAS
January 2019
(Fourth Printing)

REVISIONS

Fourth Printing (December 2019)

Updates to Figures 2 through 23 on reinforcement details.

Updates to Tables 9 through 14 on shear and deformation data.

Minor editorial changes were also made.

ABSTRACT

The use of high-strength steel bars in reinforced concrete coupling beams is expected to reduce reinforcement congestion. A series of tests was conducted to investigate the effects of high-strength reinforcement on coupling beam behavior. This report summarizes the test program and test results.

Eleven large-scale coupling beam specimens were tested under fully reversed cyclic displacements of increasing magnitude. The main variables of the test program included: yield stress of the primary longitudinal reinforcement (Grade 80, Grade 100, and Grade 120 [550, 690, and 830]), span-to-depth (aspect) ratio (1.5, 2.5, and 3.5), and layout of the primary longitudinal reinforcement (diagonal [D] and parallel [P]). All beams had the same nominal concrete compressive strength (8,000 psi [55 MPa]) and cross-sectional dimensions (12 by 18 in. [305 by 457 mm]). Beams were designed for target shear strength of $8\sqrt{f_c' \text{ psi}}\, b_w h$ ($0.67\sqrt{f_c' \text{ MPa}}\, b_w h$) for D-type beams and $6\sqrt{f_c' \text{ psi}}\, b_w d$ ($0.5\sqrt{f_c' \text{ MPa}}\, b_w d$) for P-type beams. All transverse reinforcement was Grade 80 (550), except one specimen that had Grade 120 (830) transverse reinforcement.

The test program is documented by presenting the details of specimen construction, test setup, instrumentation, and loading protocol. Documentation of test results include material properties and cyclic force-deformation response.

ACKNOWLEDGMENTS

Primary financial support for the experimental program was provided by the Charles Pankow Foundation, the Concrete Reinforcing Steel Institute, and the ACI Foundation's Concrete Research Council. Additional support was provided by Commercial Metals Company, MMFX Technologies Corporation, Harris Rebar, Midwest Concrete Materials, Nucor Corporation, and The University of Kansas through the Department of Civil, Environmental and Architectural Engineering and the School of Engineering.

Grateful acknowledgment is made to the Industry Champions, David Fields (principal at MKA, Seattle) and Ramón Gilsanz (partner at GMS, New York) and the Advisory Panel, Dominic Kelly (principal at SGH, Boston) and Conrad Paulson (principal at WJE, Los Angeles), for their ideas and constructive criticism.

Appreciation is due to the multitude of dedicated students and technicians who were involved in the construction, instrumentation, and testing of specimens.

TABLE OF CONTENTS

LIST OF TABLES

LIST OF FIGURES

CHAPTER 1: INTRODUCTION

1.1 Background and Motivation

Reinforced concrete structural walls are a common lateral force resisting system used in medium to high-rise construction. Structural walls resist lateral forces and limit building drift during earthquakes or high wind events. Perforations of a structural wall to accommodate windows, doors, and other building components reduce the stiffness and strength of the lateral force resisting system and may lead to the structural wall acting as a series of independent, smaller structural walls. Coupling beams are used to couple the actions of structural walls, restoring much of the lost stiffness and strength while retaining the openings necessary for building use. Coupling beams transfer shear between structural walls that results in wall axial tension and compression forces that form a couple in response to overturning loads. When deformed, the geometry of the system amplifies interstory wall drifts into higher coupling beam chord rotation demands. Chord rotation refers to in-plane relative deflection of a coupling beam divided by clear span. The high shear and deformation demands placed on reinforced concrete coupling beams require special reinforcement detailing. This detailing is aimed at preventing shear strength and stiffness reductions that would compromise the lateral strength and stiffness of the reinforced concrete coupled wall system.

The amount and detailing of reinforcement required in concrete coupling beams causes reinforcement congestion that increases construction costs. Reducing the quantity or size of the diagonal reinforcement by using high-strength reinforcement is one way to reduce reinforcement congestion. The ACI Building Code (ACI 318-14)[1] limits the nominal yield stress of primary longitudinal reinforcement in special seismic systems to 60 ksi (420 MPa) and confining

reinforcement to 100 ksi (690 MPa) because of limited experimental data from test of specimens constructed with high-strength reinforcement. There is reason to believe high-strength steel reinforcement can function as diagonal reinforcement in coupling beams. Typical problems associated with the use of high-strength steel, such as strain compatibility between concrete and steel reinforcement and crack width control, are not a concern in members primarily designed to resist high cyclic deformations.

The ACI Building Code[1] requires diagonal reinforcement in coupling beams with aspect ratios less than 2 and nominal shear stresses higher than $4\sqrt{f_c'}$ psi ($0.33\sqrt{f_c'}$ MPa). Coupling beams with aspect ratios (ℓ_n/h) not less than 4 are required to be designed as a beam of a special moment frame. The Code permits coupling beams with aspect ratios between two to four to be designed as diagonally-reinforced or as a special moment frame beam. Diagonal reinforcement in beams with higher aspect ratios have a smaller angle relative to the horizontal, resulting in a need for high amounts of diagonal reinforcement to resist the shear demand. Slender coupling beams ($\ell_n/h \geq 2$) may therefore greatly benefit from use of high-strength reinforcement. The effect of using high-strength steel on the behavior of coupling beams with a representative range of aspect ratios needs to be evaluated.

1.2 Research Objectives

This study was undertaken to investigate the use of high-strength steel as reinforcement in diagonally-reinforced and special moment frame coupling beams. The expected impact of this work is reduced reinforcement congestion and, as a result, lower costs for construction of robust reinforced concrete buildings.

The test results presented in this report may be useful as a basis for comparisons between coupling beams reinforced with Grade 80, 100, and 120 (550, 690, and 830) steel bars. They may be useful for developing and calibrating models for use in design of systems with high-strength reinforcement.

CHAPTER 2: EXPERIMENTAL PROGRAM

2.1 Specimens

2.1.1 Design and Detailing

Eleven coupling beam specimens were tested under reversed cyclic loading. There were specimens with three different clear span lengths (resulting in different aspect ratios), diagonal or parallel primary longitudinal reinforcement, and three grades of steel reinforcement (Grades 80, 100, and 120 [550, 690, and 830]). The coupling beams were tested rotated 90 degrees from horizontal for convenience. Each specimen consisted of a coupling beam that framed into top and bottom blocks. The end blocks had dense Grade 60 (420) reinforcement cages near the connection with the coupling beam to emulate structural wall boundary elements.

Specimens, such as D120-3.5 or P80-2.5, were named using the following rules: the first letter indicates whether it has diagonal (D) or parallel (P) primary longitudinal reinforcement (an example of which is shown in Figure 1), followed by a number that represents the reinforcement grade (in ksi), and the last number (separated by a dash) indicates the coupling beam aspect ratio (clear span to overall height, ℓ_n/h). Details of the specimens are listed in Table 1 and shown in Figures 2 through 23. Notation is defined in Appendix A.

The beams had clear span lengths of 27, 45, and 63 in. (686, 1140, and 1600 mm), a height of 18 in. (457 mm), and a width of 12 in. (305 mm), resulting in aspect ratios (ℓ_n/h) of 1.5, 2.5, and 3.5. The ACI Building Code[1] requires coupling beams with aspect ratios less than 2 to be reinforced diagonally when the shear stress demand is higher than $4\sqrt{f_c'}$ psi ($0.33\sqrt{f_c'}$ MPa). The

ACI Building Code permits coupling beams with aspect ratios between 2 and 4 to be reinforced with diagonal or special moment frame detailing.

Nine of the eleven coupling beams had primary longitudinal reinforcement arranged in two intersecting groups of diagonally-placed bars (D-type beams) with full-section confinement (rather than confinement of each group of diagonals). The remaining two coupling beams had primary longitudinal reinforcement arranged parallel (P-type beams) to the beam longitudinal axis similar to reinforcement in beams of special moment frames. Beams with the D-type reinforcement layout were designed to have a nominal shear strength of approximately $8\sqrt{f_c' \text{ psi}}\, b_w h$ ($0.67\sqrt{f_c' \text{ MPa}}\, b_w h$) based on specified f_y, in accordance with V_n calculated using ACI 318-14 Section 18.10.7.4.a[1] (Equation 2.1):

$$V_n = 2A_{vd} f_y \sin\alpha \qquad \text{Equation 2.1}$$

Beams with the P-type reinforcement layout were designed to have a nominal shear demand of approximately $6\sqrt{f_c' \text{ psi}}\, b_w d$ ($0.5\sqrt{f_c' \text{ MPa}}\, b_w d$) based on M_{pr} with specified f_y. These values are near the maximum design stresses permitted by ACI 318-14[1] of $8.5\sqrt{f_c'}$ psi ($0.71\sqrt{f_c'}$ MPa) for diagonally-reinforced coupling beams and $6\sqrt{f_c'}$ psi ($0.5\sqrt{f_c'}$ MPa) for beams of special moment frames. Design shear stresses for D-type beams in this study were 10 to 70% higher than the design shear stresses used by Naish et al.[14] in their tests of diagonally-reinforced beams using Grade 60 (420) reinforcement with full-section confinement. Naish et al.[14] had nominal shear stresses of $7.3\sqrt{f_c'}$ psi ($0.61\sqrt{f_c'}$ MPa) and $4.8\sqrt{f_c'}$ psi ($0.40\sqrt{f_c'}$ MPa) for diagonally-reinforced beams with aspect ratios of 2.4 and 3.3, respectively. In addition, the volumetric ratios of transverse

reinforcement for D-type beams in this study were approximately 16% less than those used by Naish et al.[14]

Beams had No. 6 (19) or No. 7 (22) Grade 80, 100, or 120 (550, 690, or 830) steel bars as primary longitudinal reinforcement. P-type beams were constructed with six parallel reinforcing bars, three near the top and three near the bottom of the cross-section. D-type beams were constructed with two bundles of diagonal reinforcing bars that intersected at the midpoint of the coupling beam with an angle of inclination between 10 and 23 degrees. All beams, except D120-2.5, had No. 3 (10) Grade 80 (550) steel for all non-primary reinforcement. Beam D120-2.5 was constructed using Grade 120 (830) steel. Except for P80-2.5, transverse reinforcement was provided at a 3-in. (76-mm) spacing, which corresponds to $4d_b$ for No. 6 (19) reinforcing bars and $3.4d_b$ for No. 7 (22) reinforcing bars. Beam P80-2.5 had transverse reinforcement spaced at 3.5 in. (89 mm) or 4.6 times the longitudinal bar diameter. Each layer of transverse reinforcement consisted of a hoop with seismic hooks (135 degrees) and one crosstie with 135 and 90-degree hooks in the beam strong axis. D-type beams also had two similar crossties in the beam weak axis. See beam cross-sections in Figures 2 through 23.

D-type beams had ten longitudinal No. 3 (10) bars distributed around the perimeter of the beam such that each bar was supported by either a crosstie or a corner of a hoop. This secondary longitudinal reinforcement was terminated 2 in. (51 mm) into the top and bottom blocks for all specimens aside from D120-2.5, consistent with the detailing recommended in the ACI Building Code[1] commentary. The No. 3 (10) longitudinal bars in D120-2.5 were developed into the end blocks to limit concentration of damage at the block-beam interfaces. The design data in Table 1 include the minimum embedment length (ℓ_e) of the primary longitudinal reinforcement of the

coupling beams into the top and bottom blocks. The as-built dimensions of the specimens are shown in Figures 2 through 23.

2.1.2 Materials

2.1.2.1 Concrete

Ready-mix concrete with a maximum aggregate size of 0.5 in. (13 mm), provided by a local supplier, was used to cast the specimens. The target compressive strength (f'_c) was 8,000 psi (55 MPa). The measured concrete compressive and tensile strengths (Table 2) were obtained from tests of 6 by 12 in. (152 by 305 mm) standard concrete cylinders following ASTM standards C39[9] and C496[10].

2.1.2.2 Reinforcing Steel

Deformed steel reinforcing bars were used for all reinforcement. Mill certifications for reinforcing bars used as Grade 80 (550) showed compliance with ASTM A615[6] Grade 80 (550). Mill certifications for reinforcing bars used as Grade 100 (690) showed compliance with ASTM A615[6] Grade 100 (690). Mill certifications for reinforcing bars used as Grade 120 (830) showed compliance with ASTM A1035[8] Grade120 (830). Mechanical properties of reinforcing bars (Table 3) that were used in the beams were obtained from tensile tests in accordance with ASTM A370[5]. Figure 24 shows sample tensile test results.

All reinforcement outside the coupling beams (e.g., top and bottom blocks) was Grade 60 (420) in compliance with ASTM A615[6] Grade 60 (420).

2.1.3 Construction

Photos showing various stages of specimen construction are presented in Appendix B. The specimens were cast monolithically with the top and bottom block formwork lying flat on the laboratory floor. The coupling beam concrete was supported with elevated wood formwork because it was less wide than the end blocks. Construction of each specimen included the assembly of reinforcing bar cages, installation of strain gauges to the relevant reinforcing bars, construction of wooden formwork, and placement of the concrete. After casting, specimens and cylinders were covered with wet burlap and plastic sheets until formwork removal three to five days after casting. Specimens were kept in a climate controlled laboratory from casting to testing.

2.2 Test Setup

The test setup is shown in Figures 25 through 27. For testing, the bottom block of each specimen was bolted to the laboratory strong floor with two unbonded 2.5-in. (63.5-mm) diameter high-strength threaded rods passing through the bottom block and strong floor. To distribute the hold-down forces, each of the threaded rods was connected to a steel spreader beam under the strong floor and a steel plate washer on the top surface of the bottom block. Two hydraulic actuators acting in parallel were used to load the specimens. The actuators each have a stroke length of 40 in. (1020 mm) and a force capacity of 220 kips (980 kN). The two actuators were connected to the strong wall and the specimen by means of vertically oriented HP steel sections. Actuator elevations are shown in Table 4 and Figures 28 through 30. The HP section was connected to the top block of a specimen with a series of hollow structural steel (HSS) sections for transmitting compression and six unbonded 2.25-in. (57-mm) diameter high-strength threaded rods for transmitting tension. Additional steel fixtures were used to brace the HP section against out-

of-plane motion. Mirrored steel (attached to the HP section), nylon pads (attached to the external bracing system), and white lithium grease were used to minimize friction between the HP section and the external bracing.

2.3 Instrumentation

Several instruments were used to record specimen behavior during the tests; an infrared non-contact position measurement system, two linear variable differential transformers (LVDTs) attached to the top block, one LVDT and load cell integral to each actuator, and strain gauges attached to reinforcing bars. Most collected data are not included or discussed in this report.

2.3.1 Infrared Non-Contact Position Measurement System

The motion capture system served to measure the positions of 66 to 97 optical markers attached to the surface of the specimen including three fixed positions attached to a rigid stand on the laboratory floor. The markers emit infrared light pulses that are detected by the infrared camera system. The spatial coordinates of the markers were triangulated and recorded throughout the tests. The markers were arranged in a 4-in. (102-mm) square grid over one face of the coupling beam and part of the top and bottom blocks, as shown in Figure 31.

2.3.2 Linear Variable Differential Transformers (LVDTs)

In addition to the infrared markers, redundant measurements of the top block displacement were recorded by two independent LVDTs (Figure 32). These LVDTs were attached to the face of the top block on the opposite side of the actuators, horizontally centered on the face with respect to the width of the top block and supported by an instrument stand.

2.3.3 Strain Gauges

Several 120-ohm electrical resistance strain gauges were applied to selected reinforcing bars prior to casting. D-type specimens were instrumented with at least 31 strain gauges and P-type specimens with at least 22. The different possible locations of strain gauges are shown in Figures 33 and 34 with Tables 5 and 6 identifying the strain gauges that were used in each specimen. Tables 5 and 6 also identify the strain gauges that malfunctioned. Strain gauges on primary longitudinal reinforcement were rated for 15% strain, whereas strain gauges on secondary longitudinal reinforcement and transverse reinforcement were rated for 5% strain.

2.4 Loading Protocol

Specimens were subjected to double curvature through a series of reversed cyclic displacements following the protocol in Table 7 and shown in Figure 35, patterned after the protocol recommended in FEMA 461[12]. Force-based control was used prior to yielding of the reinforcement (at approximately 0.5% chord rotation for aspect ratios of 1.5 and 2.5 and 0.75% chord rotation for an aspect ratio of 3.5. Subsequent cycles used displacement control. Applied forces or displacements were selected to minimize the rotation of the top block relative to the rotation of the bottom block.

Several small cycles were imposed prior to testing (with forces below the cracking point) to facilitate tightening of the threaded rods connecting the bottom block to the strong floor and the top block to the actuators. Testing was typically terminated when the cycle peak shear force was less than 20% of the maximum applied shear or when specimen stability became a concern.

The weight of all fixtures (including HP sections, spacer sections, steel plates, and actuators) hanging on one side of the specimen (Figure 25) caused a permanent moment of about 42 ft-kips (57 m-kN) prior to loading. An equal and opposite moment was applied using the actuators at the start of the test. The weight of the fixtures was supported by a stack of steel plates prior to testing.

The loading rate is given in Table 7 for coupling beams with 1.5 and 2.5 aspect ratios as multiples of 0.01 in./sec that increased in steps with an increase in chord rotation. Coupling beams with 3.5 aspect ratio were tested at twice the rate of the smaller aspect ratios.

Relative rotation of the end blocks is defined as the difference between the top block rotation and the bottom block rotation. Relative rotation was minimized by pausing periodically and, while holding actuator displacements constant, adjusting the ratio of actuator displacements before continuing the test.

CHAPTER 3: EXPERIMENTAL RESULTS

3.1 Shear-Chord Rotation Relationship

Chord rotation of the coupling beam, CR, is defined as the displacement of the top block relative to the bottom block divided by the length of the beam clear span and corrected for rotation of the top and bottom blocks:

$$CR = \frac{\delta_{top} - \delta_{bot}}{\ell_n} - \frac{\theta_{top} + \theta_{bot}}{2} \qquad \text{Equation 3.1}$$

Figure 36 shows a schematic of a general deformed shape of a coupling beam with displacement and rotational components identified. In this figure, top block rotation (θ_{top}) and bottom block displacement (δ_{bot}) are positive while bottom block rotation (θ_{bot}) and top block displacement (δ_{top}) are negative.

Displacement and rotation were calculated from measurements obtained with the infrared non-contact position measuring system (Section 2.3.1) and checked with data from the redundant LVDTs. The infrared markers were offset from the edges of the top and bottom blocks by approximately 2.5 in. (64 mm) to reduce the probability of the marker being on concrete that would spall during the test.

3.2 Specimen Response and Observations

The eleven specimens described in Chapter 3 were subjected to the loading protocol discussed in Section 2.4. The measured force-deformation relationships for each specimen are plotted in Figures 37 through 47 in terms of shear versus chord rotation and discussed in the following sections. Table 8 lists the maximum shear stress and deformation capacities of each

beam. Maximum shear stress is normalized by the square root of the concrete compressive strength at the time of testing (f_{cm} in Table 2).

Two different definitions were used for deformation capacity or chord rotation capacity in Table 8. The first, called Deformation Capacity A, was defined as the average of the maximum chord rotation reached in each loading direction before a 20% loss of strength in that loading direction. The second, called Deformation Capacity B, was defined as the average of the chord rotations in each loading direction where the envelope of the shear versus chord rotation curve formed by connecting the maximum chord rotation of the first cycle of each loading step intersects with 80% of the maximum applied shear. Both definitions of chord rotation capacity are provided because the distinctions may appeal to designers and researchers differently. Deformation Capacity A is the more stringent measure as it corresponds to the chord rotation that the coupling beam actually was subjected to. Deformation Capacity B is the idealized performance of the coupling beam and is less sensitive to unique occurrences within the tests. Deformation Capacity B is always higher than or equal to Deformation Capacity A. Deformation capacity in this report refers to Deformation Capacity B unless otherwise noted.

A shear-chord rotation envelope for each specimen was developed in accordance with ASCE 41-17 Section 7.6.3[4] by connecting the maximum displacement of the first cycle of each loading step. The envelopes thus generated were superimposed on the measured shear-chord rotation curves in Figures 48 through 58. Comparisons between envelopes are presented in Figures 59 through 62 for groups of beams based on their aspect ratio. Coordinates of the breakpoints for the envelopes are listed in Tables 9 through 12.

Figures 59 through 62 include the generalized force-deformation curve for coupling beams in accordance with ASCE 41-17 Table 10-19[4], where the coordinates of points A through E are specified. The force assigned to point C represents the probable strength of the member and the deformation assigned to point E represents the chord rotation capacity. In Figures 59 through 61, the target design shear force of $8\sqrt{f_c' \text{ psi}}\, b_w h$ ($0.67\sqrt{f_c' \text{ MPa}}\, b_w h$) was used to define the ordinate of point B in D-type beams, whereas in Figure 62 the target design shear force of $6\sqrt{f_c' \text{ psi}}\, b_w d$ ($0.5\sqrt{f_c' \text{ MPa}}\, b_w d$) was used to define the ordinate of point C in P-type beams. These target design shear forces are near the maximum allowed by ACI 318-14. They correspond to the beam strength calculated based on a stress of f_y in the diagonal reinforcement of D-type beams and on a stress of 1.25 f_y in the longitudinal reinforcement of P-type beams. Figures 59 through 62 show that all envelopes from the measured test data exceeded the chord rotation capacity that ASCE 41-17[4] assigns to coupling beams compliant with ACI 318-14[1].

Maximum shear among D-type beams with the same aspect ratios were very similar with the exception of D120-2.5 due to the contributions of the developed No. 3 (10) reinforcement. The chord rotation associated with maximum shear was proportional to aspect ratio. Table 13 shows measured and calculated strengths, including the measured-to-calculated ratio for each beam. The measured-to-calculated ratios averaged 1.43 for D-type beams (excluding D120-2.5) and 1.15 for P-type beams. The higher ratios for D-type beams may be because the calculated strength V_{nm} depends only on the diagonal reinforcement and neglects the contribution of concrete and transverse reinforcement. These results are consistent with those from other studies [3, 13, 14].

Test results are summarized in Table 14 in terms of key design and response parameters. General observations during testing of each specimen are summarized in Sections 3.2.1 through

3.2.11. Photos showing the condition of the beams during the last cycle to target chord rotations of 2, 4, 6, 8, and 10% are shown in Appendix C. The observed locations of fractured bars are shown in Figures 63 through 73. Bar fractures were not observed in P-type beams.

3.2.1 D80-1.5

Measured shear force is plotted versus chord rotation in Figure 37 for D80-1.5. The coupling beam completed both cycles to 6% chord rotation (Step 10 of the loading protocol in Table 7) before strength notably diminished. The second excursion to -6% reached a shear of approximately 80% of the strength after at least one bar fractured. This resulted in a deformation capacity of 6.9% (as reported in Table 8). One cycle to 8% chord rotation (Step 11 in Table 7) was completed before the test was terminated. Strength loss was initiated by buckling of the diagonal bars that was followed by bar fractures after reversing the loading direction.

3.2.2 D100-1.5

Measured shear force is plotted versus chord rotation in Figure 38 for D100-1.5. The coupling beam completed both cycles to 4% chord rotation (Step 9) before bar fractures occurred during the first cycle to 6% and strength diminished rapidly. This resulted in a deformation capacity of 5.3% (as reported in Table 8). One excursion to +8% chord rotation (Step 11) was attempted but aborted at approximately +6.1% due to stability concerns from the numerous bar fractures during the previous loading cycle (Step 10B). Strength loss was initiated by buckling of the diagonal bars followed by bar fractures in subsequent cycles.

3.2.3 D120-1.5

Measured shear force is plotted versus chord rotation in Figure 39 for D120-1.5. The coupling beam completed both cycles to 3% chord rotation (Step 8) and the first excursion to 4%.

However, an exception to the testing protocol occurred during the first excursion to -4% (Step 9). The coupling beam displaced through -5% before fracturing all reinforcing bars in one group of diagonals near the top end of the beam. The sudden bar fractures caused a high increase in top block rotation, resulting in a high increase in chord rotation to 8.1%. There was no prior evidence of bar buckling or fracture. The test resumed with cycles to 4% and 6% chord rotations (Steps 9 and 10). The deformation capacity was 5.2% (as reported in Table 8) based on the definition of Deformation Capacity B. Reinforcing bar fractures near -5% indicate that the beam would not have completed Step 10, failure was imminent despite the deviation from the testing protocol. Investigation after testing revealed that all four reinforcing bars in one of the diagonal bundles and two bars in the other diagonal bundle had fractured.

3.2.4 D80-2.5

Measured shear force is plotted versus chord rotation in Figure 40 for D80-2.5. The coupling beam completed two cycles to 6% chord rotation (Step 10) and half of a cycle to 8% chord rotation before strength diminished by more than 20%. This resulted in a deformation capacity of 7.6% (as reported in Table 8). One cycle to 10% chord rotation (Step 12) was completed before the test was terminated. Strength loss was due to fracture of diagonal bars near the ends of the coupling beam after they were observed to have buckled in a prior cycle.

3.2.5 D100-2.5

Measured shear force is plotted versus chord rotation for D100-2.5 in Figure 41. The coupling beam reached chord rotations of -4.7%[a] and +6% in each loading direction before a 20% loss of strength, resulting in a deformation capacity of 6% (as reported in Table 8). Loading

[a] A chord rotation of 4% was targeted.

continued until nearly two cycles at 8% chord rotation (Step 11) were completed. Strength loss was caused by fracture of one set of diagonal bars near the top end of the coupling beam after they were observed to have buckled in a prior cycle.

3.2.6 D120-2.5

Measured shear force is plotted versus chord rotation for D120-2.5 in Figure 42. The deformation capacity of the coupling beam was 6.9% (as reported in Table 8). Beam strength began to diminish in the first cycle to 6% with bar fractures occurring during the second excursion to +6%. Loading continued until completion of two cycles to 8% (Step 11). Strength loss was associated with hoop opening and bar buckling followed by bar fracture in both diagonal bundles near the bottom end of the coupling beam. Several longitudinal No. 3 bars also fractured. D120-2.5 had longitudinal No. 3 bars extended into the end blocks for a length sufficient to develop 1.25 times the specified yield strength of the bar at the face of the end blocks. This may have contributed to achieving a maximum shear stress of $15\sqrt{f_c'}$ psi ($1.25\sqrt{f_c'}$ MPa).

3.2.7 D80-3.5

Measured shear force is plotted versus chord rotation in Figure 43 for D80-3.5. The coupling beam completed one cycle to 8% chord rotation (Step 11) before bar fractures occurred during the second excursion to +8% with a strength loss of approximately 30%. This resulted in a deformation capacity of 8.6% (as reported in Table 8). Testing continued through one cycle of 10% (Step 12). A second excursion to +10% chord rotation was attempted but aborted due to numerous bar fractures at approximately +3%. Strength loss was due to buckling followed by fracture of diagonal bars near the ends of the coupling beam.

3.2.8 D100-3.5

Measured shear force is plotted versus chord rotation in Figure 44 for D100-3.5. The coupling beam completed one cycle to 6% chord rotation (Step 10) before bar fractures occurred during the second excursion to +6% with a strength loss of nearly 20%. This resulted in a deformation capacity of 6.8% (as reported in Table 8). Testing continued through one cycle of 10% (Step 12). Strength loss was due to fractures of diagonal bars near the ends of the coupling beam after they were observed to have buckled in previous cycles. Out-of-plane deformations as high as 2.7% of the beam length occurred during the second cycle to +6%chord rotation.

3.2.9 D120-3.5

Measured shear force is plotted versus chord rotation in Figure 45 for D120-3.5. The coupling beam completed one cycle to 6% chord rotation (Step 10) before bar fractures occurred during the second excursion to +6% with a strength loss of nearly 80%. This resulted in a deformation capacity of 6.7% (as reported in Table 8). Testing continued through two cycles of 8% (Step 11). Strength loss was due to buckling followed by fracture of diagonal bars near the ends of the coupling beam.

Continuous data from the position tracking marker system are unavailable after the second 2% cycle (Step 7) due to a recording error of the primary data acquisition system. However, shear-chord rotation coordinates were also recorded each time the test was paused with independent software that used optical character recognition to capture in real-time the display of the primary data acquisition system. These discrete data are plotted in Figure 45 as hollow points connected with dotted lines.

3.2.10 P80-2.5

Test results are plotted for P80-2.5 in terms of measured shear force versus chord rotation in Figure 46. The chord rotation capacity of the coupling beam was 3.9% (as reported in Table 8). Although strength began to diminish in the second excursion to a chord rotation of -3%, the first excursion to +4% reached a shear that was higher than 80% of the strength in the positive loading direction. Loading continued until two cycles to 6% chord rotation (Step 10) had been completed. No bar fracture was observed during the test. Strength loss was due to shear strength decay, with damage concentrated near the ends of the coupling beam.

3.2.11 P100-2.5

Results are plotted for P100-2.5 in terms of measured shear force versus chord rotation in Figure 47. The deformation capacity of the coupling beam was 4.1% (as reported in Table 8). The first cycle to +3% was the last cycle to exceed 80% of the strength in the positive loading direction. The second excursion to a chord rotation of -3% reached a shear nearly equal to 80% of the strength in the negative loading direction, while the first excursion to -4% exceeded the 80% threshold. Loading continued until two cycles to 6% chord rotation (Step 10) had been completed. No bar fracture was observed after the test. Strength loss was due to shear strength decay resulting from damage near the ends of the coupling beam.

CHAPTER 4: CONCLUDING REMARKS

Results were reported from tests of eleven large-scale reinforced concrete coupling beams subjected to reversed cyclic displacements. This research was undertaken to investigate the use of high-strength reinforcement in diagonally-reinforced (D-type) and moment frame (P-type) coupling beams. Variables included nominal yield stress of the primary longitudinal reinforcement (80, 100, and 120 ksi [550, 690, and 830 MPa]), span-to-depth (aspect) ratio (1.5, 2.5, and 3.5), and layout of primary longitudinal reinforcement (diagonal [D] and parallel [P]). All beams had the same nominal concrete compressive strength (8,000 psi [55 MPa]) and cross-sectional dimensions (12 by 18 in. [305 by 457 mm]). The D-type beams were designed for a target shear strength of $8\sqrt{f_c' \text{ psi}}\, b_w h$ ($0.67\sqrt{f_c' \text{ MPa}}\, b_w h$) and the P-type beams for $6\sqrt{f_c' \text{ psi}}\, b_w d$ ($0.5\sqrt{f_c' \text{ MPa}}\, b_w d$). All transverse reinforcement was Grade 80 (550) except one beam with Grade 120 (830) transverse reinforcement (D120-2.5). The main findings and observations from this study are summarized as follows:

(1) Chord rotation capacities of D-type beams with Grade 100 or Grade 120 (690 or 830) diagonal reinforcement were similar, with average deformation capacities of approximately 5, 6, and 7% for beams with aspect ratios of 1.5, 2.5, and 3.5, respectively. Deformation capacity was based on the average chord rotation (for positive and negative loading directions) corresponding to 20% loss of strength. These deformation capacities exceeded the minimum chord rotation capacities in ASCE 41-17 [4] for diagonally-reinforced coupling beams.

(2) D-type beams with Grade 80 (550) diagonal reinforcement exhibited approximately 25% higher chord rotation capacities, on average, than their Grade 100 or Grade 120 (690 or 830) counterparts. The increased rotation capacity of the beams with Grade 80 diagonal bars may

be attributed to their lower ratio of f_y to s/d_b, where f_y is the yield stress of the diagonal bar, d_b is the diameter of the diagonal bar, and s is the spacing of the hoops.

(3) Chord rotation capacities of P-type beams with Grade 80 or Grade 100 (550 or 690) longitudinal reinforcement were similar, with an average chord rotation capacity of approximately 4% for beams with an aspect ratio of 2.5.

(4) Measured strength of D-type beams, on average, was nearly 50% higher than the calculated nominal shear strength (V_{nm} for a diagonally-reinforced coupling beam based on f_{ym}).

(5) Measured strength of P-type beams, on average, was approximately 15% higher than the calculated nominal flexural strength (M_{nm} for a moment frame beam based on f_{cm} and f_{ym}).

REFERENCES

1. ACI 318 (2014). “Building Code Requirements for Structural Concrete (ACI 318-14) and Commentary (ACI 318R-14).” American Concrete Institute, Farmington Hills, Michigan.
2. ACI 408 (2003). “Bond and Development of Straight Reinforcing Bars in Tension (ACI 408R-03).” American Concrete Institute, Farmington Hills, Michigan.
3. Ameen, S. (2019). “Diagonally-Reinforced Concrete Coupling Beams with High-Strength Steel Bars.” PhD Dissertation, The University of Kansas, Lawrence, Kansas.
4. ASCE 41 (2017). “Seismic Evaluation and Retrofit of Existing Buildings (ASCE/SEI 41-17).” American Society of Civil Engineers, Reston, Virginia.
5. ASTM A370 (2017). “Standard Test Methods and Definitions for Mechanical Testing of Steel Products (ASTM A370-17).” ASTM International, West Conshohocken, Pennsylvania.
6. ASTM A615 (2016). “Standard Specification for Deformed and Plain Carbon-Steel Bars for Concrete Reinforcement (A615-16/A615M-16).” ASTM International, West Conshohocken, Pennsylvania.
7. ASTM A706 (2016). “Standard Specification for Deformed and Plain Low-Alloy Steel Bars for Concrete Reinforcement (ASTM A706/A706M-16).” ASTM International, West Conshohocken, Pennsylvania.
8. ASTM A1035 (2016). “Standard Specification for Deformed and Plain, Low-Carbon, Chromium, Steel Bars for Concrete Reinforcement (ASTM A1035-16b).” ASTM International, West Conshohocken, Pennsylvania.
9. ASTM C39 (2017). “Standard Test Method for Compressive Strength of Cylindrical Concrete Specimens (ASTM C39/C39M-17a).” ASTM International, West Conshohocken, Pennsylvania.
10. ASTM C496 (2011). “Standard Test Method for Splitting Tensile Strength of Cylindrical Concrete Specimens (ASTM C496/C496M-11).” ASTM International, West Conshohocken, Pennsylvania.
11. ASTM E8 (2016). “Standard Test Methods for Tension Testing of Metallic Materials (ASTM E8/E8M-16a).” ASTM International, West Conshohocken, Pennsylvania.
12. FEMA 461 (2007). “Interim Testing Protocols for Determining the Seismic Performance Characteristics of Structural and Nonstructural Components.” Applied Technology Council, Redwood City, California.
13. Lequesne, R.D. (2011). “Behavior and Design of High-Performance Fiber-Reinforced Concrete Coupling Beams and Coupled-Wall Systems.” PhD Dissertation, University of Michigan, Ann Arbor, Michigan.
14. Naish, D., Fry, A., Klemencic, R., and Wallace, J. (2013). “Reinforced Concrete Coupling Beams – Part I: Testing.” ACI Structural Journal, 110 (6), 1057-1066.

TABLES

Table 1 – Design data for coupling beam specimens [a]
(1 in. = 25.4 mm, 1 ksi = 1,000 psi = 6.89 MPa)

Coupling Beam[b]				Primary Longitudinal Reinforcement							Transverse Reinforcement			
Id.	v_e	$\frac{\ell_n}{h}$	ℓ_n	f_y	n	d_b	ℓ_e [c]	A_{vd}	α	A_s	Weak Axis[d]	Strong Axis[e]	f_{yt}	s
	$\sqrt{f'_c}$, psi		in.	ksi		in.	in.	in.^{2}	degrees	in.^{2}	in.^{2}	in.^{2}	ksi	in.
D80-1.5	8.4	1.5	27	80	6	0.75	21	2.64	22.7	-	0.44	0.33	80	3
D100-1.5	8.8	1.5	27	100	5	0.75	27	2.20	22.7	-	0.44	0.33	80	3
D120-1.5	8.4	1.5	27	120	4	0.75	34	1.76	22.7	-	0.44	0.33	80	3
D80-2.5	8.0	2.5	45	80	9	0.75	21	3.96	14.2	-	0.44	0.33	80	3
D100-2.5	7.8	2.5	45	100	7	0.75	27	3.08	14.2	-	0.44	0.33	80	3
D120-2.5	8.0	2.5	45	120	6	0.75	34	2.64	14.2	-	0.44	0.33	120	3
D80-3.5	7.8	3.5	63	80	9	0.875	24	5.40	10.0	-	0.44	0.33	80	3
D100-3.5	7.3	3.5	63	100	9	0.75	27	3.96	10.3	-	0.44	0.33	80	3
D120-3.5	7.8	3.5	63	120	8	0.75	34	3.52	10.3	-	0.44	0.33	80	3
P80-2.5	5.2	2.5	45	80	3	0.75	21	-	-	1.32	0.22	0.33	80	3.5
P100-2.5	6.4	2.5	45	100	3	0.75	27	-	-	1.32	0.22	0.33	80	3

[a] For notation and definitions, see APPENDIX A: NOTATION.

[b] All specimens have $f'_c = 8{,}000$ psi, $h = 18$ in., $b_w = 12$ in., and $c_c = 0.75$ in. to No. 3 (10) transverse reinforcement. Specimen Id. starts with D for cases with diagonal reinforcement and P for cases with parallel reinforcement, see Figure 1.

[c] Minimum straight embedment length based on ACI 408R-03 Eq. 4.11.a[2] using $\phi = \omega = \alpha = \beta = \lambda = 1$, $(c\ \omega + K_{tr})/d_b = 4$, $1.25 f_y$ psi, and $f'_c = 8{,}000$ psi. Grade 80 (550) No. 3 (10) longitudinal reinforcing bars were terminated approximately 2 in. into the top and bottom blocks consistent with the detailing recommendations in the ACI Building Code[1] commentary, except for Grade 120 (830) No. 3 (10) longitudinal reinforcing bars in D120-2.5 with a minimum straight embedment length of 17 in. into the top and bottom blocks.

[d] Transverse reinforcement along the 12-in. width of the coupling beam; 4 legs of No. 3 (10) bars at spacing *s* for D-type beams and 2 legs of No. 3 (10) bars for P-type beams.

[e] Transverse reinforcement along the 18-in. depth of the coupling beam; 3 legs of No. 3 (10) bars at spacing *s*.

Table 2 – Measured compressive and tensile strengths of concrete[a] (1,000 psi = 6.89 MPa)

Coupling Beam Identification	Cast Date	Test Date	Age (days)	f_{cm} [b] (psi)	f_{ct} [c] (psi)
D80-1.5	3 Nov 17	1 May 18	179	7,600	710
D100-1.5	3 Nov 17	9 Apr 18	157	8,200	720
D120-1.5	3 Nov 17	31 May 18	209	7,600	610
D80-2.5	16 Jun 17	3 Oct 17	109	8,400	620
D100-2.5	30 Jun 17	29 Nov 17	152	8,000	790
D120-2.5	18 Aug 17	6 Mar 18	200	7,800	760
D80-3.5	26 Jul 17	19 Jun 18	328	7,800	660
D100-3.5	26 Jul 17	6 Jul 18	345	7,900	650
D120-3.5	18 Aug 17	25 Jul 18	341	8,200	660
P80-2.5	16 Jun 17	10 Nov 17	147	8,300	790
P100-2.5	30 Jun 17	12 Dec 17	165	7,500	790

[a] For notation and definitions, see APPENDIX A: NOTATION.

[b] Tested in accordance with ASTM C39[9], average of two tests of 6 by 12 in. (150 by 300 mm) cylinders

[c] Tested in accordance with ASTM C496[10], average of two tests of 6 by 12 in. (150 by 300 mm) cylinders

Table 3 – Reinforcing steel properties [a] (1 in. = 25.4 mm, 1 ksi = 6.89 MPa)

Coupling Beam Identification	Bar Size	Nominal Bar Diameter	Yield Stress[b]		Tensile Strength[b]	Uniform Elongation[c]	Fracture Elongation[d]
	No.	d_b in.	f_{ym} ksi	f_{ytm} ksi	f_t ksi	ε_{su} %	ε_{sf} %
D80-1.5 D80-2.5 P80-2.5	3 (10)	0.375		89	113	9.7	12.9
	6 (19)	0.75	83		110	9.2	13.3
D80-3.5	3 (10)	0.375		89	113	9.7	12.9
	7 (22)	0.875	84		114	10.0	16.4
D100-1.5 D100-2.5 D100-3.5 P100-2.5	3 (10)	0.375		89	113	9.7	12.9
	6 (19)	0.75	108		125	6.8	9.8
D120-1.5 D120-3.5	3 (10)	0.375		89	113	9.7	12.9
	6 (19)	0.75	116		163	5.2	9.9
D120-2.5	3 (10)	0.375		133	173	4.5	6.3
	6 (19)	0.75	116		163	5.2	9.9

[a] For notation and definitions, see APPENDIX A: NOTATION.

[b] Tested in accordance with ASTM A370[5]

[c] Corresponds to strain at peak stress, in accordance with ASTM E8[11]

[d] Calculated strain corresponding to zero stress on a line with slope equal to modulus of elasticity and passing through the fracture point.

Table 4 – Specimen and actuators nominal elevations relative to strong floor (1 in. = 25.4 mm)

$\frac{l_n}{h}$	Top of Bottom Block (in.)	Bottom of Top Block (in.)	Actuator A Centerline (in.)	Actuator B Centerline (in.)
1.5	39.5	66.5	21	87
2.5	36.5	81.5	45	87
3.5	36.5	99.5	51	130

Table 5 – List of strain gauges on primary and secondary longitudinal reinforcement

			Coupling Beam Identification										
			D80-1.5	D100-1.5	D120-1.5	D80-2.5	D100-2.5	D120-2.5	D80-3.5	D100-3.5	D120-3.5	P80-2.5	P100-2.5
Primary Reinforcement	Diagonal	D1	X	X	X	X	X	X	X	O	X		
		D2	X	O	X	O	X	X	X	X	X		
		D3	X	X	X	X	X	X	X	O	X		
		D4	X	X	X	X	X	X	X	X	X		
		D5	X	X	X	X	O	X	X	X	X		
		D6	X	X	X	X	X	X	X	X	X		
		D7	X	X	X	X	X	X	X	X	X		
		D8	X	X	X	X	X	X	O	X	X		
		D9	O	X	X	O	X	O	X	X	X		
		D10	X	X	X	X	X	X	X	X	X		
		D11	X	X	X	X	O	X	X	X	X		
		D12	X	X	X	X	O	X	X	X	X		
		D13	X	X	O	O	X	X	X	X	X		
		D14	X	X	X	X	X	X	X	X	X		
	Parallel[a]	P1										X	X
		P2										X	O
		P3										X	X
		P4										X	X
		P5										X	X
		P6										X	O
		P7										X	X
		P8										X	O
		P9										X	X
		P10										X	X
		P11										X	X
		P12										X	X
Secondary Reinforcement	Parallel[b]	H1	X	O	O	X	X	X	X	X	X		
		H2	X	O	X	X	O	X	O	X	X		
		H3	X	X	X	X	O	X	O	X	X		
		H4	X	X	X	X	X	X	X	O	X		
		H5	X	X	O	X	X	O	X	O	X		
		H6	X	X	X		X	O	X	X			
		H7		X	O				O	X			
		H8		O	X				X				
		H9	X	X	X								
		H10		X	X								
		H11	X	O	X								
		H12	X	X									
		H13	X										
		H14	X										

"X" indicates strain gauge is present.
"O" indicates strain gauge is present but data not available due to instrument malfunction.

[a] No. 6 (19) reinforcement placed parallel to the longitudinal axis of the P-type beams.

[b] No. 3 (10) reinforcement placed parallel to the longitudinal axis of the D-type beams.

Table 6 – List of strain gauges on transverse reinforcement

			Coupling Beam Identification										
			D80-1.5	D100-1.5	D120-1.5	D80-2.5	D100-2.5	D120-2.5	D80-3.5	D100-3.5	D120-3.5	P80-2.5	P100-2.5
Transverse Reinforcement	Closed Stirrups	S1	O	O	X	O	X	O	O	O	O	X	X
		S2	X	X	X	X	X	X	X	X	X	X	X
		S3	X	X	X	X	X	X	X	X	X	O	X
		S4	X	X	X	X	X	X	X	X	X	O	X
		S5	X	X	X	X	O	X	X	X	X	X	X
		S6	X	O	X	X	X	X	X	X	X	X	X
		S7	X	X	X	X	X	X	X	X	X	X	X
		S8	X	X	X	X	X	X	X	X	X	X	X
		S9	X	X	X	X	X	X	X	O	X	X	X
		S10						X					
		S11						X					
		S12						X					
		S13						X					
		S14						X					
		S15						X					
		S16						X					
		S17						X					
		S18						O					
	Crossties	T1	X	X	O	X	X	X	X	X	X	X	X
		T2	X	X	O	X	X	X	X	X	X		
		T3	X	X	X	O	X	X	X	X	X		
		T4	X	X	X								
		T5		X	X								
		T6			X								

"X" indicates strain gauge is present.
"O" indicates strain gauge is present but data not available due to instrument malfunction.

Table 7 – Loading protocol (1 in. = 25.4 mm)

Step[a]	Chord Rotation[b] %	Loading Rate in./s [c]
1	0.20	0.01
2	0.30	0.01
3	0.50	0.01
4	0.75	0.01
5	1.00	0.02
6	1.50	0.02
7	2.00	0.02
8	3.00	0.03
9	4.00	0.03
10	6.00	0.04
11	8.00	0.04
12	10.00	0.04

[a] Two cycles of loading in each step, following recommendations in FEMA 461[12], see Figure 35.

[b] Based on the relative lateral displacement between end blocks divided by the beam clear span (excluding contributions due to sliding of the specimen and rotation of the end blocks).

[c] Loading rate of coupling beams with aspect ratios of 1.5 and 2.5. Coupling beams with an aspect ratio of 3.5 were tested at twice these rates.

Table 8 – Coupling beam maximum shear stress and deformation capacity[a]
(1,000 psi = 6.89 MPa, 1 kip = 4.45 kN)

Coupling Beam Id.	Maximum Applied Shear V_{max} kips	Maximum Applied Shear Stress $\frac{v_{max}}{\sqrt{f_{cm}}}$, psi	Deformation Capacity A [b] %	Deformation Capacity B [c] %
D80-1.5	254	13.5	6.1	6.9
D100-1.5	257	13.1	4.9	5.3
D120-1.5	264	14.0	4.6	5.2
D80-2.5	220	11.1	7.1	7.6
D100-2.5	220	11.4	5.3	6.0
D120-2.5	286	15.0	6.6	6.9
D80-3.5	219	11.5	8.3	8.6
D100-3.5	196	10.2	6.3	6.8
D120-3.5	216	11.0	6.5	6.7
P80-2.5	91	5.0	3.6	3.9
P100-2.5	110	6.4	3.6	4.1

[a] For notation and definitions, see APPENDIX A: NOTATION.

[b] The average of the highest chord rotations reached in each loading direction before strength diminished to less than 80% of the maximum applied shear.

[c] The average of the chord rotations in each loading direction where the envelope curve formed by connecting the maximum chord rotation of the first cycle of each loading step intersects with 80% of the maximum applied shear.

Table 9 – Force-deformation envelope for D-type coupling beams with aspect ratio of 1.5 (1 kip = 4.45 kN)

Target Chord Rot.	D80-1.5			D100-1.5			D120-1.5		
	Actual Chord Rot.	Shear		Actual Chord Rot.	Shear		Actual Chord Rot.	Shear	
CR	CR[a]	V	V / V_{max}[b]	CR[a]	V	V / V_{max}[b]	CR[a]	V	V / V_{max}[b]
%	%	kips		%	kips		%	kips	
-10									
-8	-8.23	-31.75	0.13				-8.56	-31.43	0.12
-6	-6.07	-226.30	0.95	-6.61	-151.45	0.59			
-4	-4.09	-235.70	0.99	-4.24	-216.96	0.84	-4.88	-237.76	0.91
-3	-3.01	-235.67	0.99	-3.08	-241.74	0.94	-3.20	-261.53	1.00
-2	-1.90	-229.89	0.96	-2.05	-246.26	0.96	-2.06	-254.64	0.97
-1.5	-1.54	-223.37	0.93	-1.74	-257.10	1.00	-1.60	-246.66	0.94
	-1.44	-228.92	0.96						
-1	-1.12	-238.91	1.00	-1.04	-238.81	0.93	-1.05	-209.23	0.80
-.75	-0.78	-221.76	0.93	-0.78	-202.63	0.79	-0.77	-177.18	0.68
-.5	-0.51	-171.53	0.72	-0.52	-168.44	0.66	-0.52	-138.50	0.53
-.3	-0.31	-124.27	0.52	-0.32	-123.83	0.48	-0.31	-92.79	0.35
-.2	-0.21	-96.21	0.40	-0.22	-103.48	0.40	-0.20	-68.89	0.26
0	0.00	1.37	0.01	0.00	3.83	0.02	0.00	2.37	0.01
.2	0.20	80.68	0.32	0.22	82.98	0.33	0.21	71.26	0.27
.3	0.30	103.95	0.41	0.31	99.00	0.39	0.31	91.17	0.35
.5	0.50	150.30	0.59	0.51	142.57	0.57	0.52	120.71	0.46
.75	0.75	197.28	0.78	0.77	185.55	0.74	0.76	157.36	0.60
1	0.99	229.39	0.90	1.01	223.96	0.89	1.02	189.37	0.72
1.5	1.48	248.17	0.98	1.47	251.72	1.00	1.52	231.26	0.88
2	2.12	254.24	1.00	2.03	240.36	0.95	2.08	254.60	0.96
	2.69	252.05	0.99						
3	2.98	251.50	0.99	2.95	241.39	0.96	2.99	264.11	1.00
4	3.87	248.72	0.98	3.99	229.06	0.91	4.16	243.43	0.92
				5.60	218.95	0.87	5.44	192.14	0.73
6	6.11	246.22	0.97	6.04	185.41	0.74	6.09	141.53	0.54
8	8.22	170.00	0.67	8.30	20.79	0.08			
10									

[a] The actual chord rotation, *CR*, associated with the peak force for each loading step. *CR* is the measured displacement of the top block relative to the bottom block divided by the coupling beam clear span, ℓ_n, and correcting for relative rotation of the end blocks.

[b] V_{max} is the maximum measured shear force in the respective loading direction.

Table 10 – Force-deformation envelope for D-type coupling beams with aspect ratio of 2.5 (1 kip = 4.45 kN)

Target Chord Rot.	D80-2.5			D100-2.5			D120-2.5		
	Actual Chord Rot.	Shear		Actual Chord Rot.	Shear		Actual Chord Rot.	Shear	
CR	CR[a]	V	V / V_{max}[b]	CR[a]	V	V / V_{max}[b]	CR[a]	V	V / V_{max}[b]
%	%	kips		%	kips		%	kips	
-10	-10.01	-20.96	0.10						
-8	-7.91	-131.70	0.60	-7.99	-46.15	0.21	-8.35	-119.57	0.42
-6	-5.91	-216.84	0.99	-6.04	-127.65	0.58	-6.42	-243.63	0.86
-4	-3.85	-215.74	0.98	-4.67	-216.89	0.99	-4.30	-283.46	1.00
-3	-3.11	-220.13	1.00				-3.15	-272.27	0.96
-2	-2.03	-213.19	0.97	-2.48	-220.12	1.00	-2.04	-241.03	0.85
-1.5	-1.51	-201.65	0.92	-1.50	-207.61	0.94	-1.56	-217.28	0.77
-1	-0.99	-170.95	0.78	-0.98	-167.82	0.76	-1.00	-162.48	0.57
-.75	-0.70	-144.26	0.66	-0.75	-138.02	0.63	-0.74	-134.47	0.47
-.5	-0.47	-108.58	0.49	-0.50	-101.22	0.46	-0.53	-105.53	0.37
-.3	-0.28	-80.44	0.37	-0.29	-73.03	0.33	-0.31	-65.09	0.23
-.2	-0.23	-72.21	0.33	-0.19	-60.27	0.27	-0.20	-40.35	0.14
0	0.00	0.00	0.00	0.00	0.00	0.00	0.01	2.10	0.01
.2	0.23	63.45	0.29	0.20	58.02	0.27	0.20	40.13	0.14
.3	0.38	92.87	0.43	0.33	76.62	0.36	0.31	64.96	0.23
.5	0.48	106.54	0.49	0.54	102.19	0.48	0.61	116.76	0.41
.75	0.76	142.91	0.66	0.81	144.25	0.67	0.77	138.26	0.48
1	0.98	166.18	0.76	1.04	170.74	0.80	1.01	168.12	0.59
1.5	1.89	212.34	0.97	1.45	203.97	0.95	1.50	216.83	0.76
2	2.06	193.89	0.89	2.16	214.25	1.00	2.10	251.95	0.88
3	2.92	209.56	0.96	3.06	210.68	0.98	3.15	277.43	0.97
4	3.94	207.45	0.95	4.02	194.51	0.91	4.29	285.94	1.00
							5.80	271.60	0.95
6	6.00	217.95	1.00	6.01	191.05	0.89	6.68	251.57	0.88
8	8.17	180.68	0.83	8.12	124.04	0.58	9.11	94.56	0.33
10									

[a] The actual chord rotation, *CR*, associated with the peak force for each loading step. *CR* is the measured displacement of the top block relative to the bottom block divided by the coupling beam clear span, ℓ_n, and correcting for relative rotation of the end blocks.

[b] V_{max} is the maximum measured shear force in the respective loading direction.

Table 11 – Force-deformation envelope for D-type coupling beams with aspect ratio of 3.5 (1 kip = 4.45 kN)

Target Chord Rot.	D80-3.5			D100-3.5			D120-3.5		
	Actual Chord Rot.	Shear		Actual Chord Rot.	Shear		Actual Chord Rot.	Shear	
CR	CR[a]	V	V / V_{max}[b]	CR[a]	V	V / V_{max}[b]	CR[a]	V	V / V_{max}[b]
%	%	kips		%	kips		%	kips	
-10	-10.29	-53.91	0.25	-10.25	-38.06	0.20			
-8	-8.24	-182.26	0.84	-8.09	-102.84	0.54	-7.91	-93.00	0.43
-6	-6.04	-217.50	1.00	-6.35	-180.91	0.94	-6.38	-184.10	0.85
-4	-4.13	-209.83	0.96	-4.12	-186.92	0.97	-4.08	-215.70	1.00
-3	-3.09	-207.46	0.95	-3.10	-191.73	1.00	-3.01	-214.54	0.99
-2	-2.16	-204.24	0.94	-2.11	-189.19	0.99	-1.97	-191.87	0.89
-1.5	-1.56	-195.04	0.90	-1.58	-175.56	0.92	-1.58	-172.44	0.80
-1	-1.08	-164.62	0.76	-1.05	-134.79	0.70	-1.03	-129.45	0.60
-.75	-0.77	-125.98	0.58	-0.76	-106.16	0.55	-0.77	-105.13	0.49
-.5	-0.51	-95.35	0.44	-0.51	-77.91	0.41	-0.51	-78.48	0.36
-.3	-0.30	-66.42	0.31	-0.31	-55.74	0.29	-0.31	-55.70	0.26
-.2	-0.22	-46.14	0.21	-0.22	-45.86	0.24	-0.20	-40.57	0.19
0	0.00	-0.16	0.00	0.00	1.63	0.01	0.00	0.06	0.00
.2	0.22	49.87	0.23	0.26	52.65	0.27	0.23	43.16	0.20
.3	0.34	71.92	0.33	0.31	57.99	0.30	0.33	57.05	0.27
.5	0.51	95.47	0.44	0.53	86.95	0.44	0.53	79.80	0.38
.75	0.78	130.92	0.60	0.77	114.71	0.59	0.78	104.60	0.49
1	1.08	166.34	0.76	1.02	139.32	0.71	1.02	126.60	0.60
1.5	1.55	196.19	0.90	1.57	177.08	0.90	1.55	161.65	0.76
2	2.03	206.40	0.95	2.02	187.53	0.96	2.07	182.77	0.86
3	3.13	212.97	0.98	3.16	195.99	1.00	3.04	211.46	1.00
4	4.16	211.81	0.97	4.36	189.27	0.97	4.14	212.40	1.00
6	5.96	219.40	1.00	6.20	184.12	0.94	6.53	191.10	0.90
8	8.28	211.74	0.97	8.11	94.05	0.48	8.48	62.12	0.29
10	10.20	84.96	0.39	10.25	34.29	0.17			

[a] The actual chord rotation, *CR*, associated with the peak force for each loading step. *CR* is the measured displacement of the top block relative to the bottom block divided by the coupling beam clear span, ℓ_n, and correcting for relative rotation of the end blocks.

[b] V_{max} is the maximum measured shear force in the respective loading direction.

Table 12 – Force-deformation envelope for P-type coupling beams with aspect ratio of 2.5 (1 kip = 4.45 kN)

Target Chord Rot.	P80-2.5			P100-2.5		
	Actual Chord Rot.	Shear		Actual Chord Rot.	Shear	
CR	CR[a]	V	V / V_{max}[b]	CR[a]	V	V / V_{max}[b]
%	%	kips		%	kips	
-10						
-8						
-6	-6.03	-16.81	0.19	-6.53	-29.39	0.27
-4	-4.06	-39.15	0.44	-4.02	-96.44	0.89
-3	-3.04	-77.09	0.86	-3.23	-106.60	0.98
-2	-1.98	-89.56	1.00	-2.05	-108.48	1.00
-1.5	-1.50	-87.17	0.97	-1.46	-104.53	0.96
-1	-1.01	-82.07	0.92	-0.99	-95.65	0.88
-.75	-0.84	-80.11	0.89	-0.73	-82.75	0.76
-.5	-0.47	-66.10	0.74	-0.50	-67.15	0.62
-.3	-0.35	-58.97	0.66	-0.29	-50.74	0.47
-.2	-0.19	-42.31	0.47	-0.23	-44.38	0.41
0	0.00	0.00	0.00	0.00	0.00	0.00
.2	0.18	42.34	0.47	0.23	41.34	0.38
.3	0.31	52.68	0.58	0.35	51.10	0.47
.5	0.55	73.64	0.81	0.58	63.98	0.58
.75	0.82	84.79	0.94	0.77	83.49	0.76
1	1.00	84.80	0.94	1.09	98.78	0.90
1.5	1.58	88.92	0.98	1.76	109.85	1.00
2	1.93	88.61	0.98	2.11	107.52	0.98
3	2.86	90.58	1.00	3.18	106.76	0.97
4	4.09	80.15	0.88	4.10	76.02	0.69
6	7.09	30.53	0.34	6.15	48.95	0.45
8						
10						

[a] The actual chord rotation, *CR*, associated with the peak force for each loading step. *CR* is the measured displacement of the top block relative to the bottom block divided by the coupling beam clear span, ℓ_n, and correcting for relative rotation of the end blocks.

[b] V_{max} is the maximum measured shear force in the respective loading direction.

Table 13 – Coupling beam measured and calculated strengths[a]
(1,000 psi = 6.89 MPa, 1 kip = 4.45 kN)

Coupling Beam Id.	Measured		Calculated			Measured-to-Calculated Ratio[b]
	V_{max} kips	v_{max} $\sqrt{f_{cm}}$, psi	V_{nm} kips	$2M_{nm}/\ell_n$ kips	v_{nm} $\sqrt{f_{cm}}$, psi	
D80-1.5	254	13.5	169	-	9.0	1.50
D100-1.5	257	13.1	183	-	9.4	1.40
D120-1.5	264	14.0	158	-	8.4	1.68
D80-2.5	220	11.1	161	-	8.1	1.36
D100-2.5	220	11.4	163	-	8.4	1.35
D120-2.5	286	15.0	150	-	7.9	1.90
D80-3.5	219	11.5	158	-	8.3	1.39
D100-3.5	196	10.2	153	-	8.0	1.28
D120-3.5	216	11.0	146	-	7.5	1.48
P80-2.5	91	5.0	-	77	4.3	1.18
P100-2.5	110	6.4	-	99	5.8	1.11

[a] For notation and definitions, see APPENDIX A: NOTATION.

[b] The average of measured-to-calculated ratios is 1.43 for D-type beams (excluding D120-2.5) and 1.15 for P-type beams.

Table 14 – Summary of test data[a]
(1 ksi = 1000 psi = 6.89 MPa)

Coupling Beam Id.	Reinforcement Type	$\frac{\ell_n}{h}$	f_{cm}	f_{ym}	f_{ytm}	v_{max} [b]	v_{nm} [c]	Measured Chord Rotation Capacity[d]	ASCE 41-17 Chord Rotation Capacity[e]
			psi	ksi	ksi	$\sqrt{f_{cm}}$, psi	$\sqrt{f_{cm}}$, psi	%	%
D80-1.5	Diagonal	1.5	7,600	83	89	13.5	9.0	6.9	5.0
D100-1.5	Diagonal	1.5	8,200	108	89	13.1	9.4	5.3	5.0
D120-1.5	Diagonal	1.5	7,600	116	89	14.0	8.4	5.2	5.0
D80-2.5	Diagonal	2.5	8,400	83	89	11.1	8.1	7.6	5.0
D100-2.5	Diagonal	2.5	8,000	108	89	11.4	8.4	6.0	5.0
D120-2.5	Diagonal	2.5	7,800	116	133	15.0	7.9	6.9	5.0
D80-3.5	Diagonal	3.5	7,800	84	89	11.5	8.3	8.6	5.0
D100-3.5	Diagonal	3.5	7,900	108	89	10.2	8.0	6.8	5.0
D120-3.5	Diagonal	3.5	8,200	116	89	11.0	7.5	6.7	5.0
P80-2.5	Parallel	2.5	8,300	83	89	5.0	4.3	3.9	4.0[f]
P100-2.5	Parallel	2.5	7,500	108	89	6.4	5.8	4.1	4.0[f]

[a] For notation and definitions, see APPENDIX A: NOTATION.

[b] Shear stress associated with maximum applied shear V_{max}.
For D-type beams, $v_{max} = V_{max}/(b_w h)$.
For P-type beams, $v_{max} = V_{max}/(b_w d)$.

[c] For D-type beams, $v_{nm} = (2A_{vd}\, f_{ym} \sin \alpha)/(b_w h)$.
For P-type beams, $v_{nm} = (2M_{nm}/\ell_n)/(b_w d)$.

[d] The average of the chord rotations in each loading direction where the envelope curve formed by connecting the maximum chord rotation of the first cycle of each loading step intersects with 80% of the maximum applied shear.

[e] Chord rotation capacity from ASCE 41-17[4] Table 10-19 corresponding to the maximum chord rotation associated with the residual strength defined by segment D-E in ASCE 41-17[4] Figure 10-1(b). It is important to note that the measured chord rotation capacity (see footnote d) corresponds to a higher residual strength than those used in ASCE 41-17[4], where the residual strength is defined as 80% of the strength at point B in Figure 10-1(b)[4].

[f] The reported ASCE 41-17[4] chord rotation capacity is taken from Table 10-19[4] and corresponds to a residual strength of 50% of the strength at point B in Figure 10-1(b)[4]. In contrast, the measured chord rotation capacity (see footnote d) corresponds to the chord rotation associated with a post-peak strength of 80% of the maximum applied shear.

FIGURES

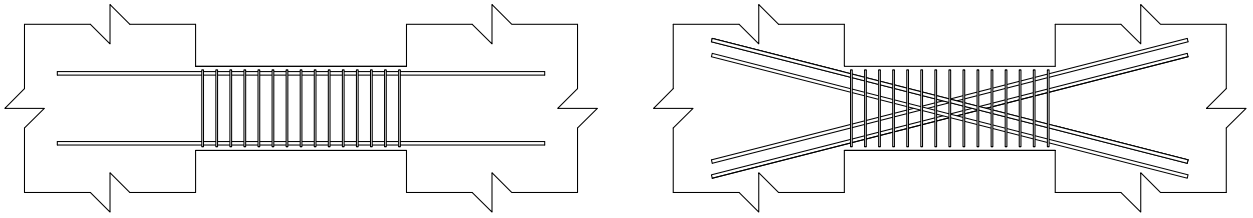

(a) P-type beam (b) D-type beam

Figure 1 – Reinforcement layout types, parallel (P) and diagonal (D)

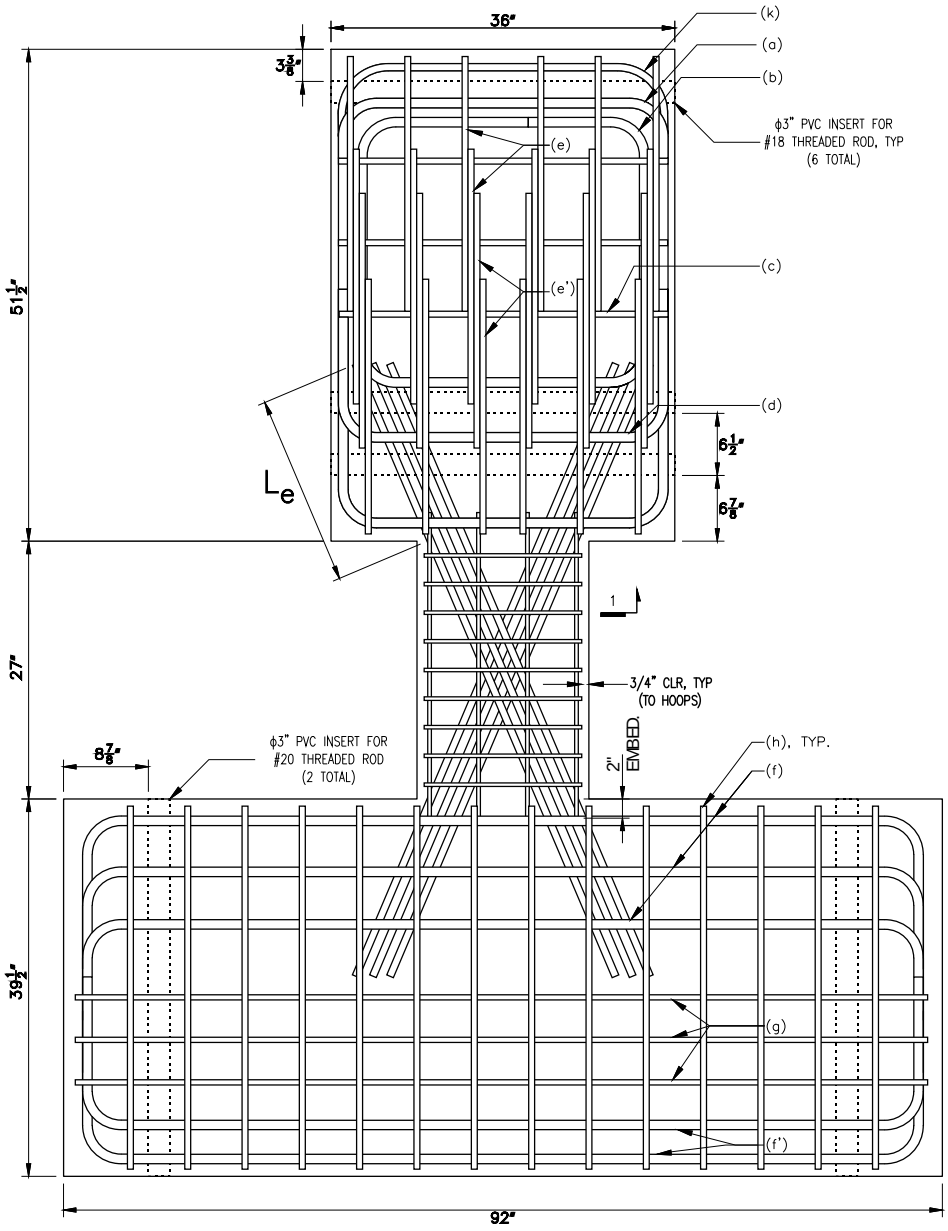

Figure 2 – Elevation view of D80-1.5 (1 in. = 25.4 mm)

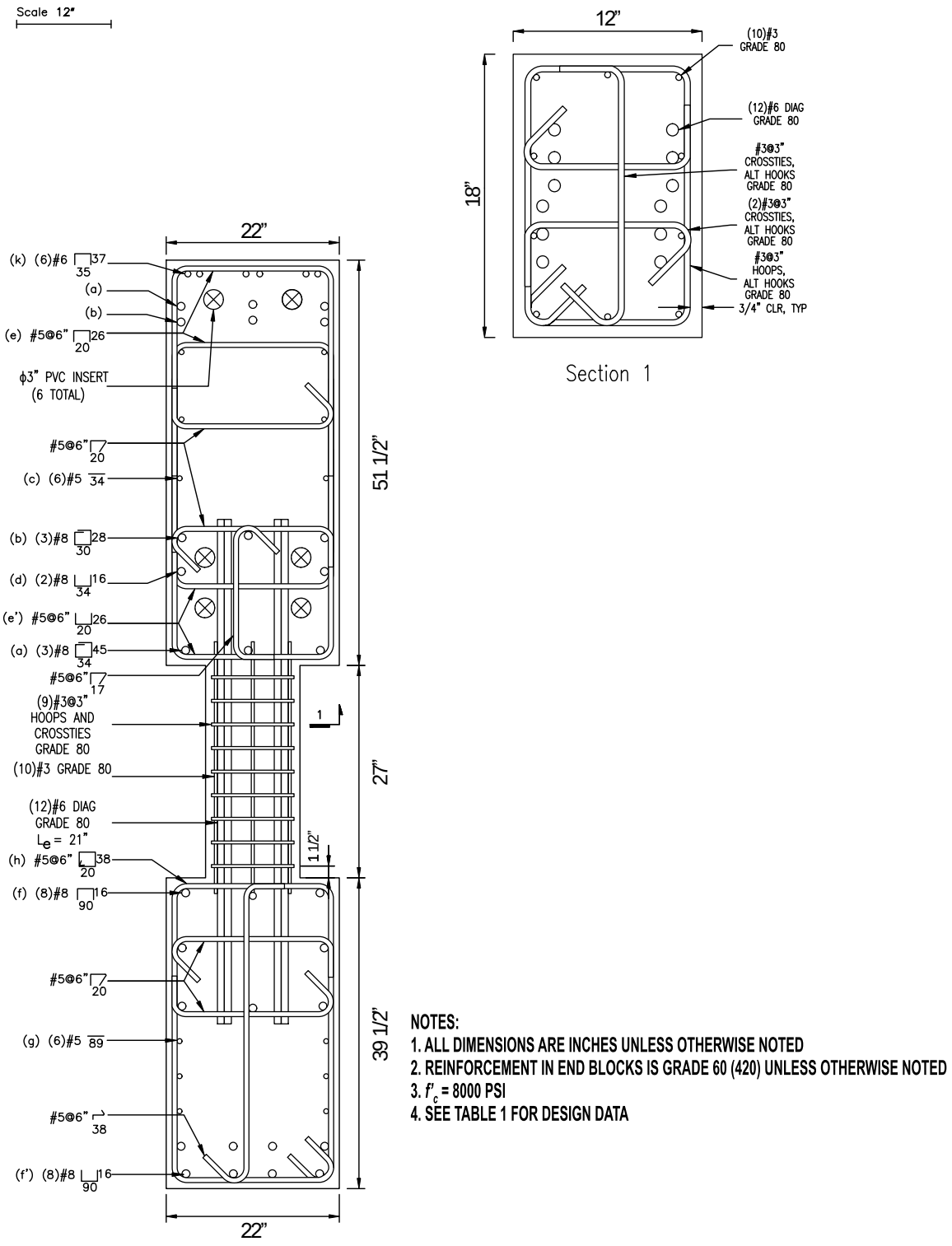

Figure 3 – Reinforcement details of D80-1.5 (1 in. = 25.4 mm, 1 ksi = 1,000 psi = 6.89 MPa)

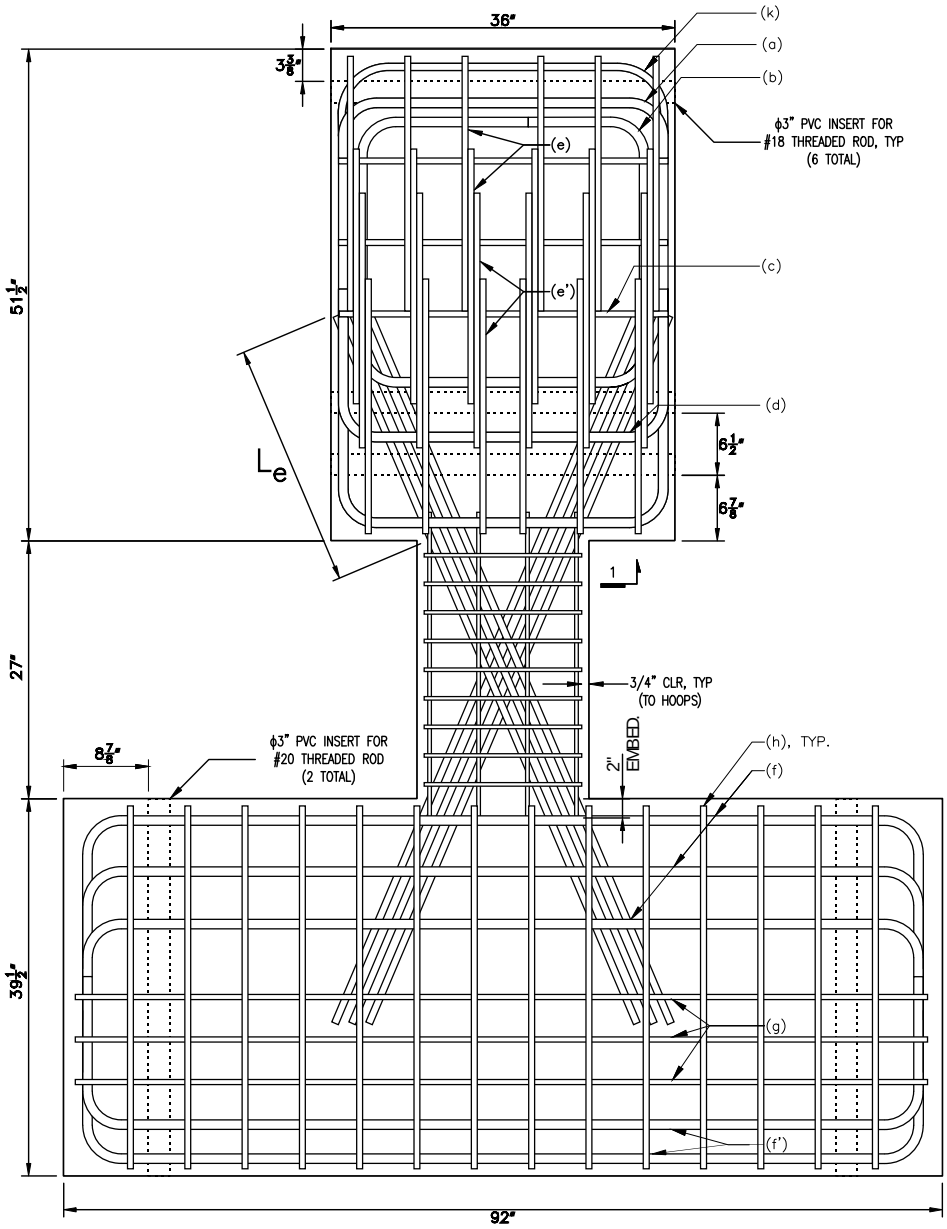

Figure 4 – Elevation view of D100-1.5 (1 in. = 25.4 mm)

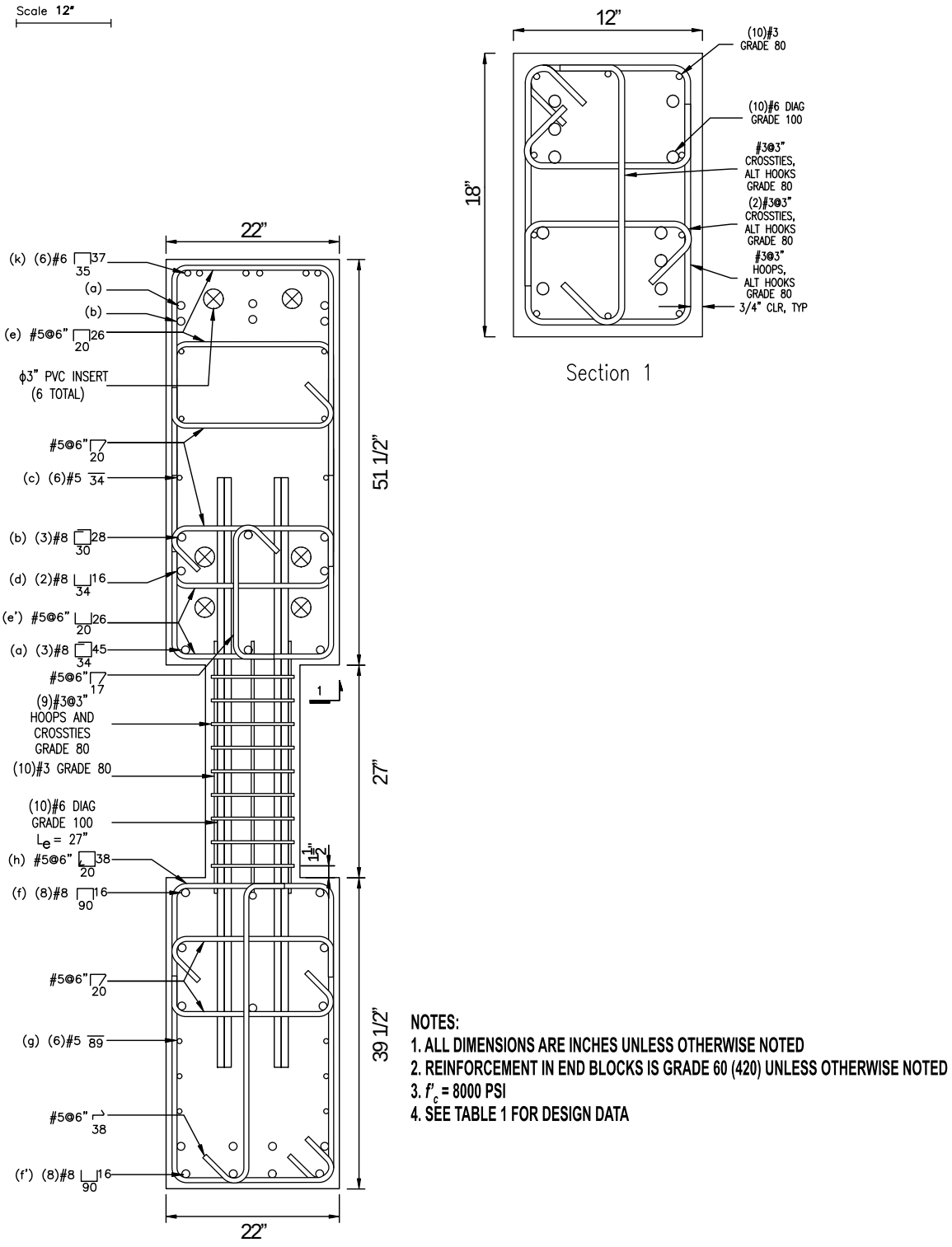

Figure 5 – Reinforcement details of D100-1.5 (1 in. = 25.4 mm, 1 ksi = 1,000 psi = 6.89 MPa)

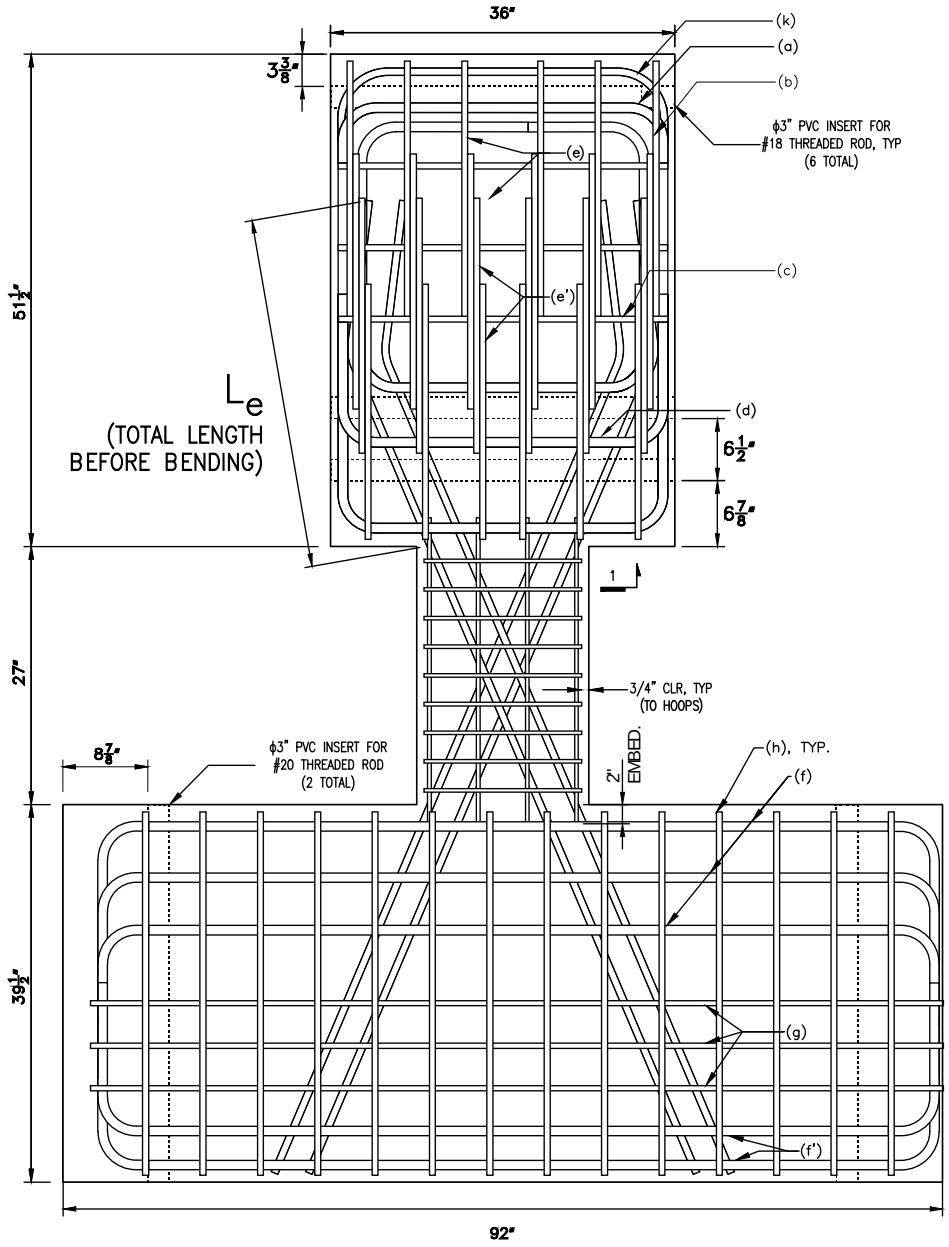

Figure 6 – Elevation view of D120-1.5 (1 in. = 25.4 mm)

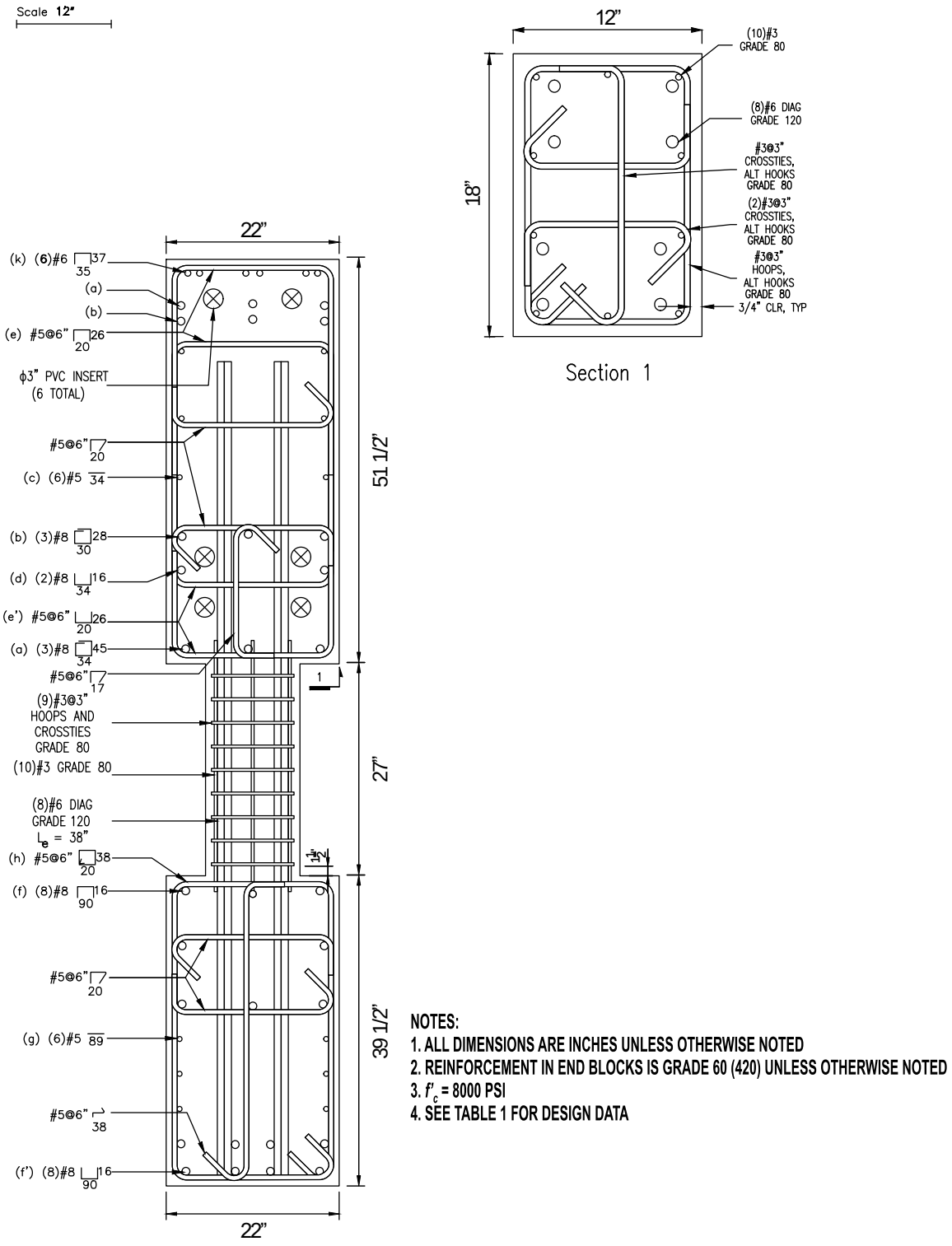

Figure 7 – Reinforcement details of D120-1.5 (1 in. = 25.4 mm, 1 ksi = 1,000 psi = 6.89 MPa)

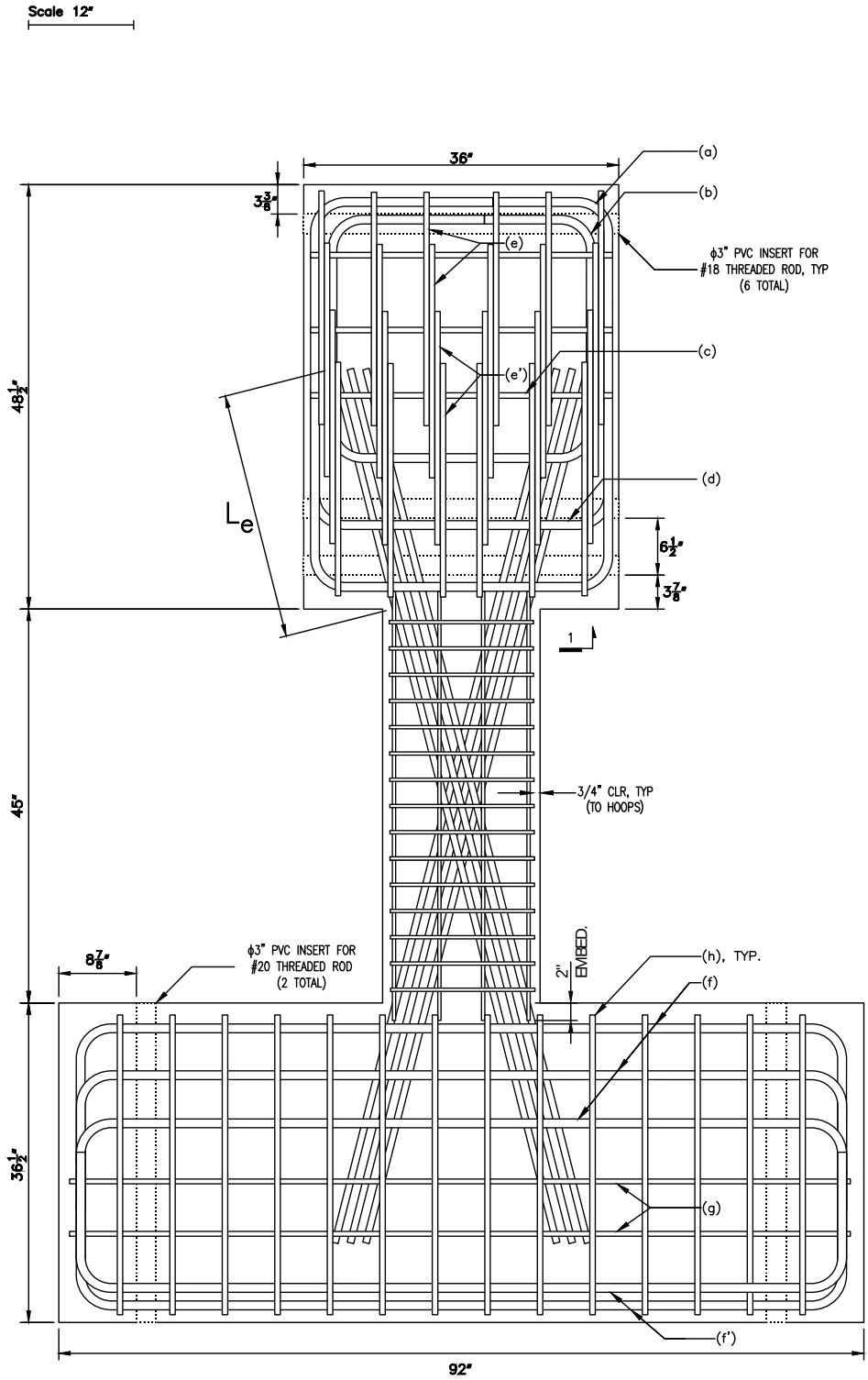

Figure 8 – Elevation view of D80-2.5 (1 in. = 25.4 mm)

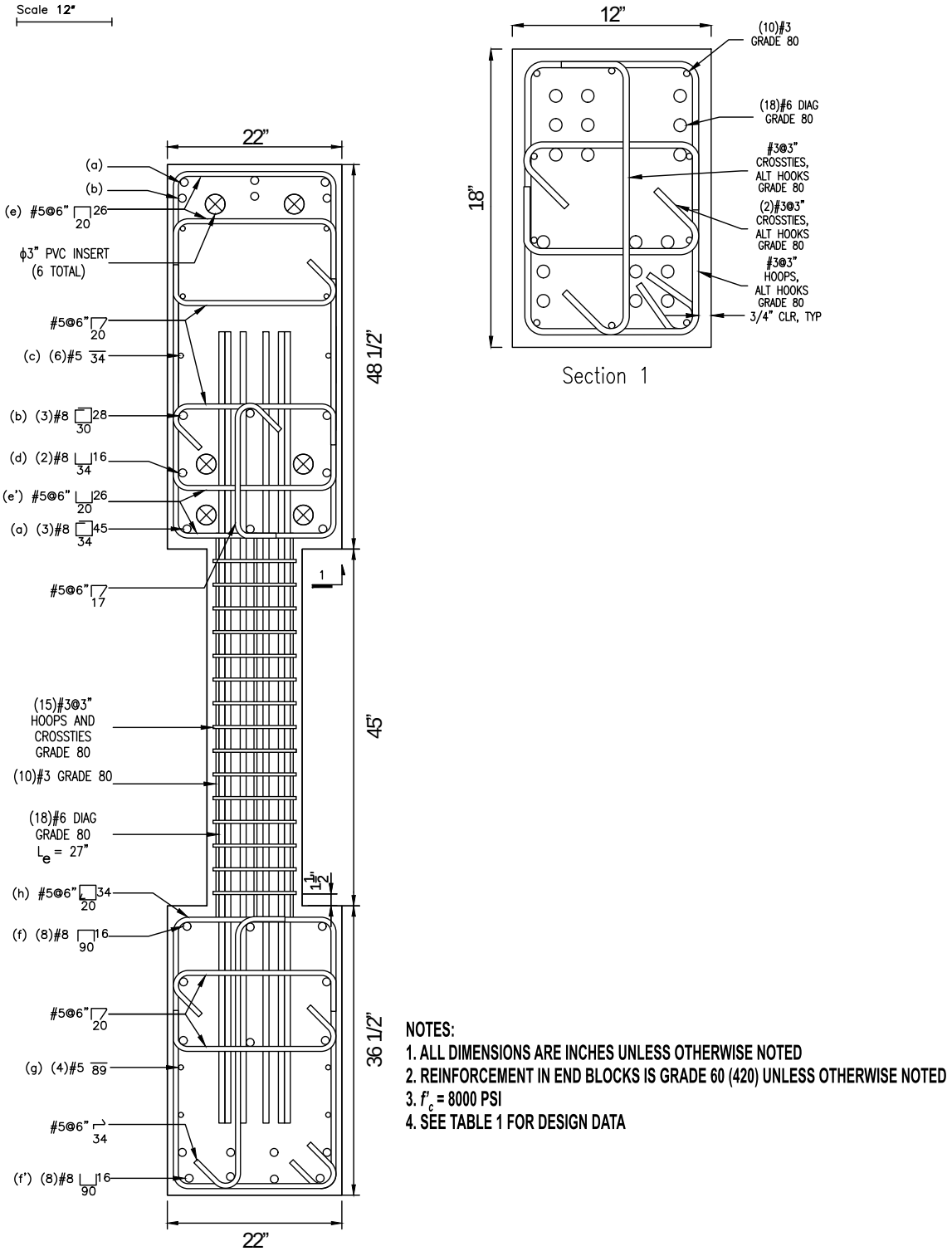

Figure 9 – Reinforcement details of D80-2.5 (1 in. = 25.4 mm, 1 ksi = 1,000 psi = 6.89 MPa)

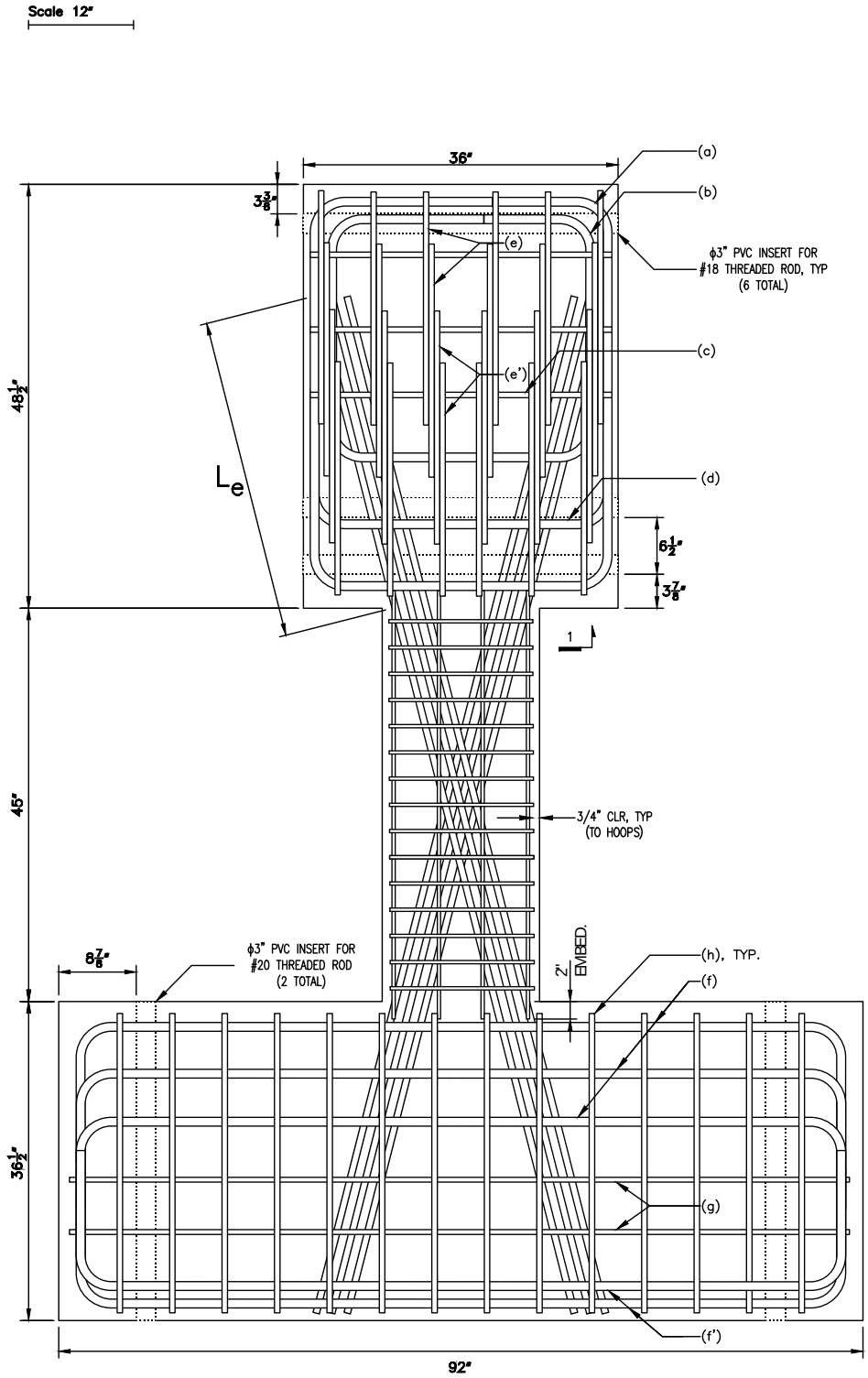

Figure 10 – Elevation view of D100-2.5 (1 in. = 25.4 mm)

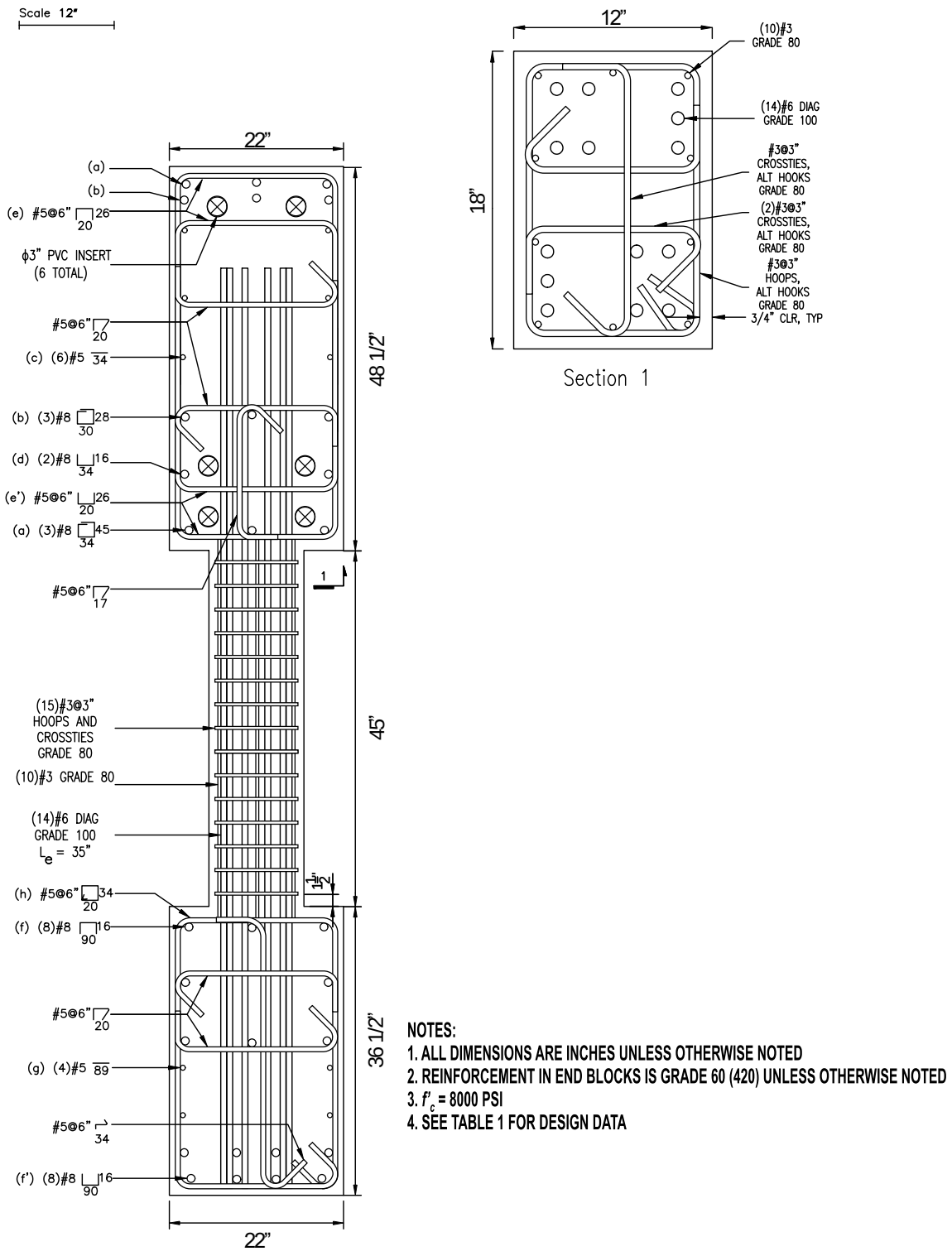

Figure 11 – Reinforcement details of D100-2.5 (1 in. = 25.4 mm, 1 ksi = 1,000 psi = 6.89 MPa)

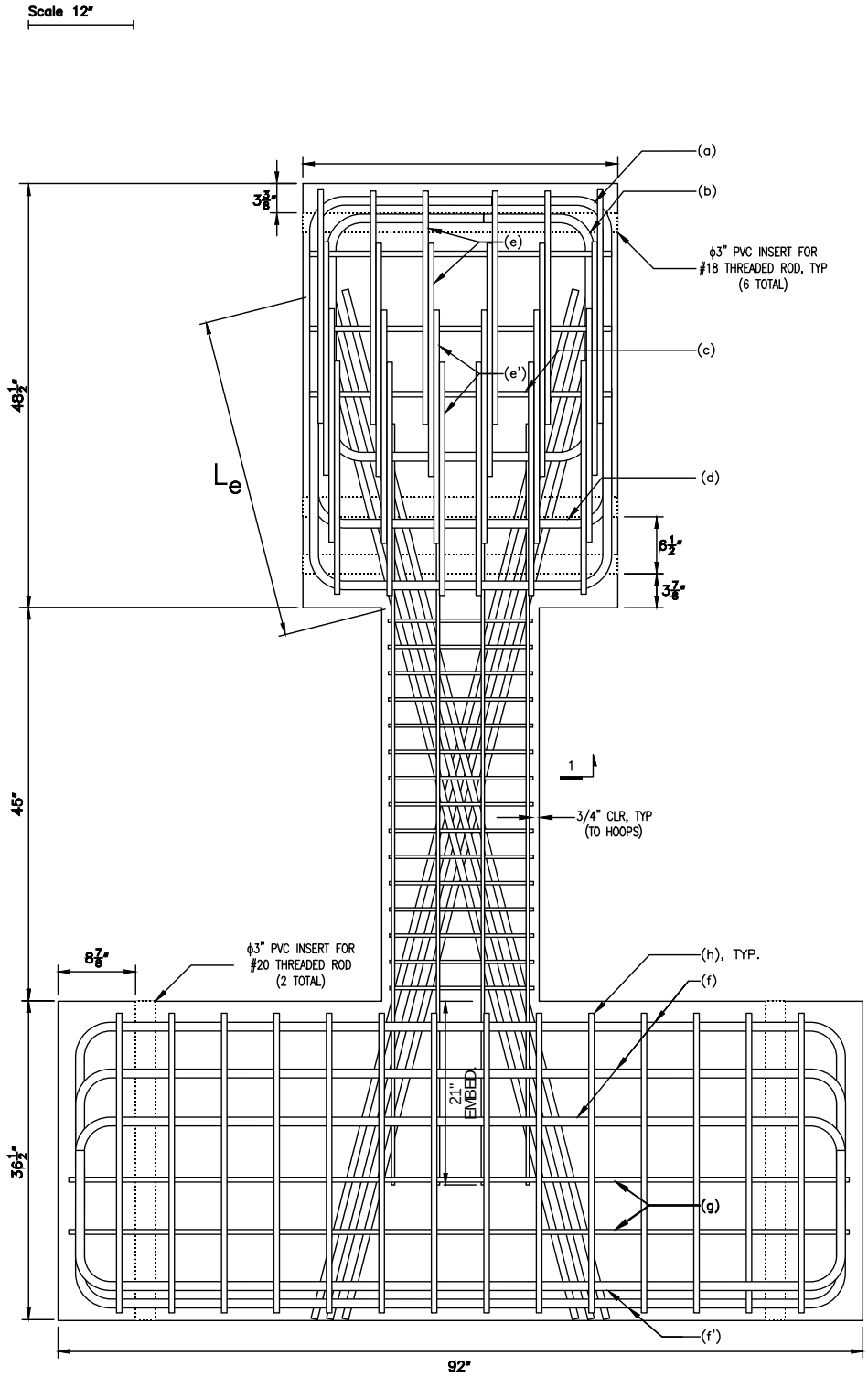

Figure 12 – Elevation view of D120-2.5 (1 in. = 25.4 mm)

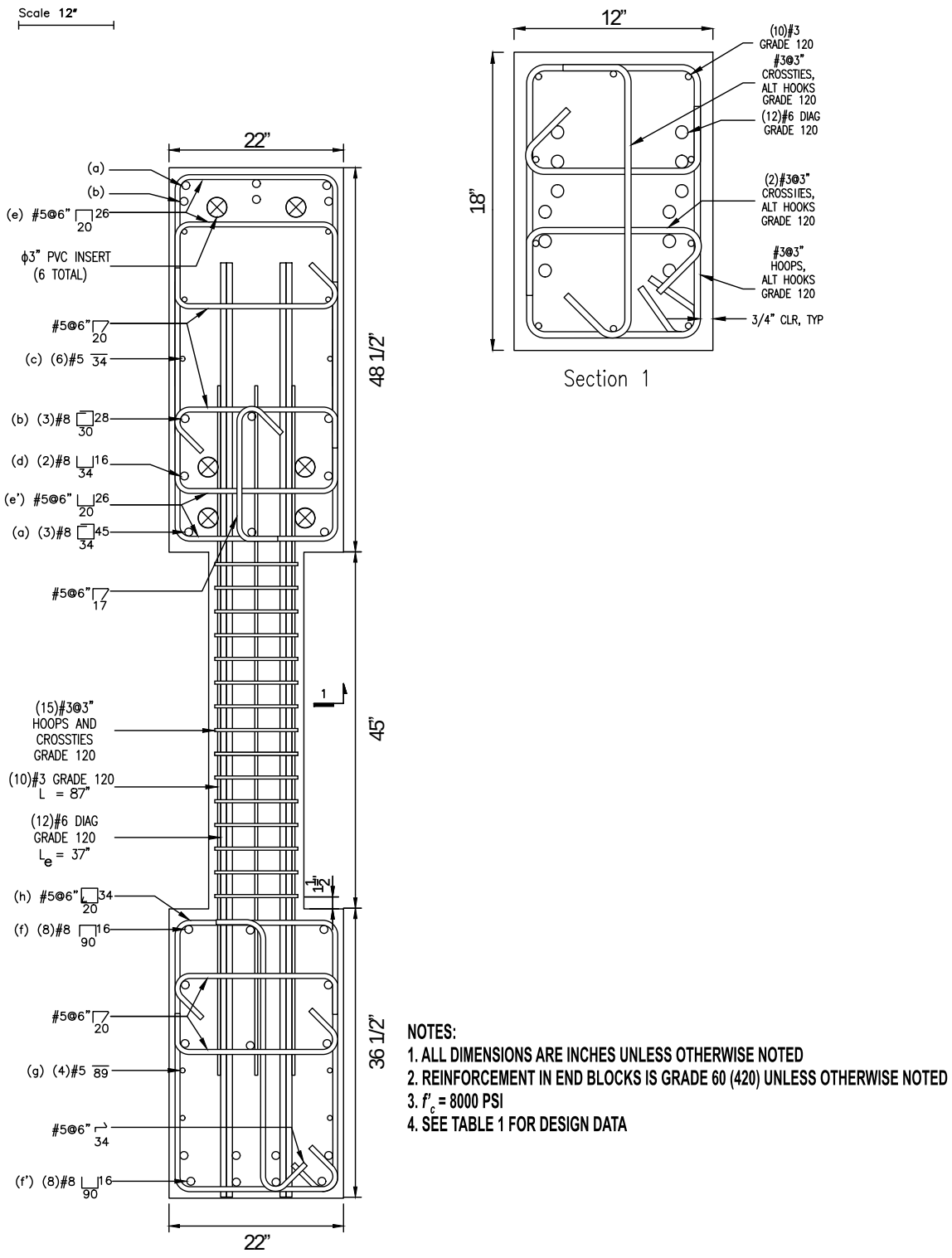

Figure 13 – Reinforcement details of D120-2.5 (1 in. = 25.4 mm, 1 ksi = 1,000 psi = 6.89 MPa)

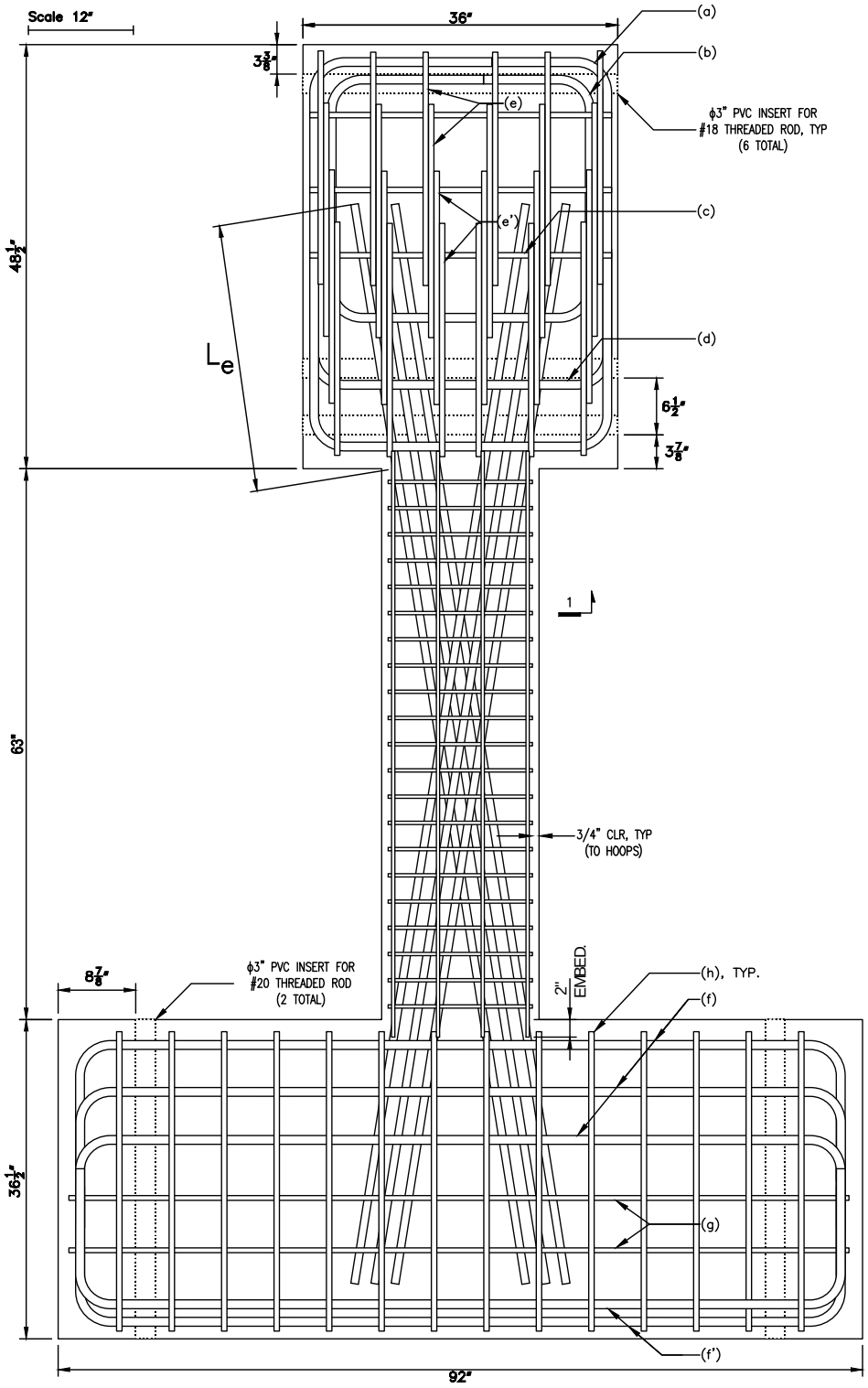

Figure 14 – Elevation view of D80-3.5 (1 in. = 25.4 mm)

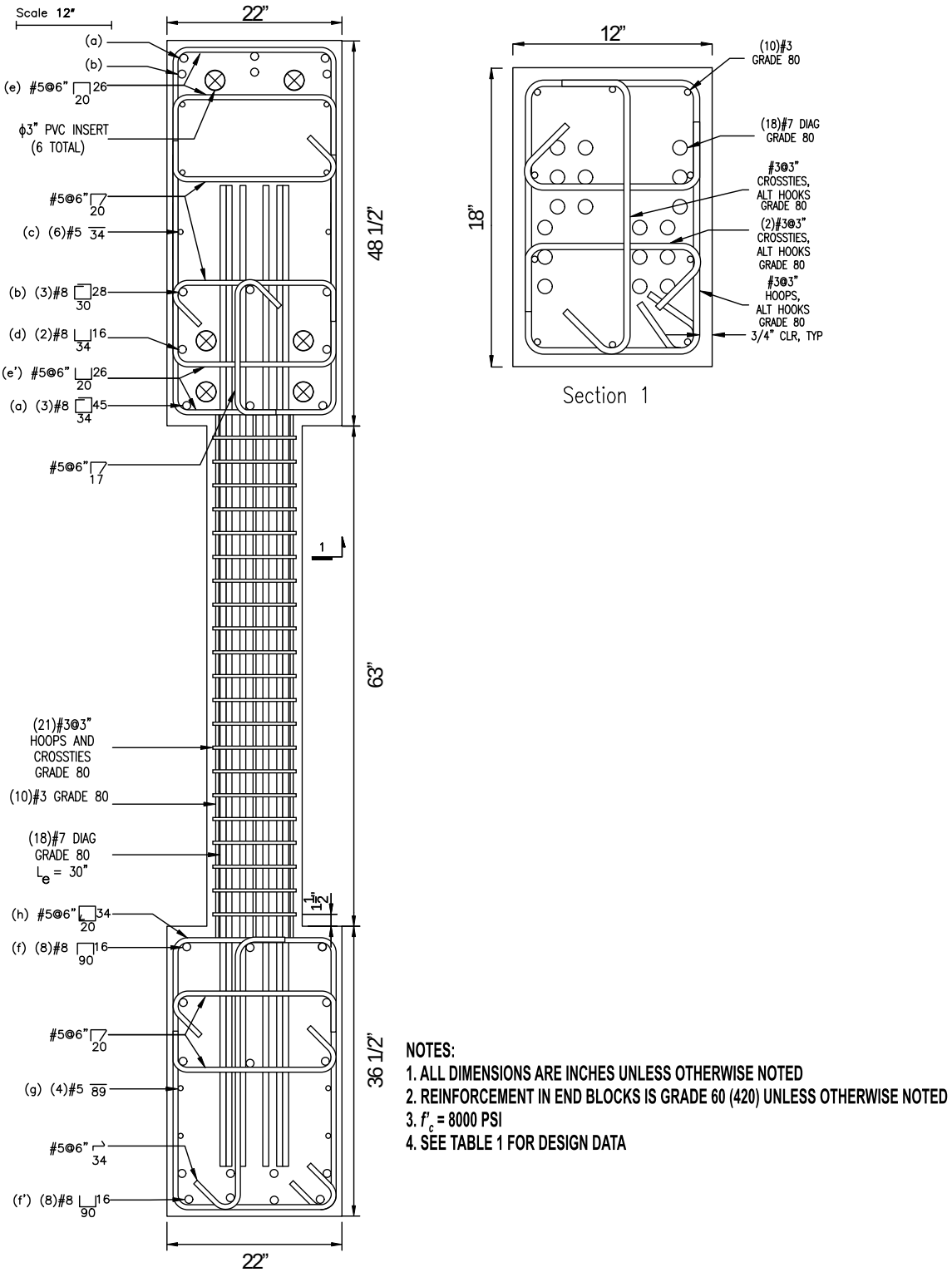

Figure 15 – Reinforcement details of D80-3.5 (1 in. = 25.4 mm, 1 ksi = 1,000 psi = 6.89 MPa)

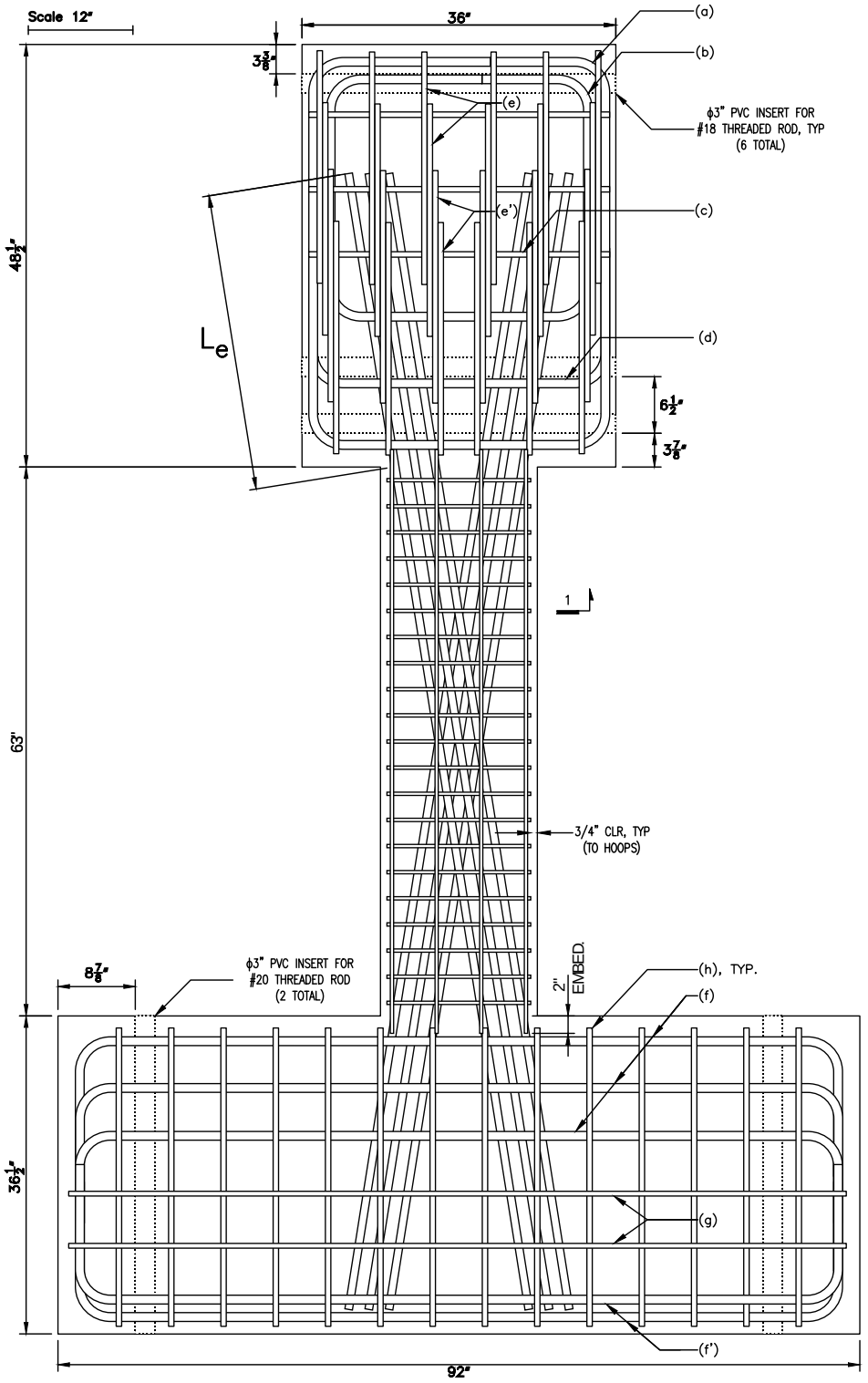

Figure 16 – Elevation view of D100-3.5 (1 in. = 25.4 mm)

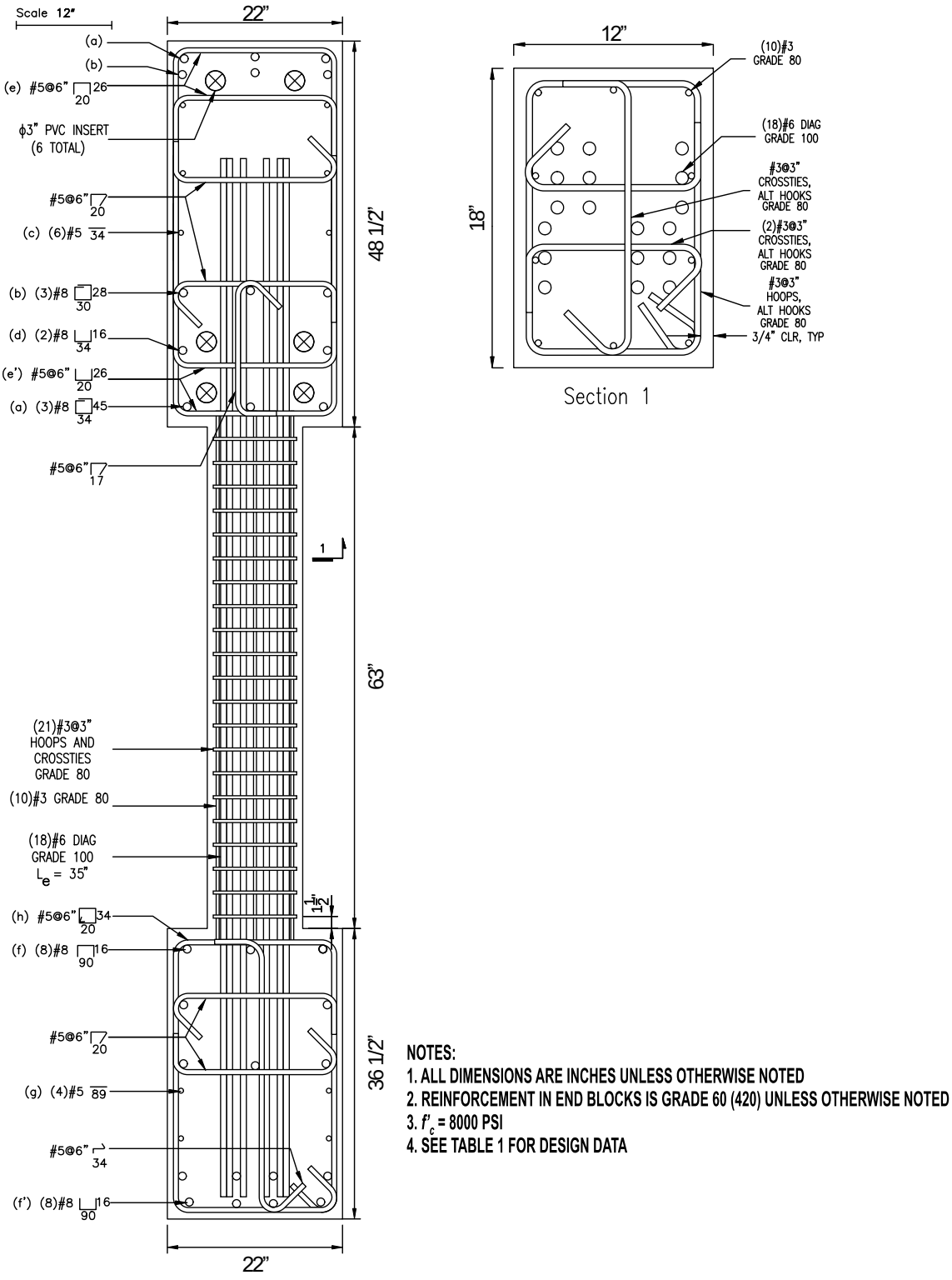

Figure 17 – Reinforcement details of D100-3.5 (1 in. = 25.4 mm, 1 ksi = 1,000 psi = 6.89 MPa)

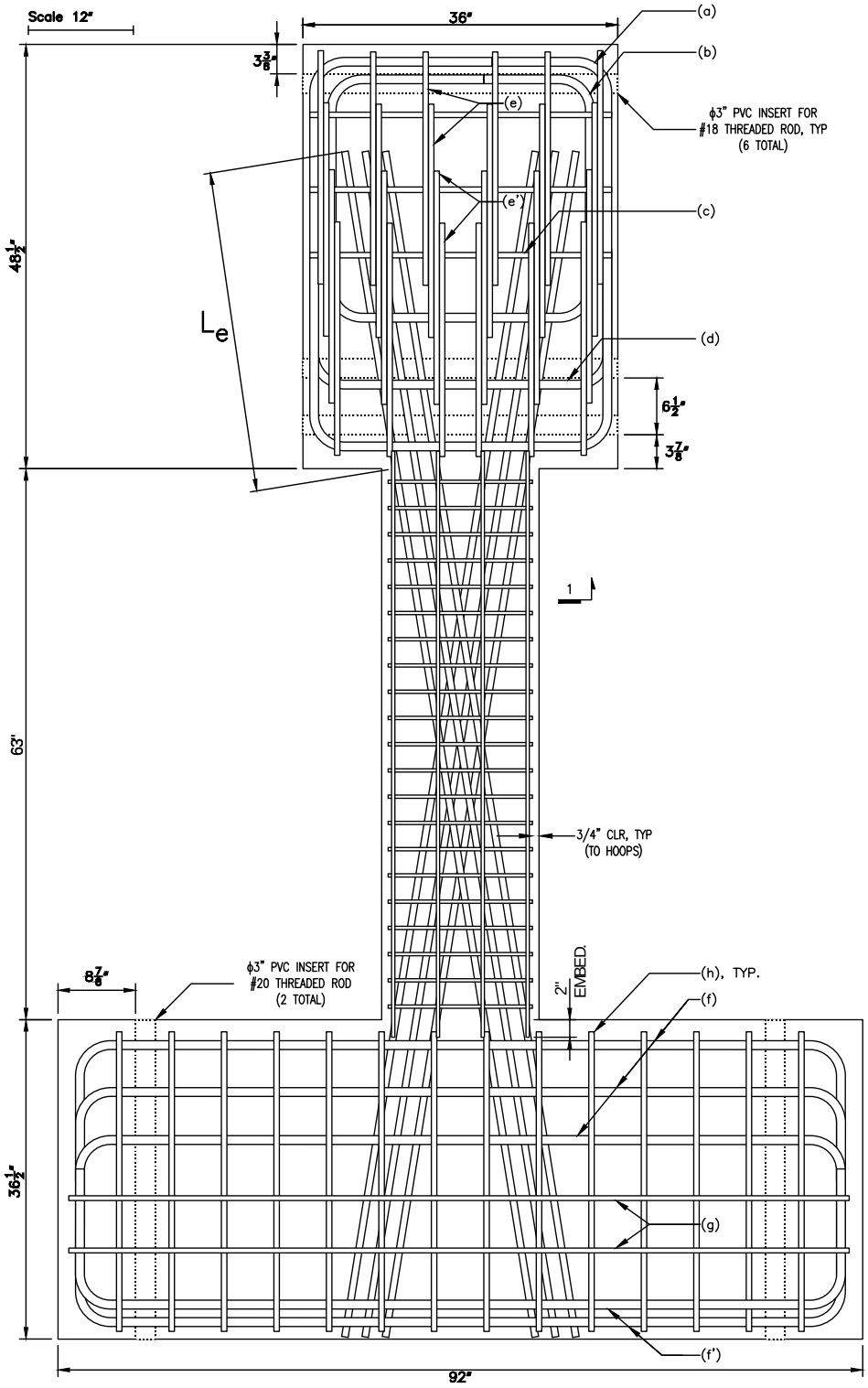

Figure 18 – Elevation view of D120-3.5 (1 in. = 25.4 mm)

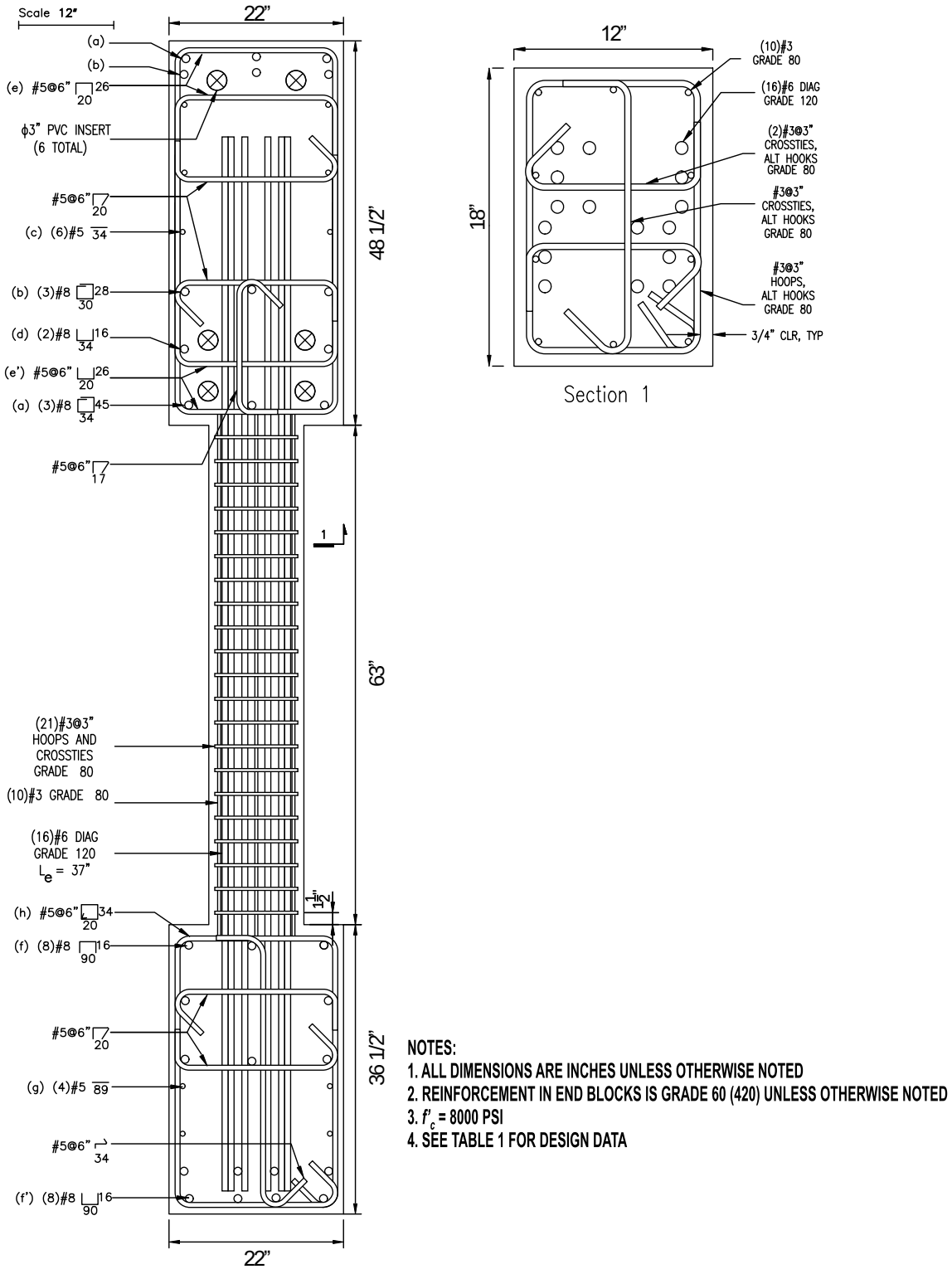

Figure 19 – Reinforcement details of D120-3.5 (1 in. = 25.4 mm, 1 ksi = 1,000 psi = 6.89 MPa)

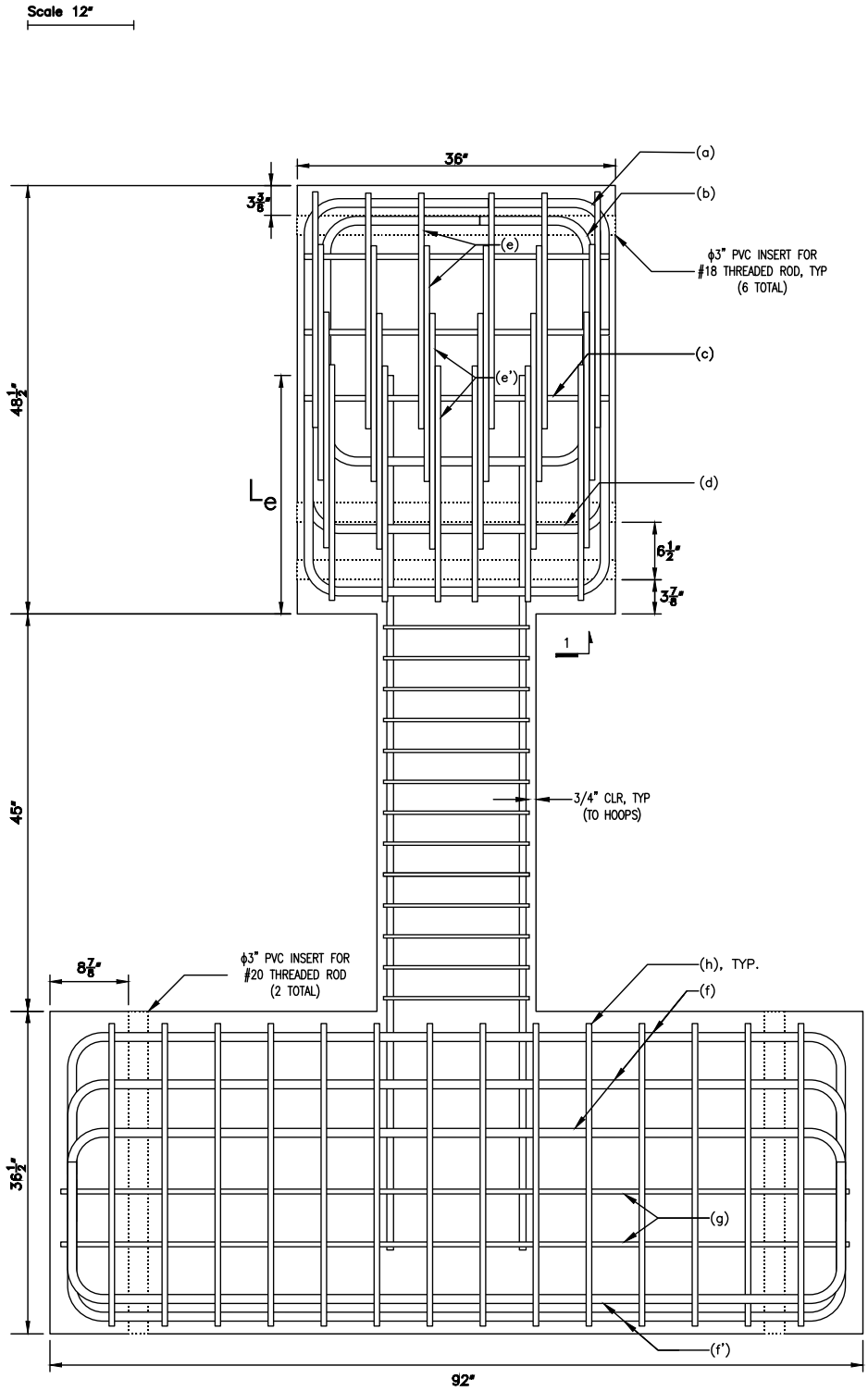

Figure 20 – Elevation view of P80-2.5 (1 in. = 25.4 mm)

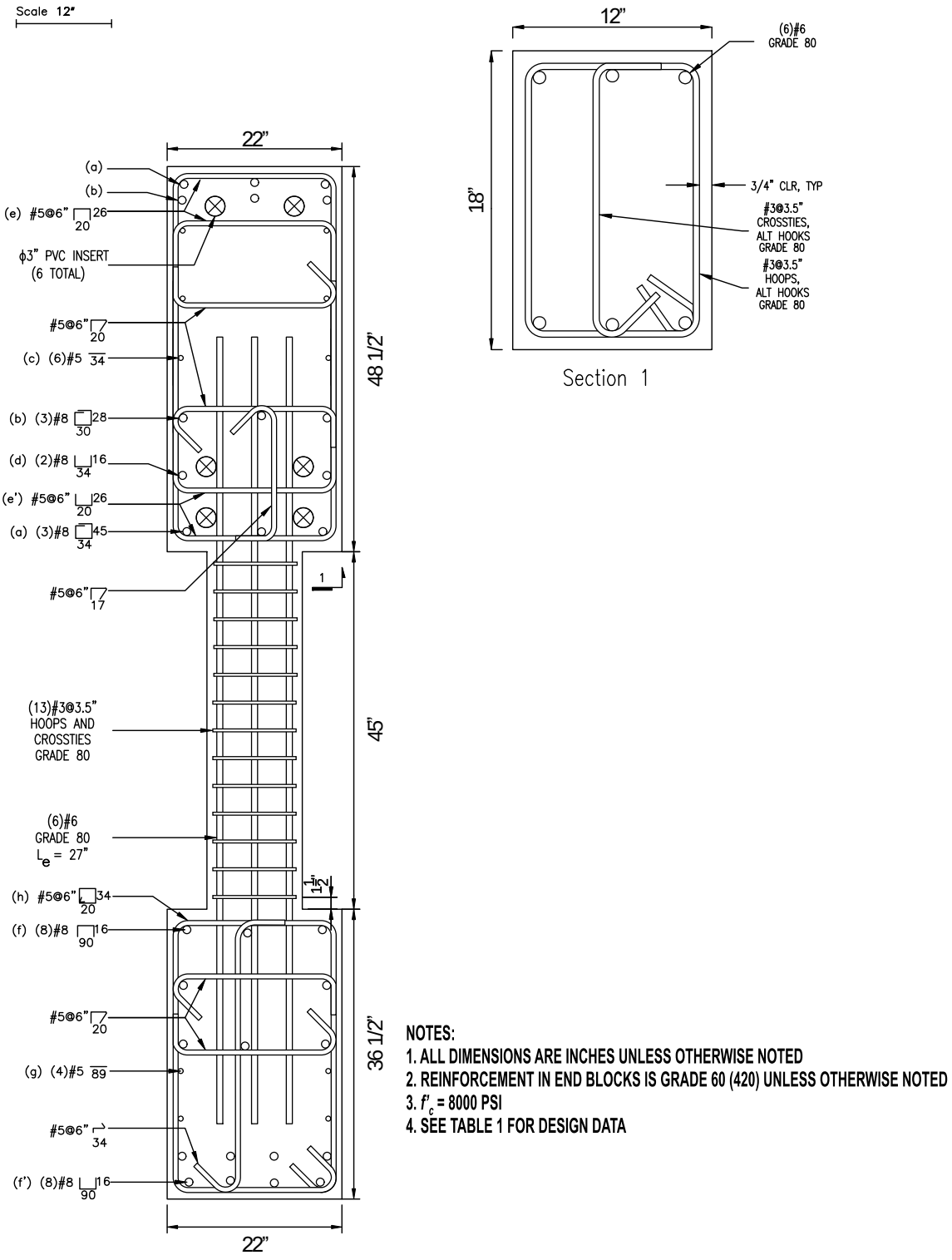

Figure 21 – Reinforcement details of P80-2.5 (1 in. = 25.4 mm, 1 ksi = 1,000 psi = 6.89 MPa)

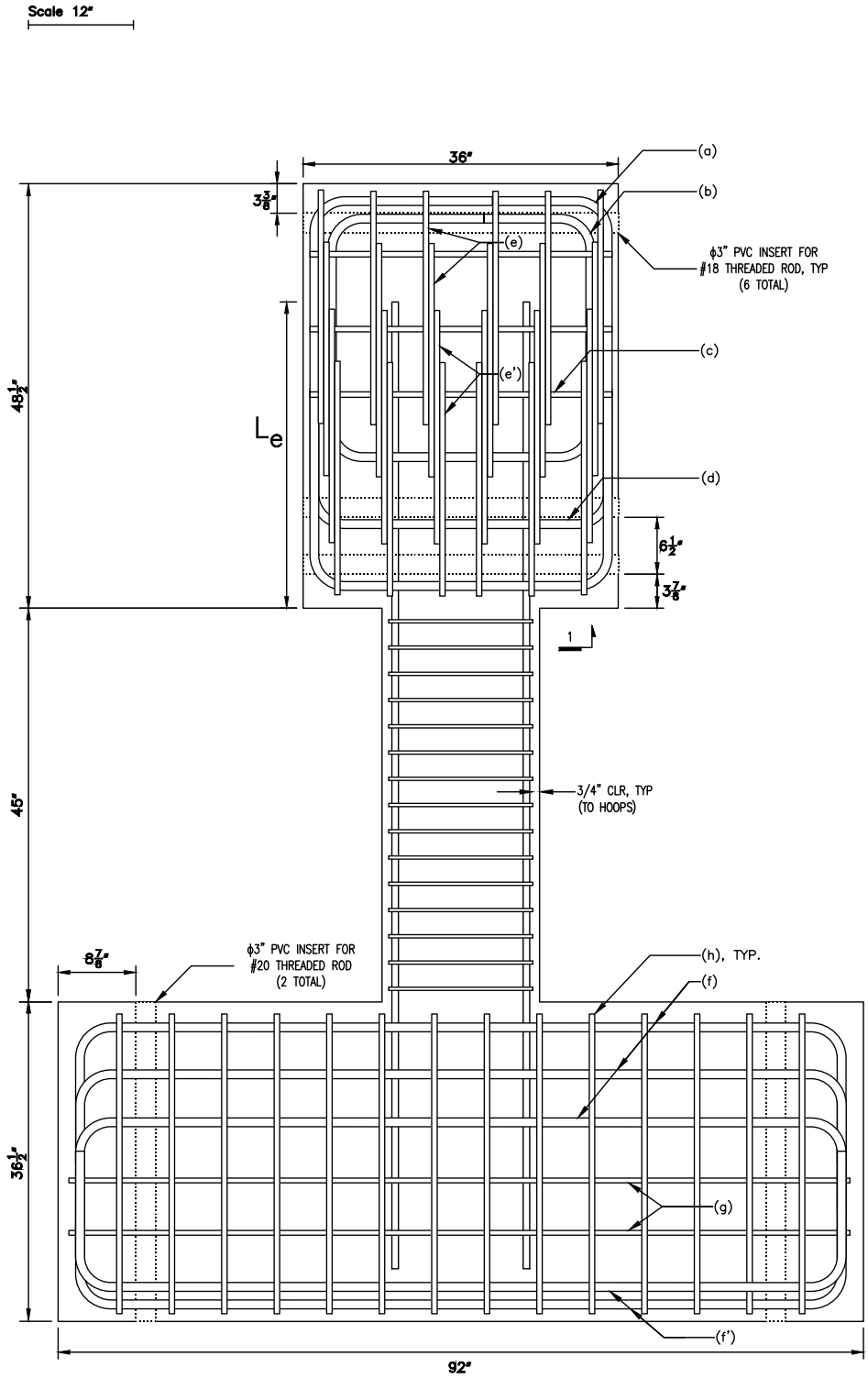

Figure 22 – Elevation view of P100-2.5 (1 in. = 25.4 mm)

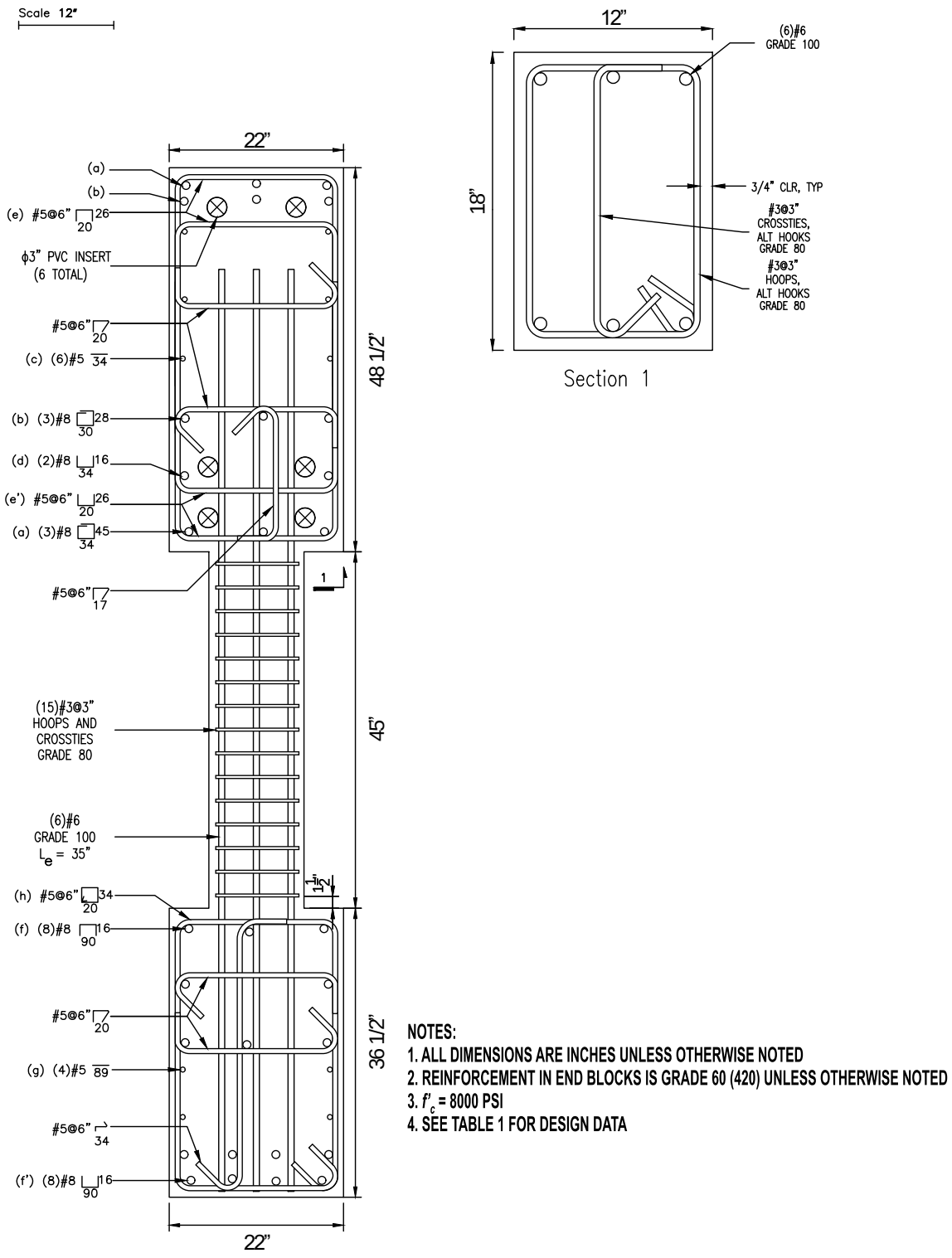

Figure 23 – Reinforcement details of P100-2.5 (1 in. = 25.4 mm, 1 ksi = 1,000 psi = 6.89 MPa)

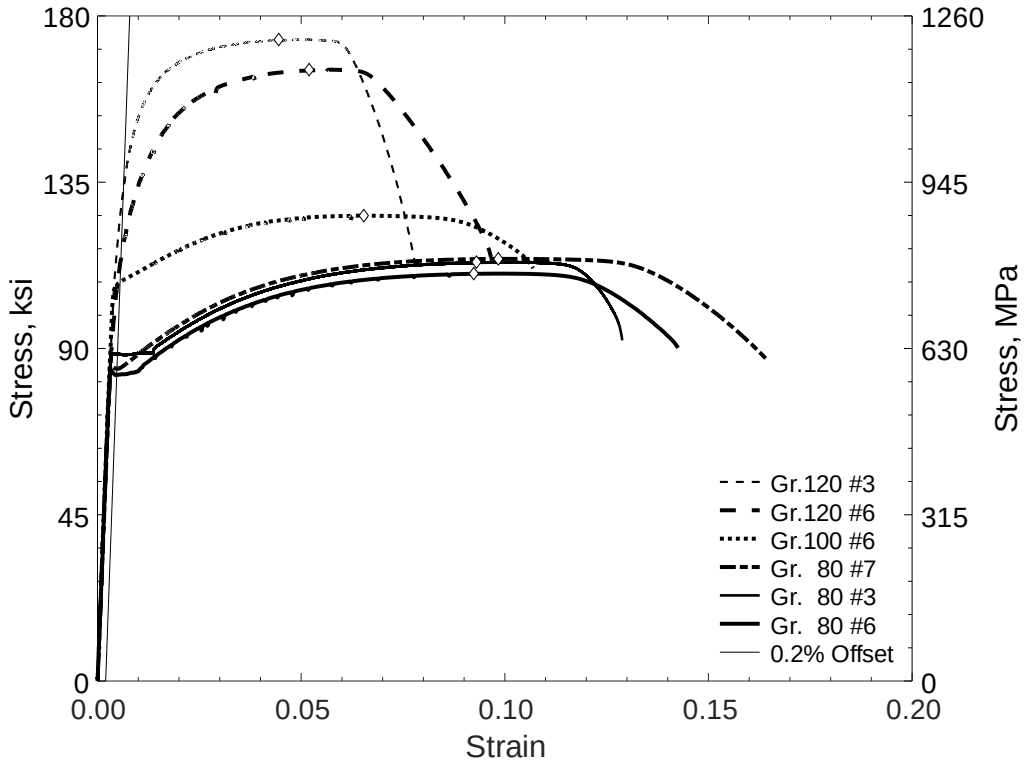

Figure 24 – Measured stress versus strain for reinforcement

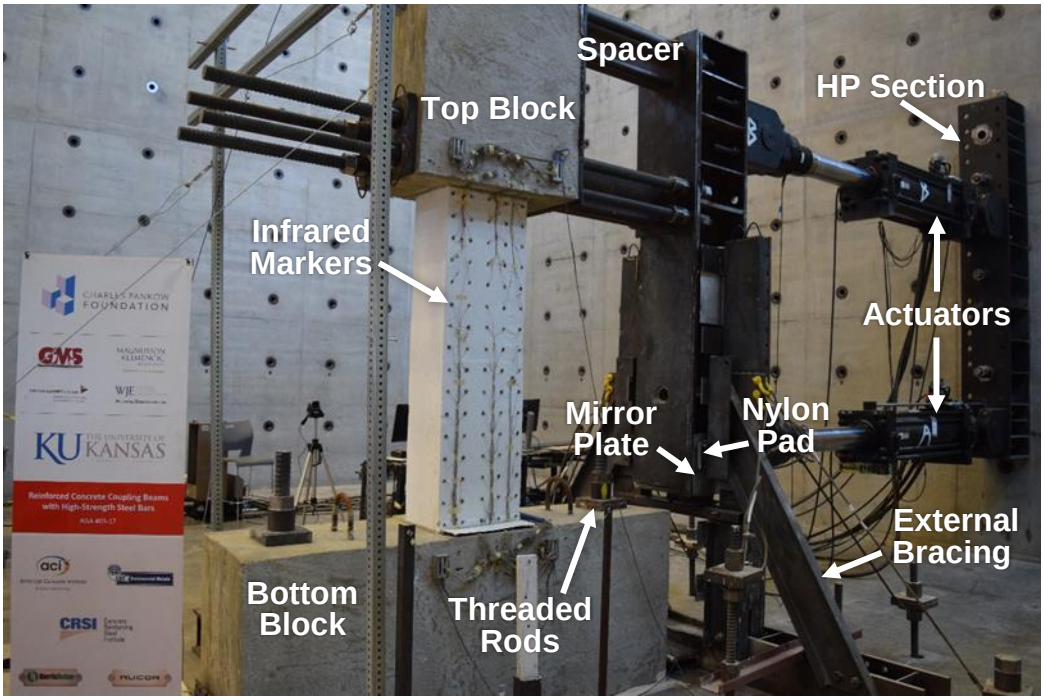

Figure 25 – Test setup, view from northeast

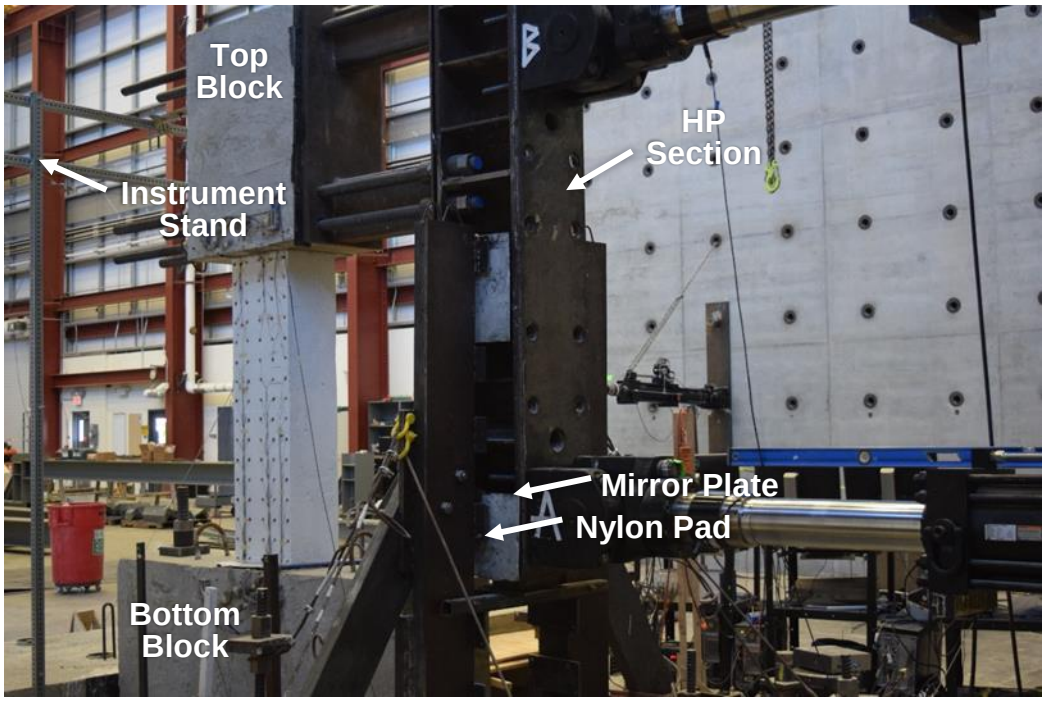

Figure 26 – Test setup, view from northwest

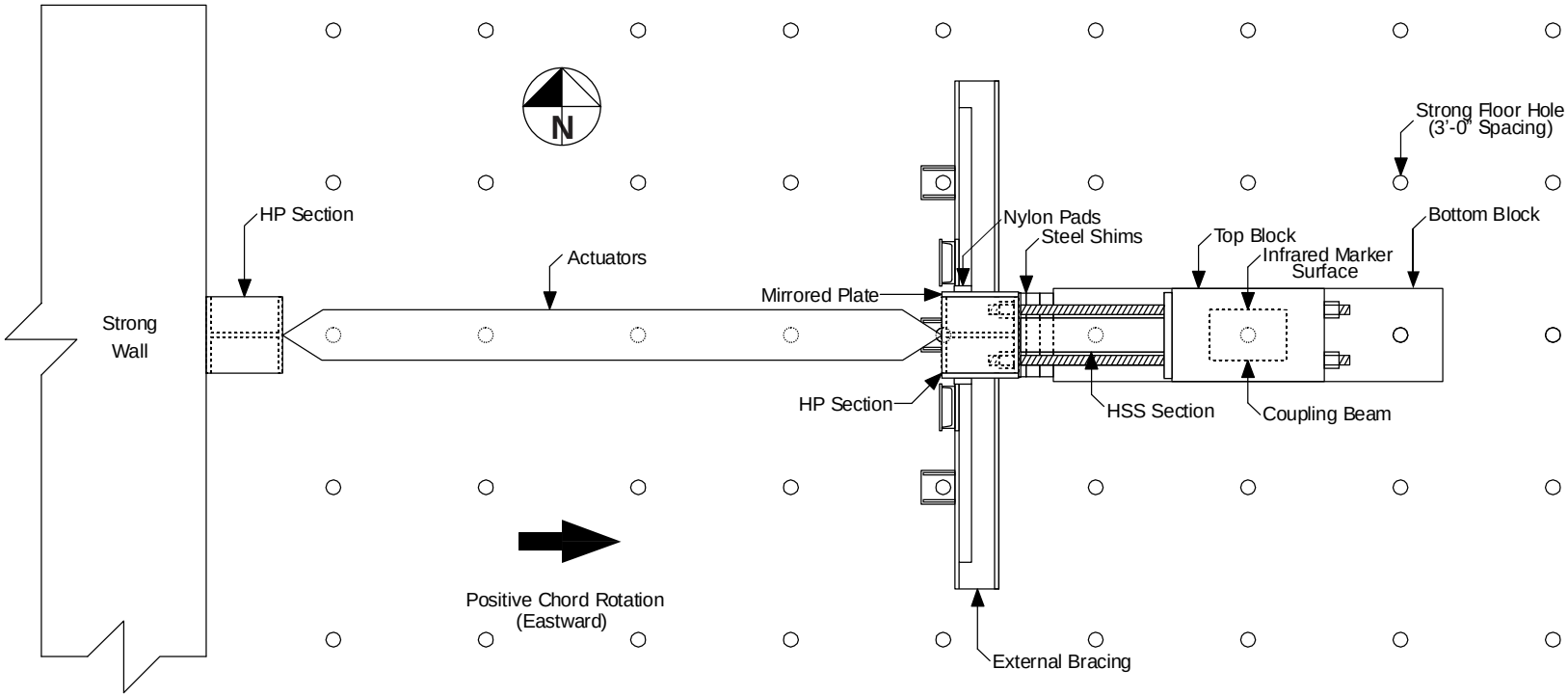

Figure 27 – Test setup, plan view

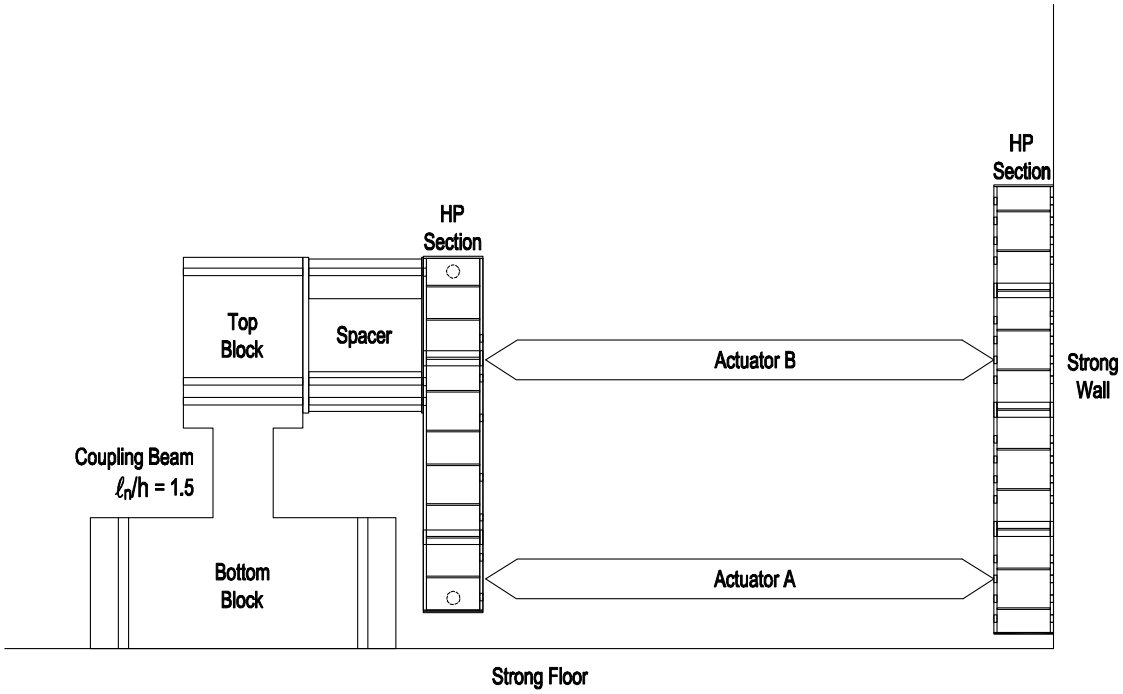

Figure 28 – Test setup for coupling beams with aspect ratio of 1.5[a]

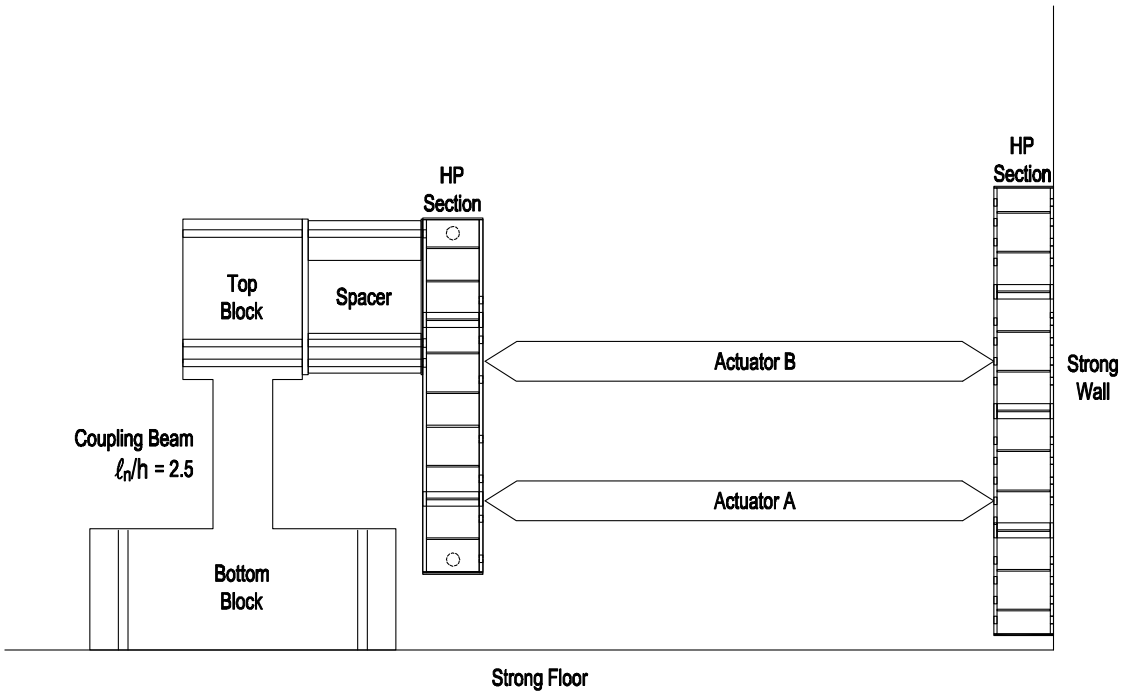

Figure 29 – Test setup for coupling beams with aspect ratio of 2.5[a]

[a] External bracing omitted for clarity. Actuator and coupling beam elevations in Table 4.

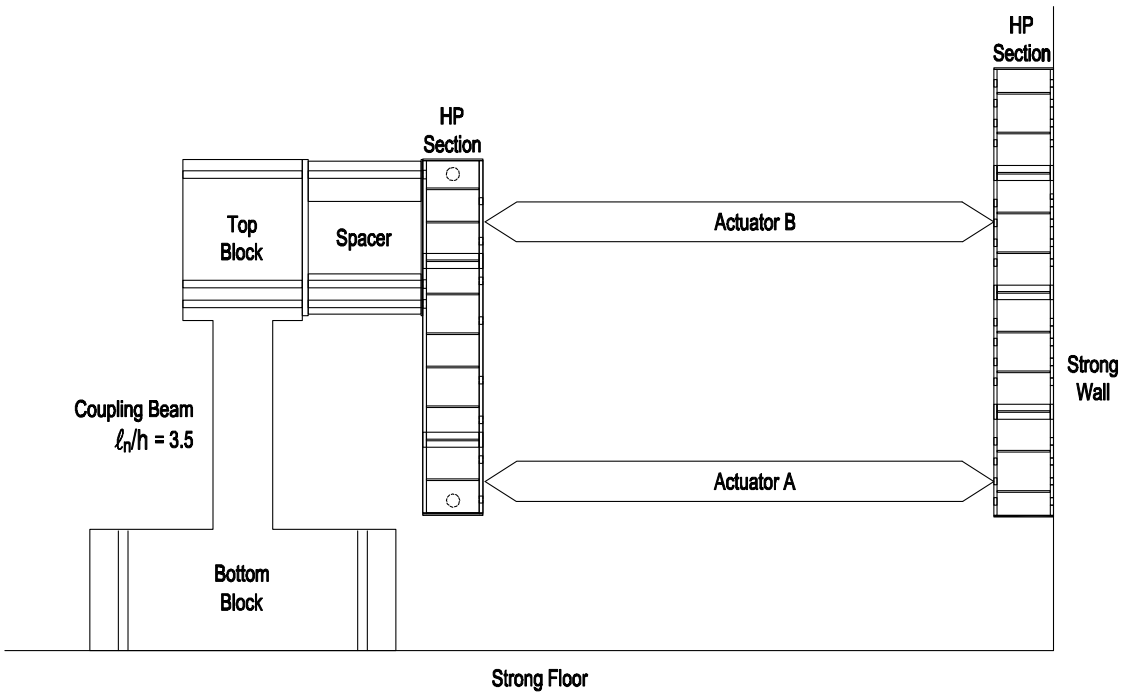

Figure 30 – Test setup for coupling beams with aspect ratio of 3.5[a]

[a] External bracing omitted for clarity. Actuator and coupling beam elevations in Table 4.

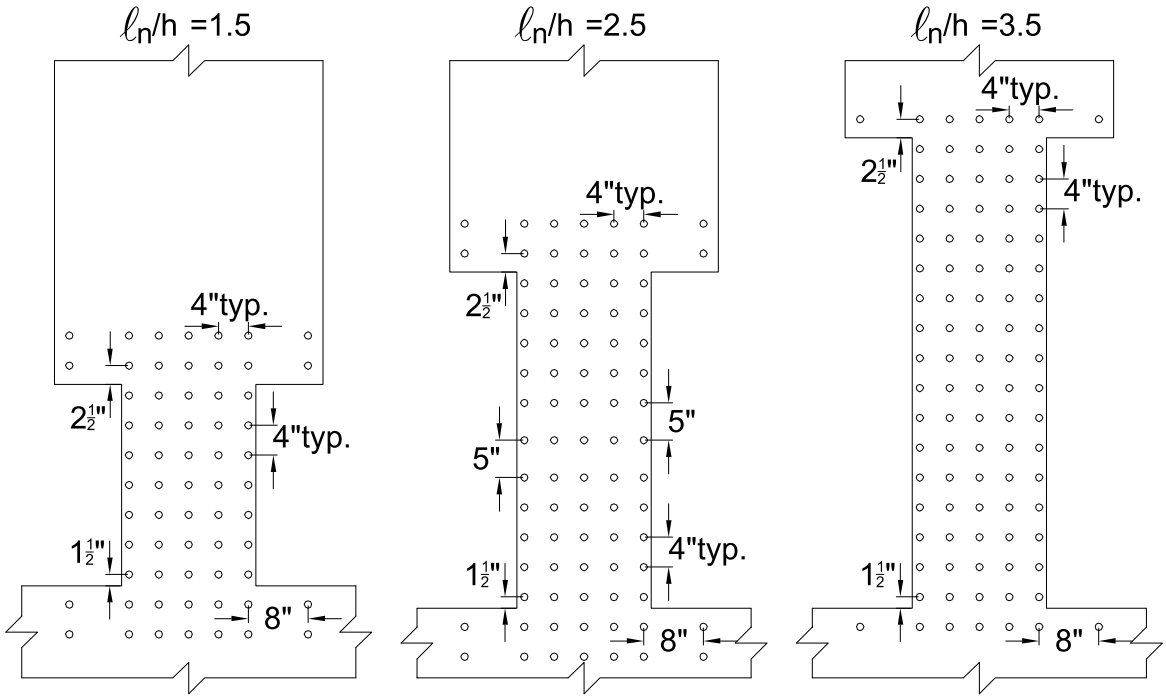

Figure 31 – Infrared marker positions (1 in. = 25.4 mm)

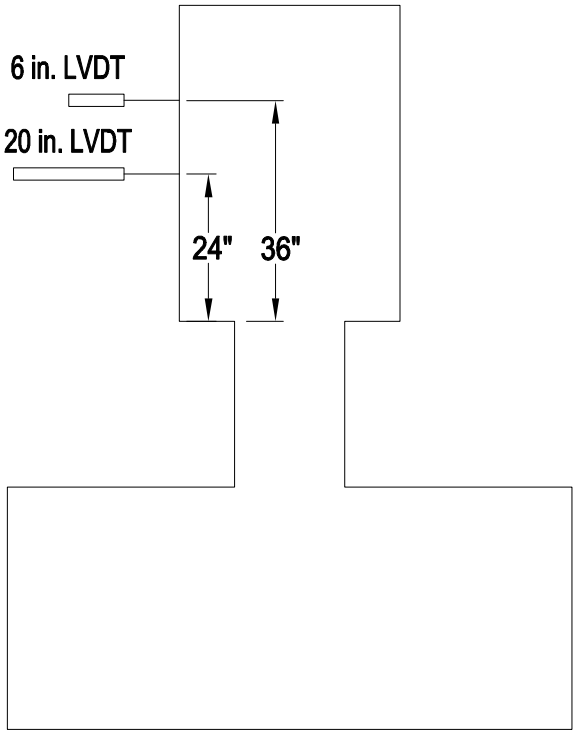

Figure 32 – LVDT locations (1 in. = 25.4 mm)

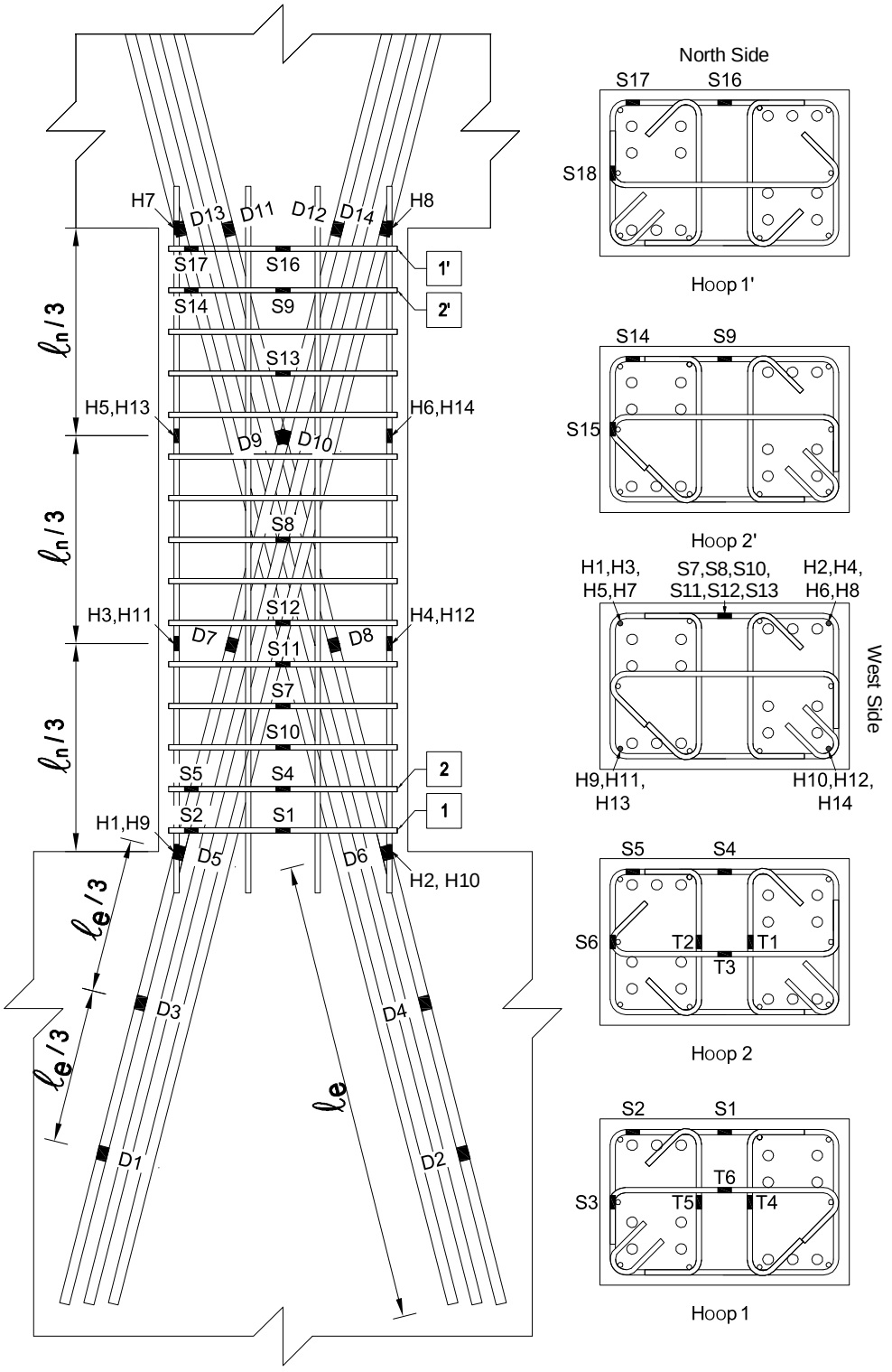

Figure 33 – Strain gauge layout (view from north), D-type specimens

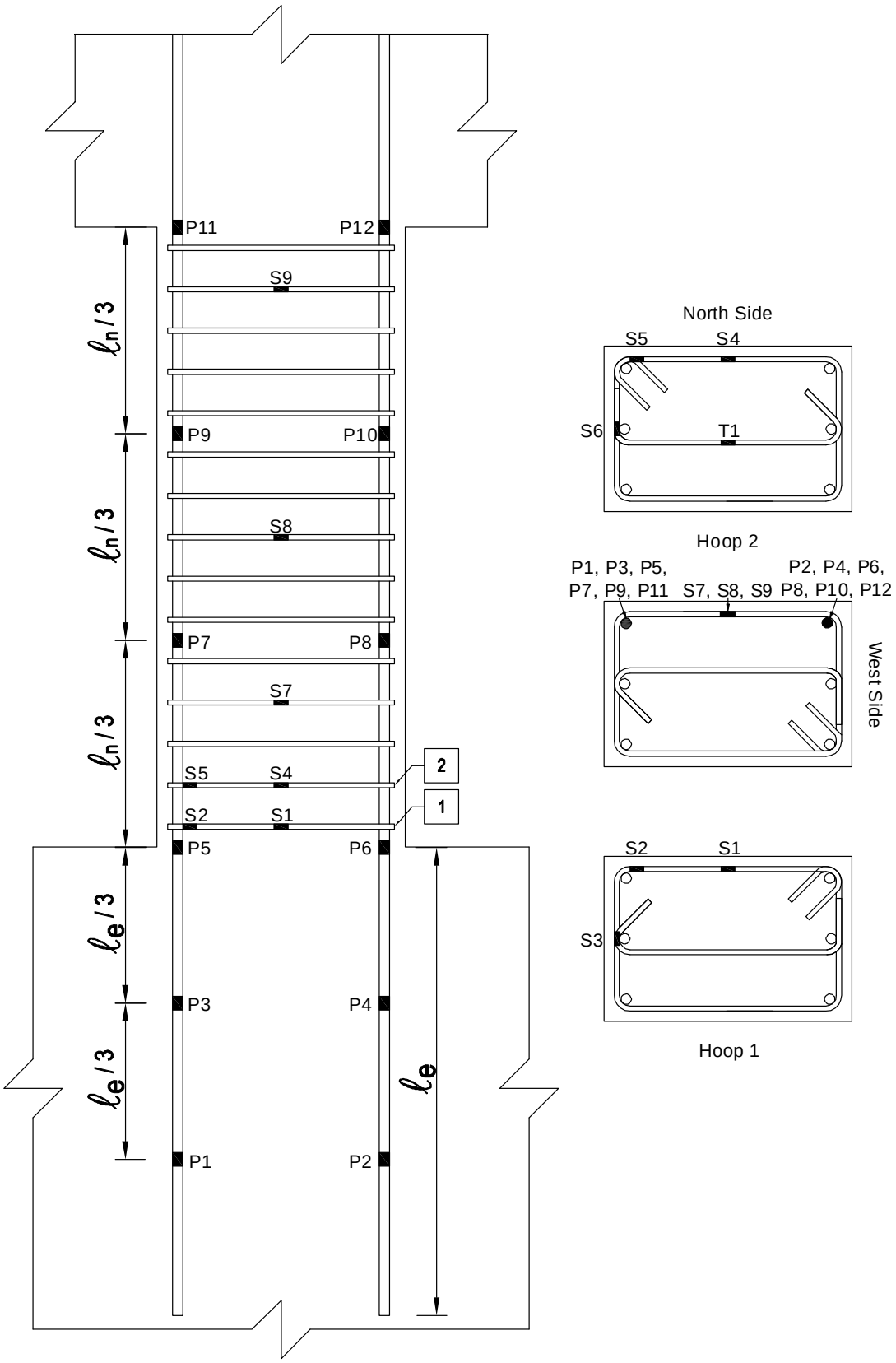

Figure 34 – Strain gauge layout (view from north), P-type specimens

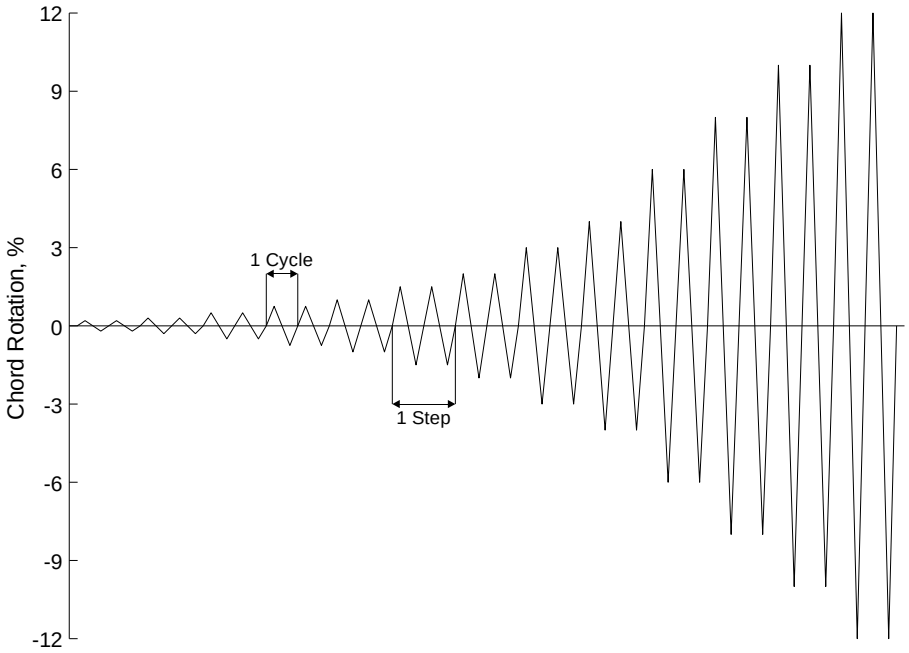

Figure 35 – Loading protocol[a]

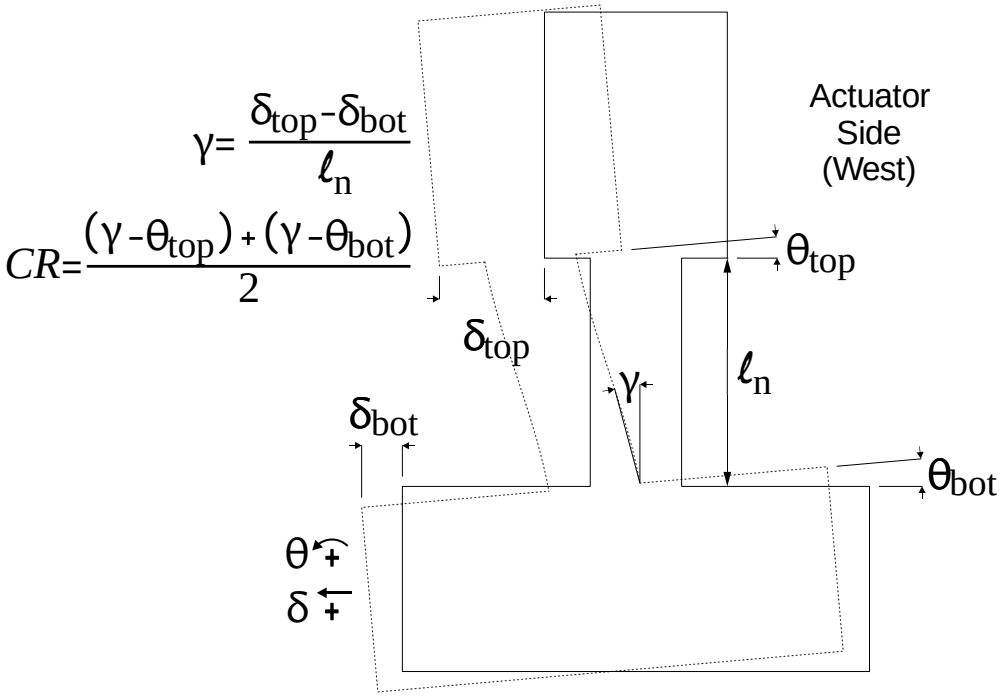

Figure 36 – General deformed shape of specimen, view from north[b]

[a] Values listed in Table 7.

[b] Positive displacement corresponds to actuator extension toward laboratory east.

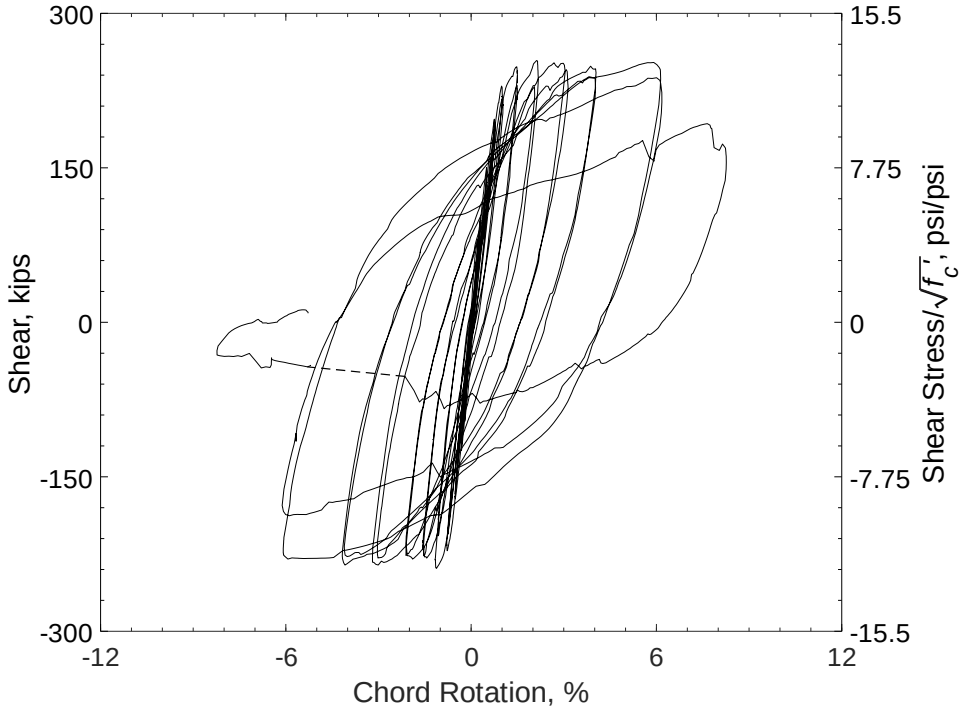

Figure 37 – Shear versus chord rotation for D80-1.5
(1,000 psi = 6.89 MPa, 1 kip = 4.45 kN)

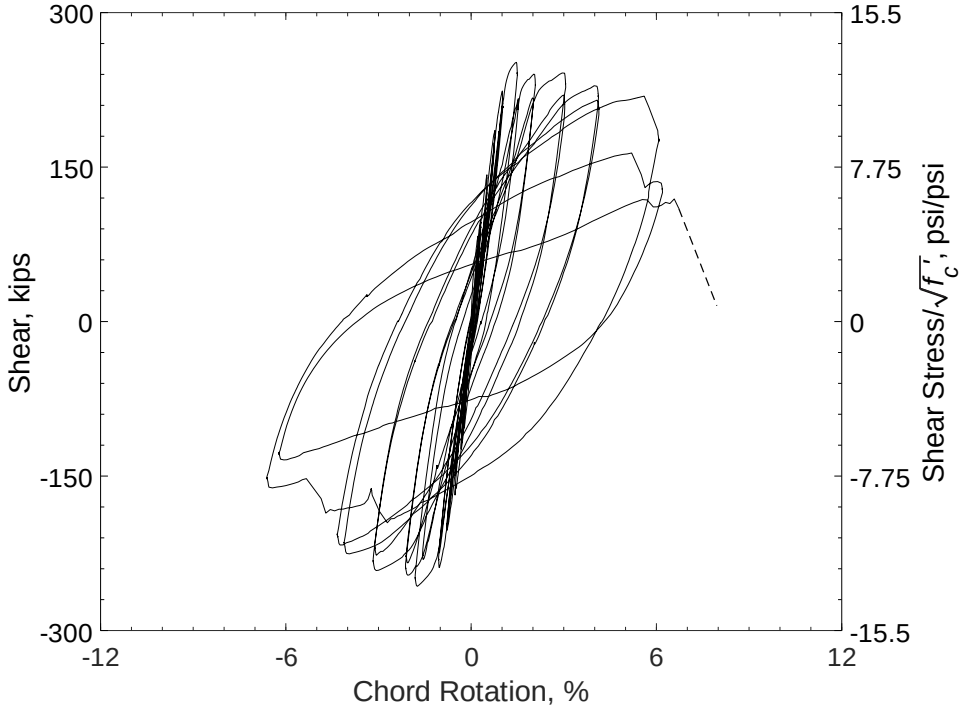

Figure 38 – Shear versus chord rotation for D100-1.5
(1,000 psi = 6.89 MPa, 1 kip = 4.45 kN)

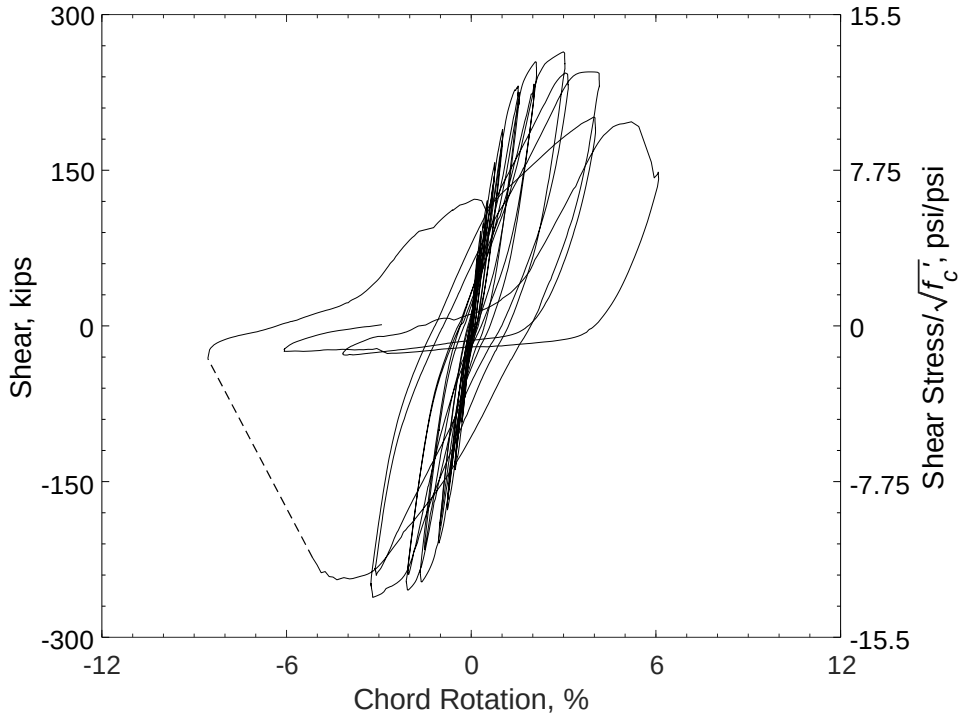

Figure 39 – Shear versus chord rotation for D120-1.5
(1,000 psi = 6.89 MPa, 1 kip = 4.45 kN)

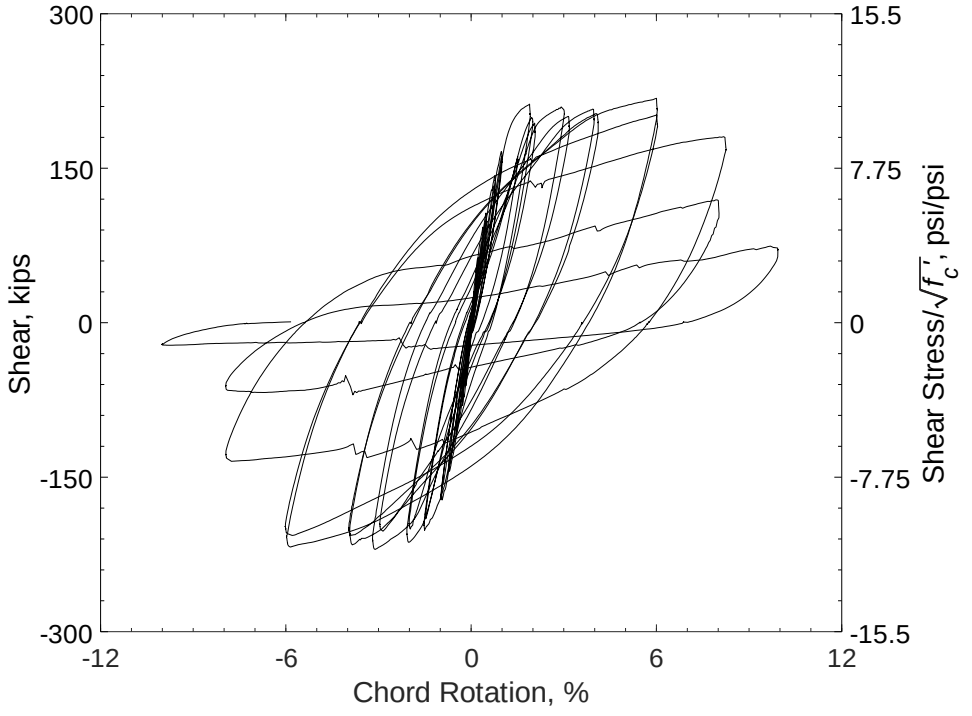

Figure 40 – Shear versus chord rotation for D80-2.5
(1,000 psi = 6.89 MPa, 1 kip = 4.45 kN)

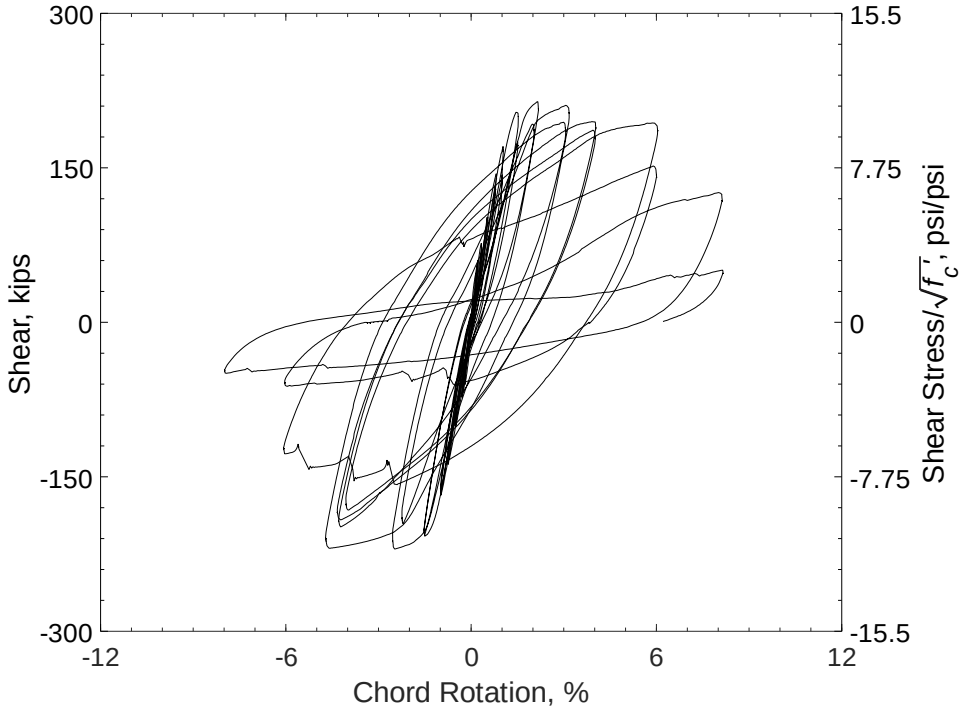

Figure 41 – Shear versus chord rotation for D100-2.5
(1,000 psi = 6.89 MPa, 1 kip = 4.45 kN)

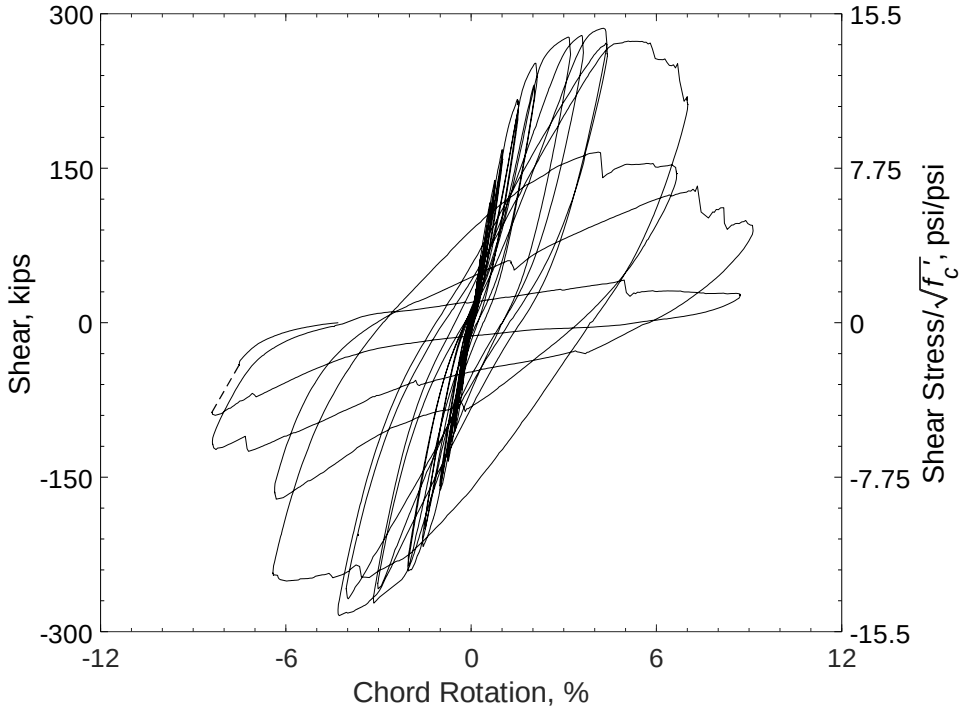

Figure 42 – Shear versus chord rotation for D120-2.5
(1,000 psi = 6.89 MPa, 1 kip = 4.45 kN)

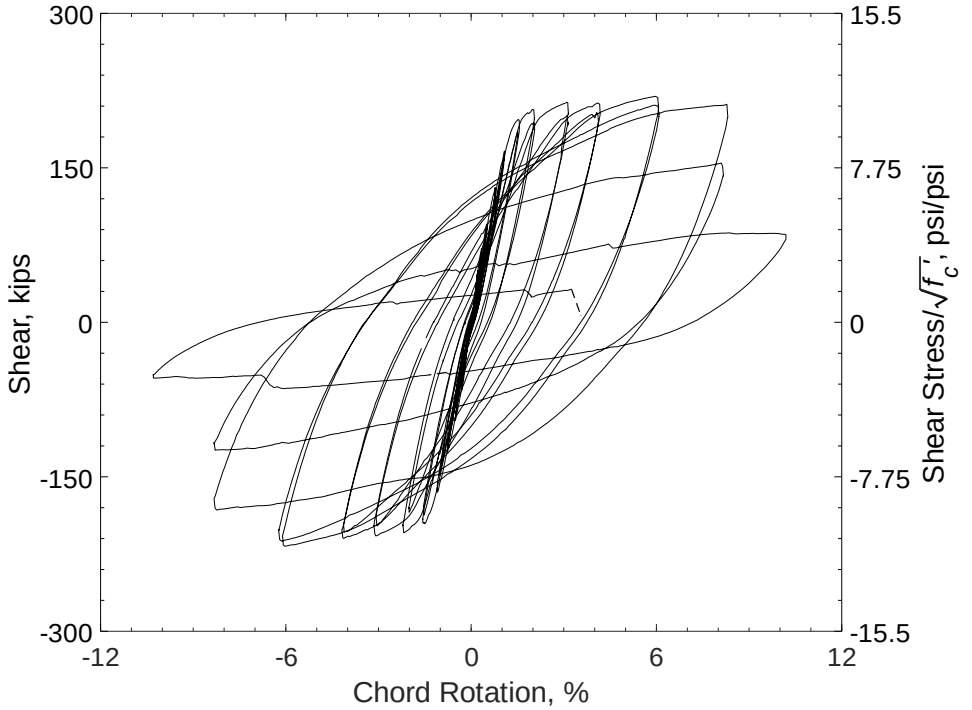

Figure 43 – Shear versus chord rotation for D80-3.5
(1,000 psi = 6.89 MPa, 1 kip = 4.45 kN)

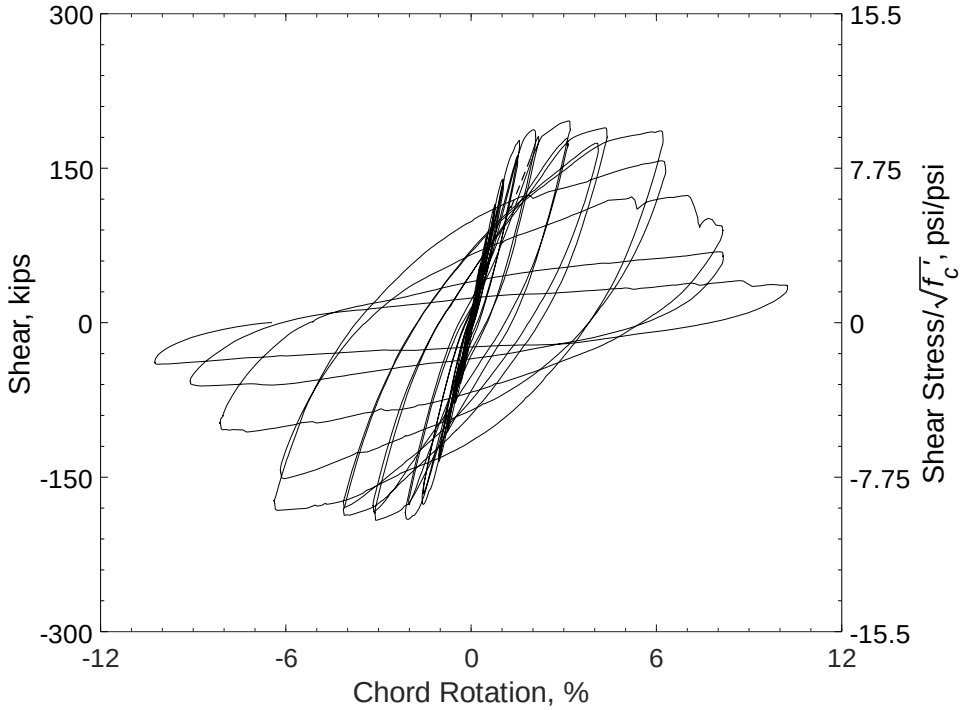

Figure 44 – Shear versus chord rotation for D100-3.5
(1,000 psi = 6.89 MPa, 1 kip = 4.45 kN)

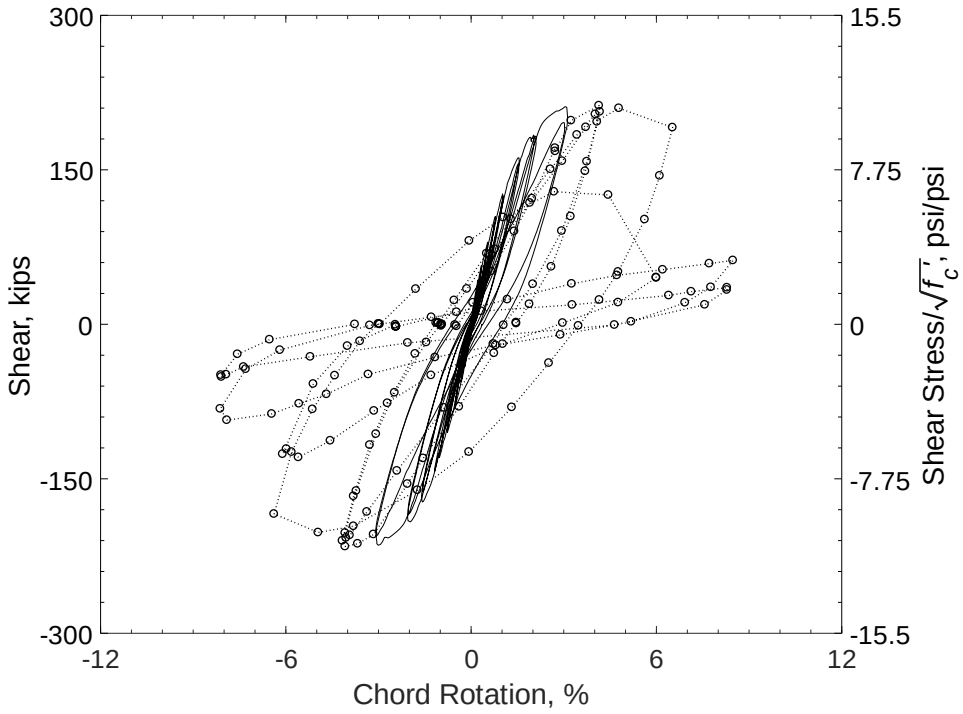

Figure 45 – Shear versus chord rotation for D120-3.5
(1,000 psi = 6.89 MPa, 1 kip = 4.45 kN)

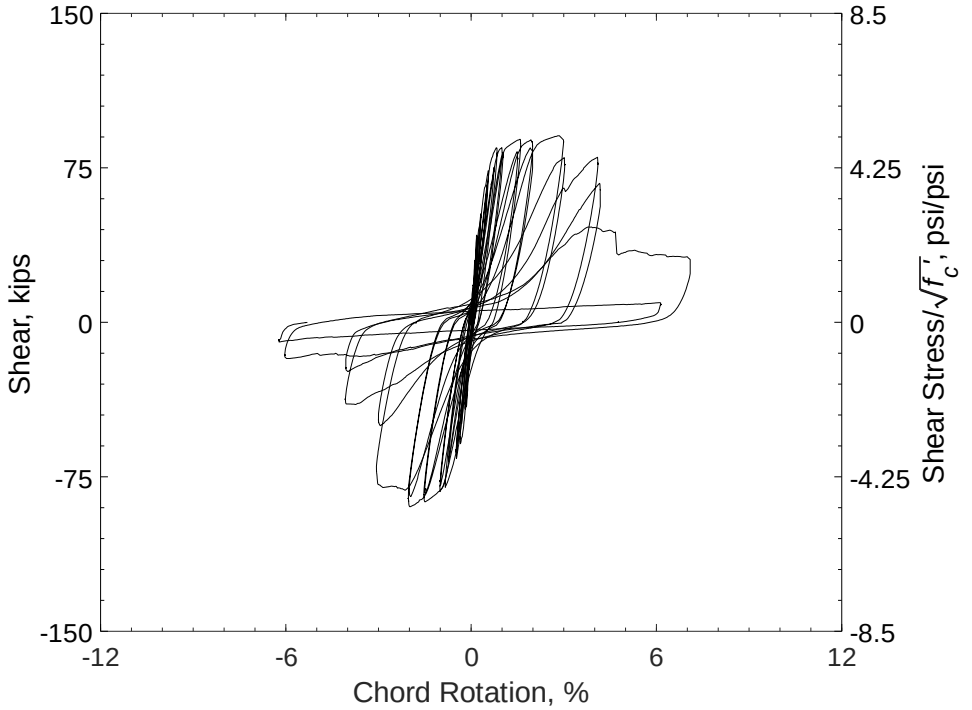

Figure 46 – Shear versus chord rotation for P80-2.5
(1,000 psi = 6.89 MPa, 1 kip = 4.45 kN)

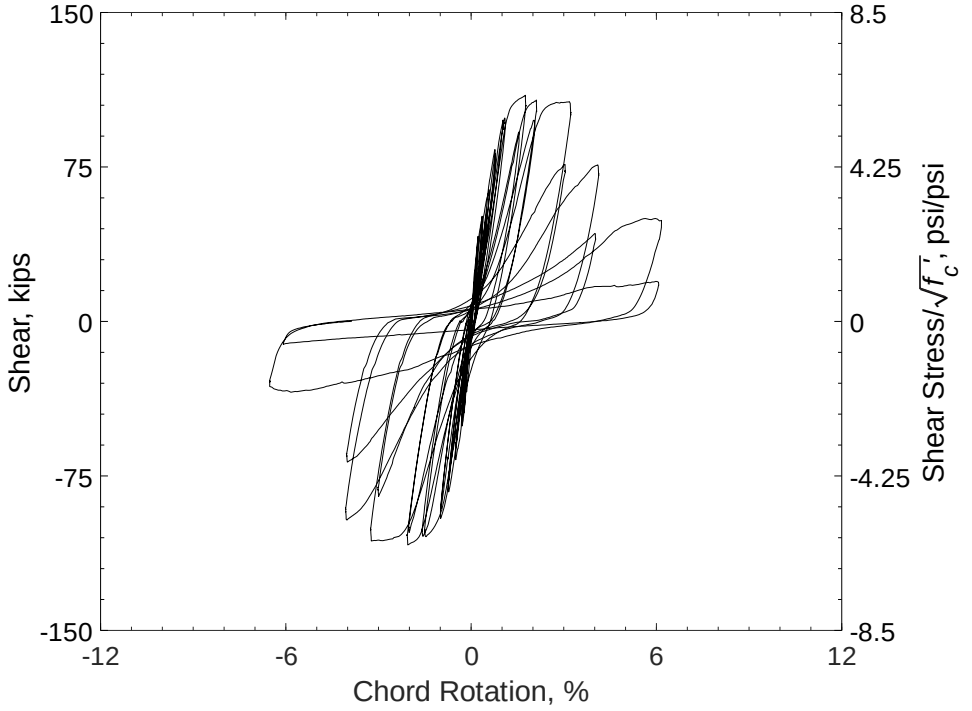

Figure 47 – Shear versus chord rotation for P100-2.5
(1,000 psi = 6.89 MPa, 1 kip = 4.45 kN)

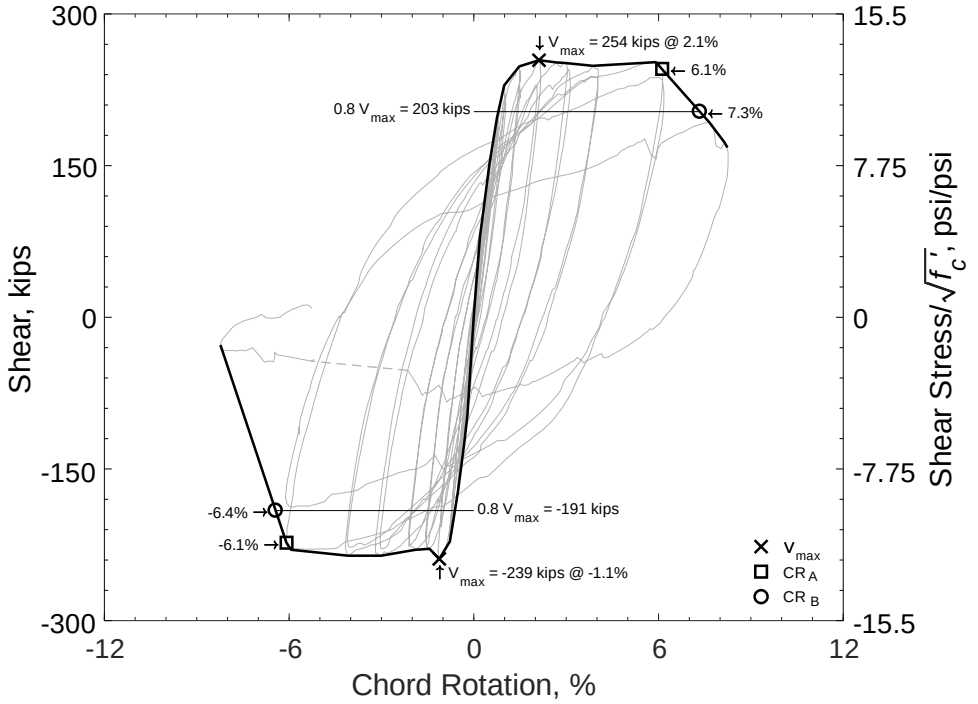

Figure 48 – Shear versus chord rotation envelope for D80-1.5
(1,000 psi = 6.89 MPa, 1 kip = 4.45 kN)

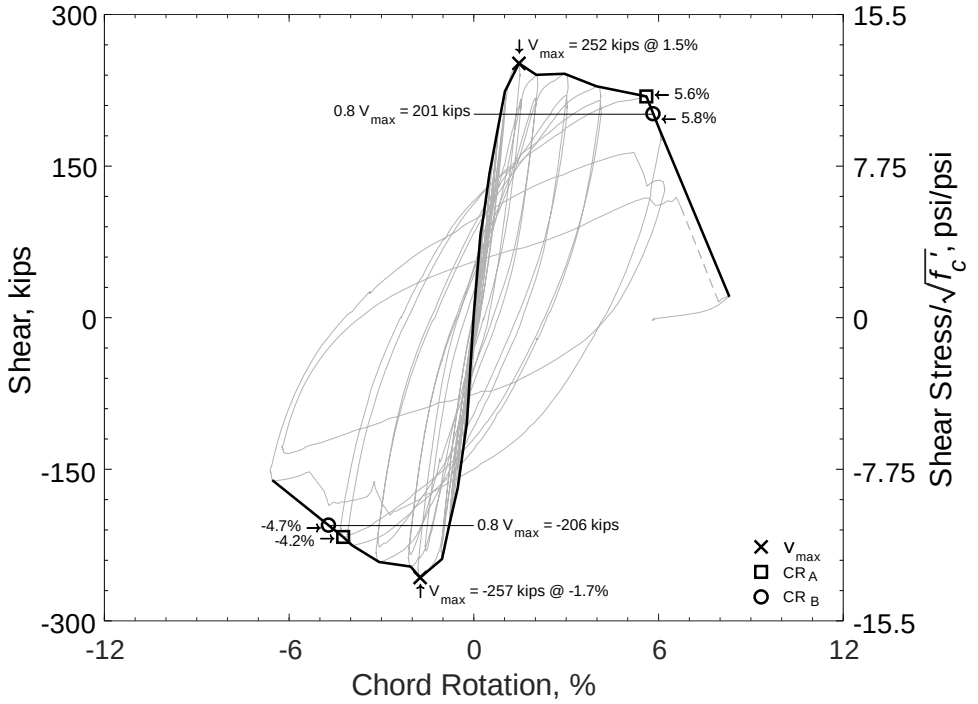

Figure 49 – Shear versus chord rotation envelope for D100-1.5
(1,000 psi = 6.89 MPa, 1 kip = 4.45 kN)

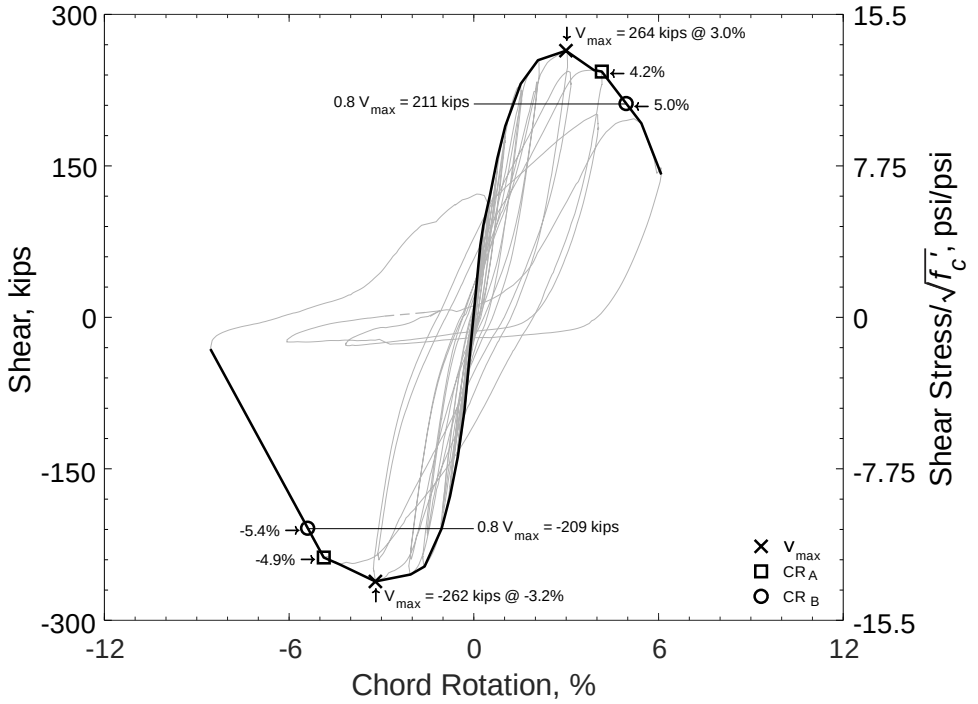

Figure 50 – Shear versus chord rotation envelope for D120-1.5
(1,000 psi = 6.89 MPa, 1 kip = 4.45 kN)

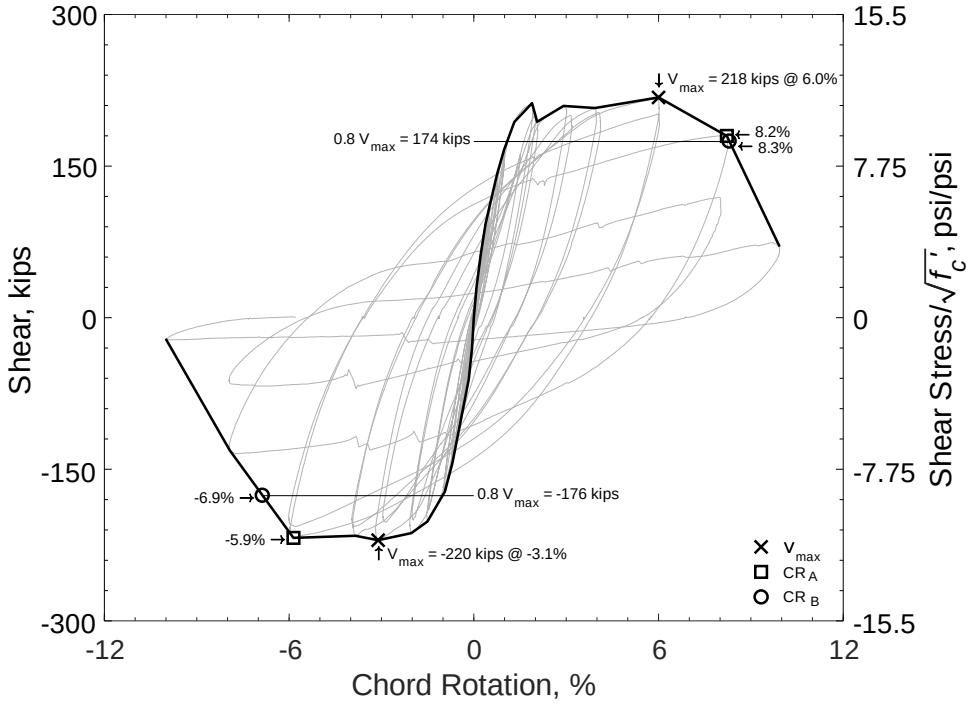

Figure 51 – Shear versus chord rotation envelope for D80-2.5
(1,000 psi = 6.89 MPa, 1 kip = 4.45 kN)

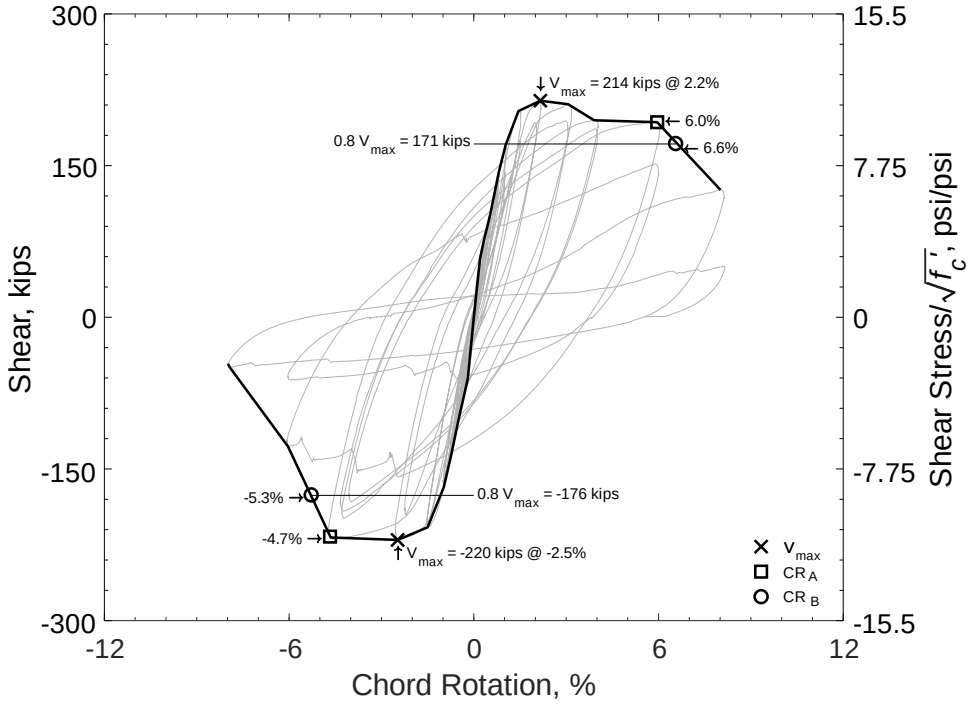

Figure 52 – Shear versus chord rotation envelope for D100-2.5
(1,000 psi = 6.89 MPa, 1 kip = 4.45 kN)

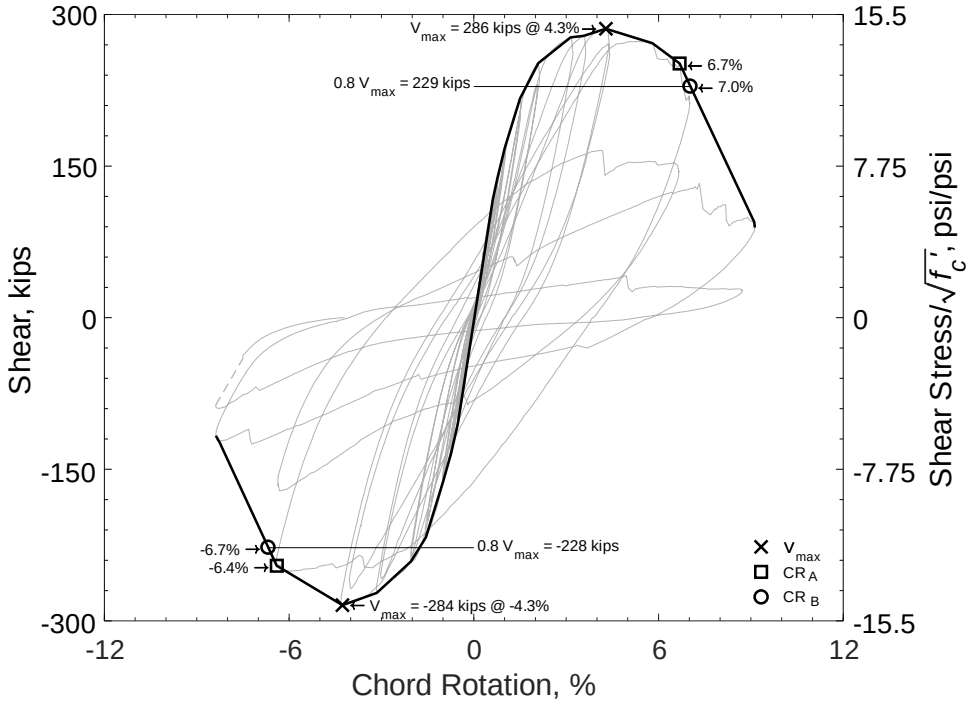

Figure 53 – Shear versus chord rotation envelope for D120-2.5
(1,000 psi = 6.89 MPa, 1 kip = 4.45 kN)

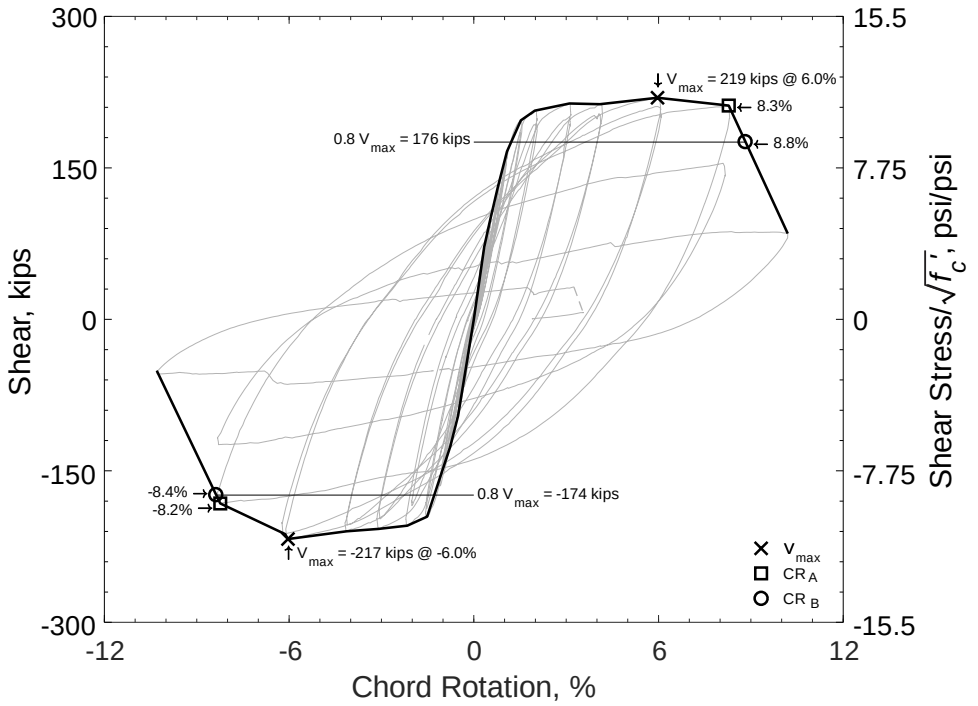

Figure 54 – Shear versus chord rotation envelope for D80-3.5
(1,000 psi = 6.89 MPa, 1 kip = 4.45 kN)

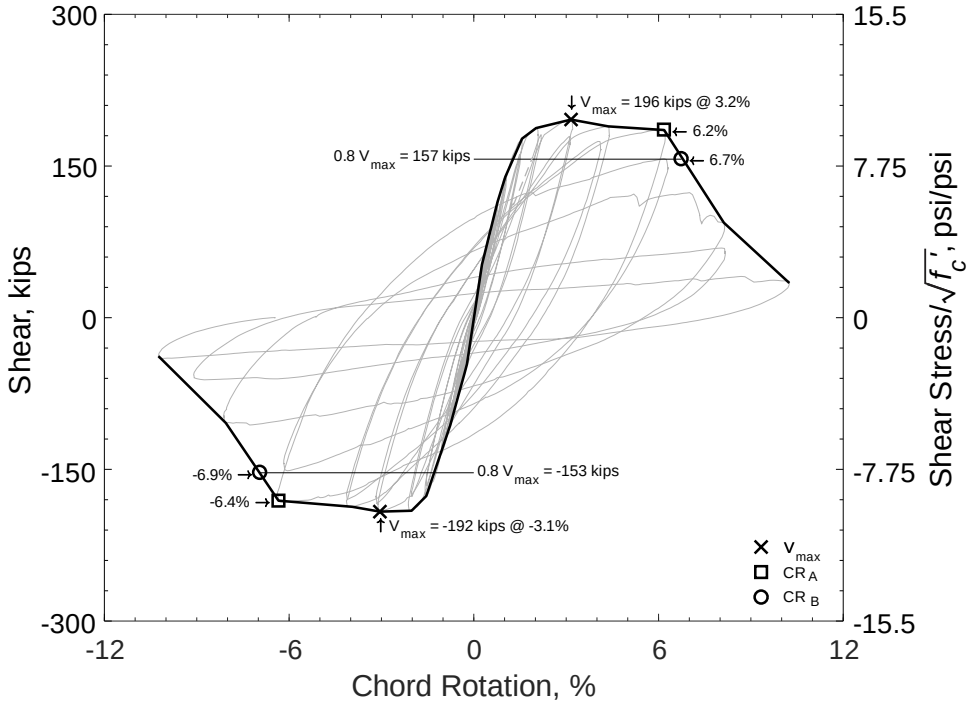

Figure 55 – Shear versus chord rotation envelope for D100-3.5
(1,000 psi = 6.89 MPa, 1 kip = 4.45 kN)

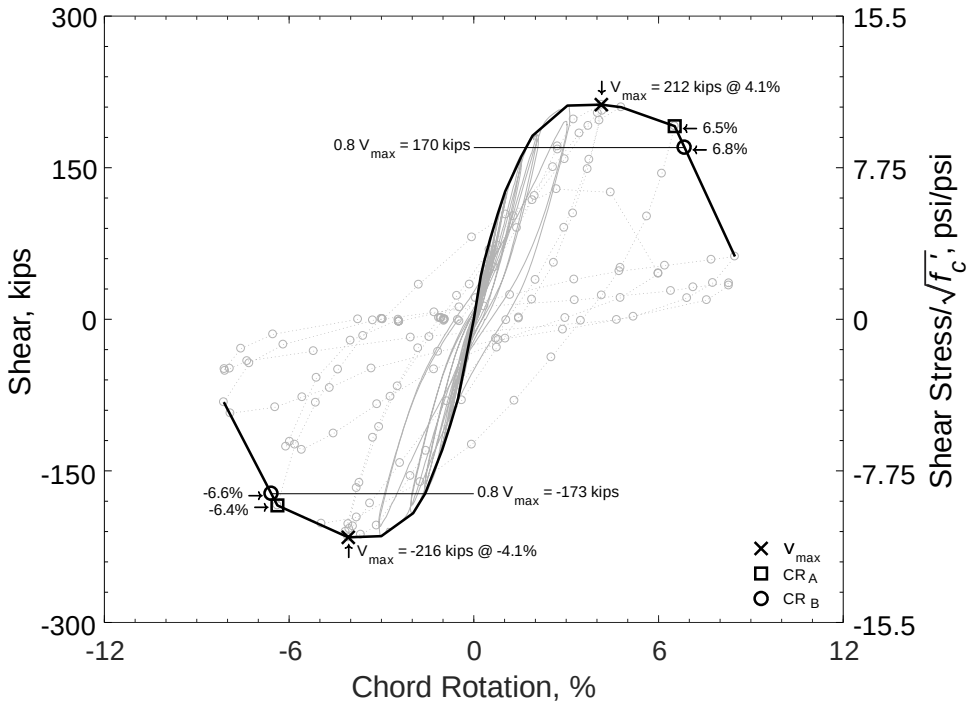

Figure 56 – Shear versus chord rotation envelope for D120-3.5
(1,000 psi = 6.89 MPa, 1 kip = 4.45 kN)

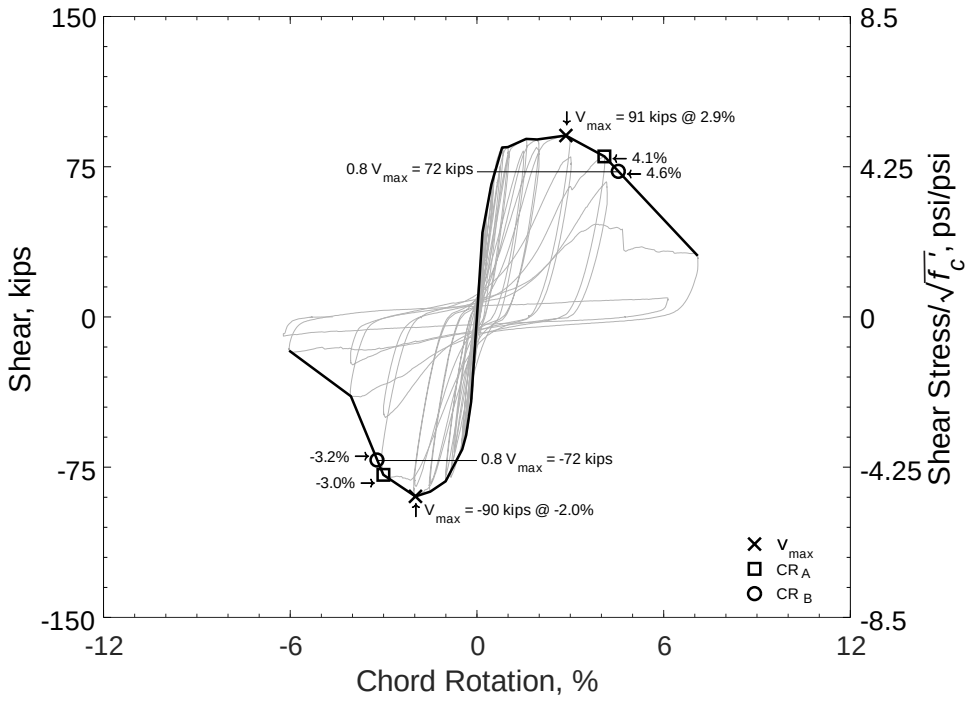

Figure 57 – Shear versus chord rotation envelope for P80-2.5
(1,000 psi = 6.89 MPa, 1 kip = 4.45 kN)

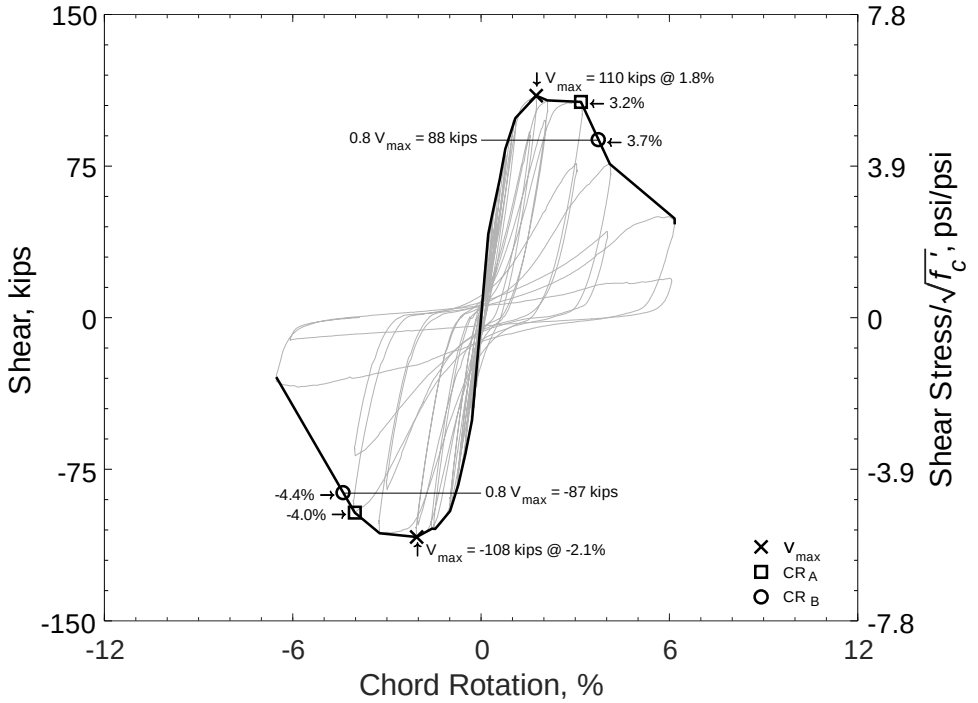

Figure 58 – Shear versus chord rotation envelope for P100-2.5
(1,000 psi = 6.89 MPa, 1 kip = 4.45 kN)

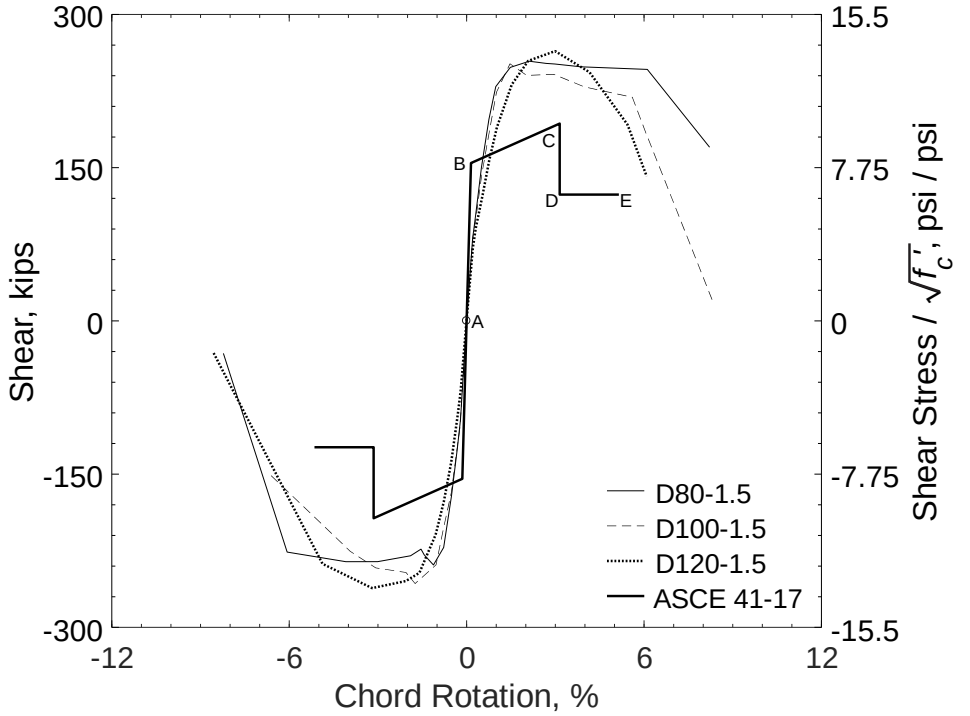

Figure 59 – Shear versus chord rotation envelopes for D80-1.5, D100-1.5, and D120-1.5 (1,000 psi = 6.89 MPa, 1 kip = 4.45 kN)

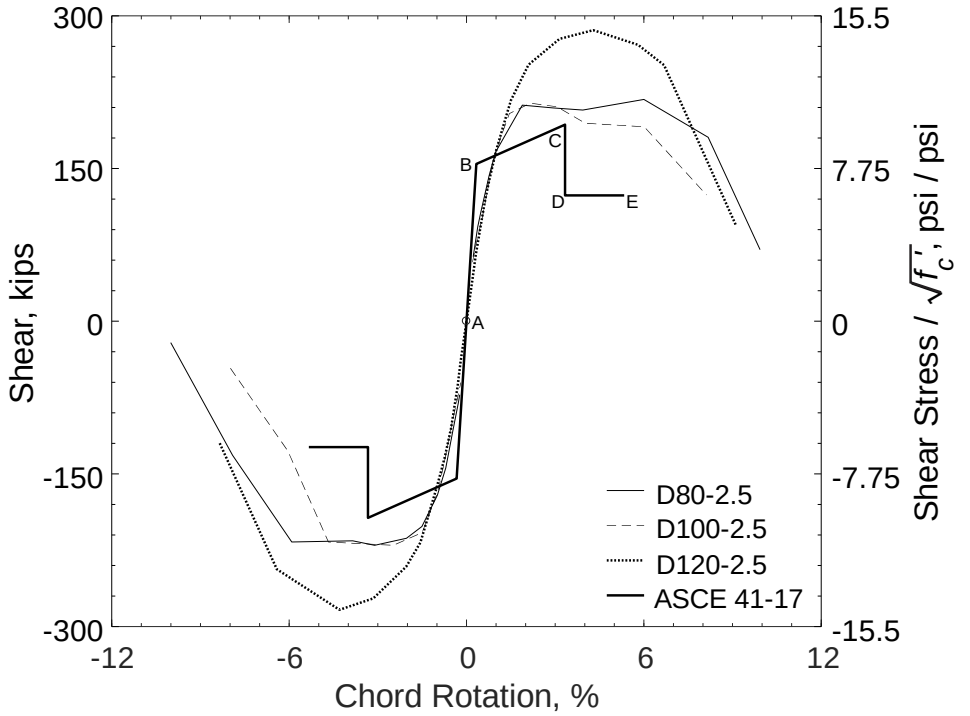

Figure 60 – Shear versus chord rotation envelopes for D80-2.5, D100-2.5, and D120-2.5 (1,000 psi = 6.89 MPa, 1 kip = 4.45 kN)

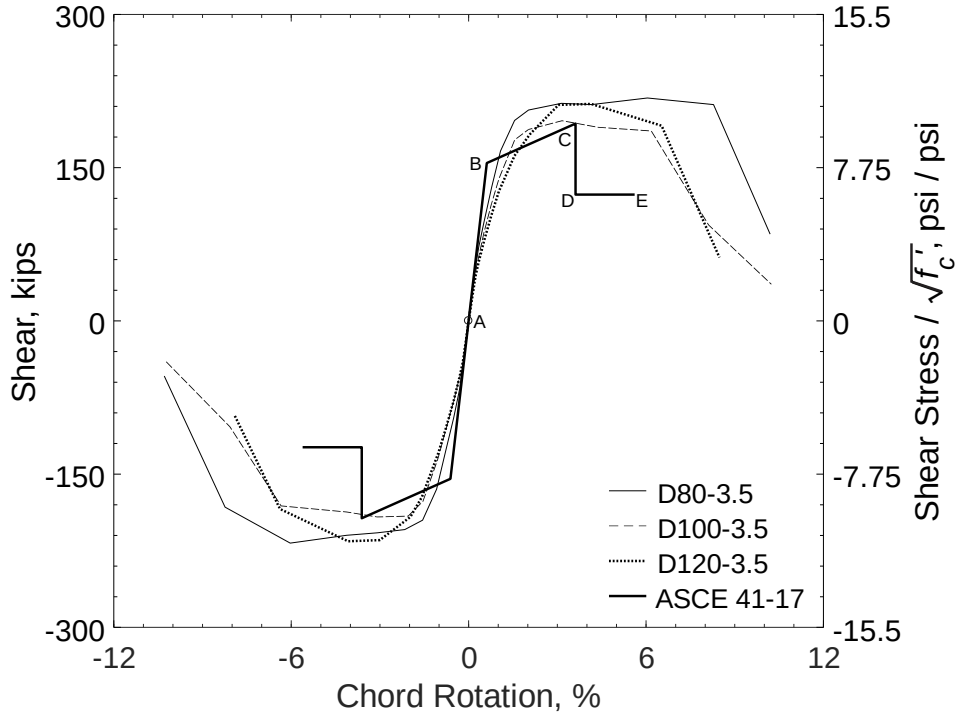

Figure 61 – Shear versus chord rotation envelopes for D80-3.5, D100-3.5, and D120-3.5
(1,000 psi = 6.89 MPa, 1 kip = 4.45 kN)

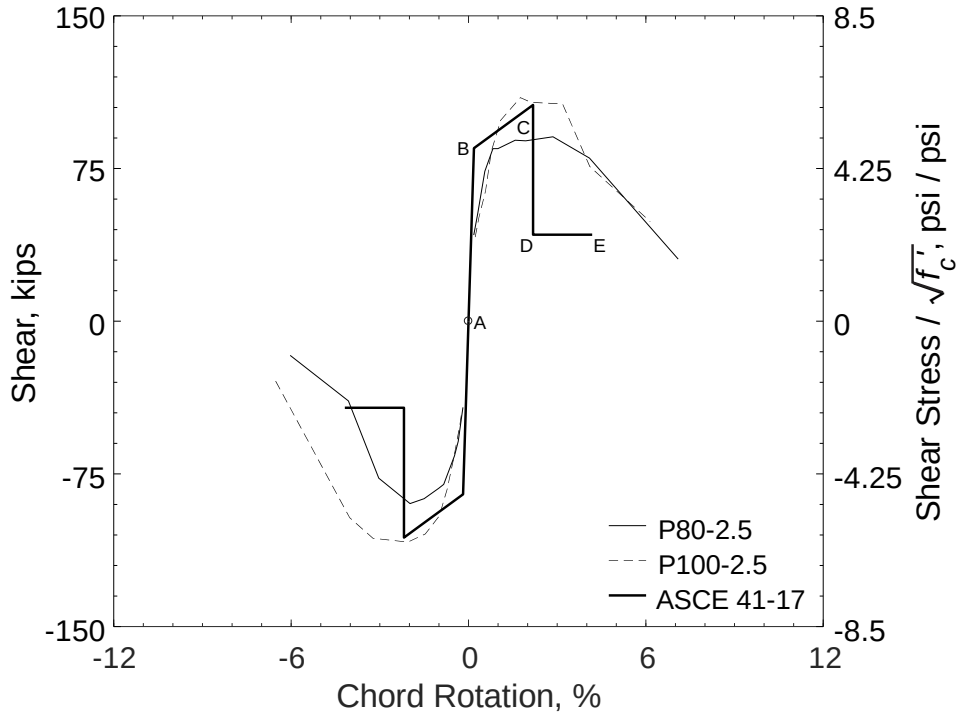

Figure 62 – Shear versus chord rotation envelopes for P80-2.5 and P100-2.5
(1,000 psi = 6.89 MPa, 1 kip = 4.45 kN)

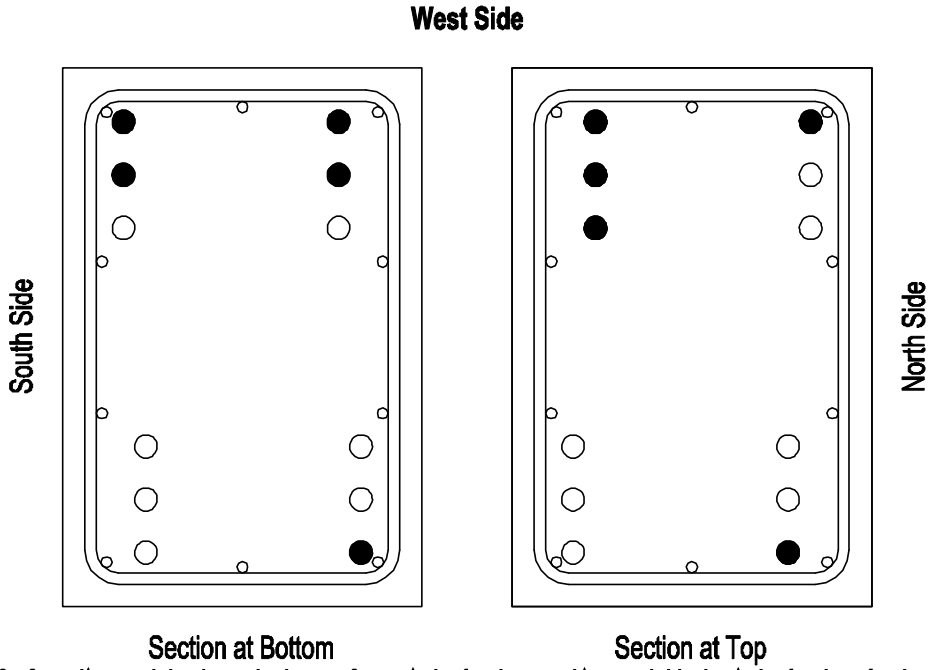

Figure 63 – Reinforcing bar fracture locations, D80-1.5

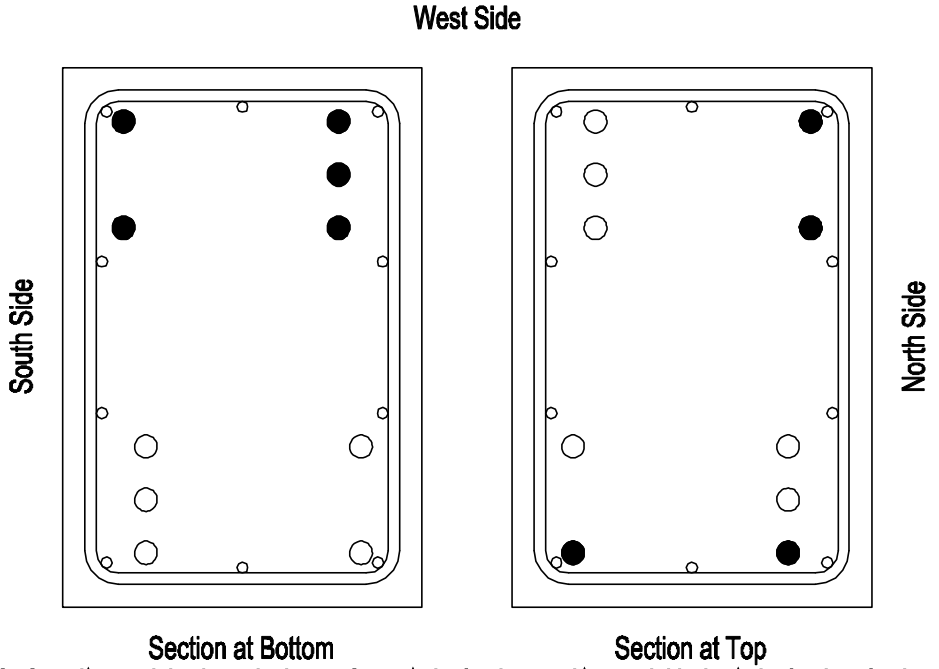

Figure 64 – Reinforcing bar fracture locations, D100-1.5

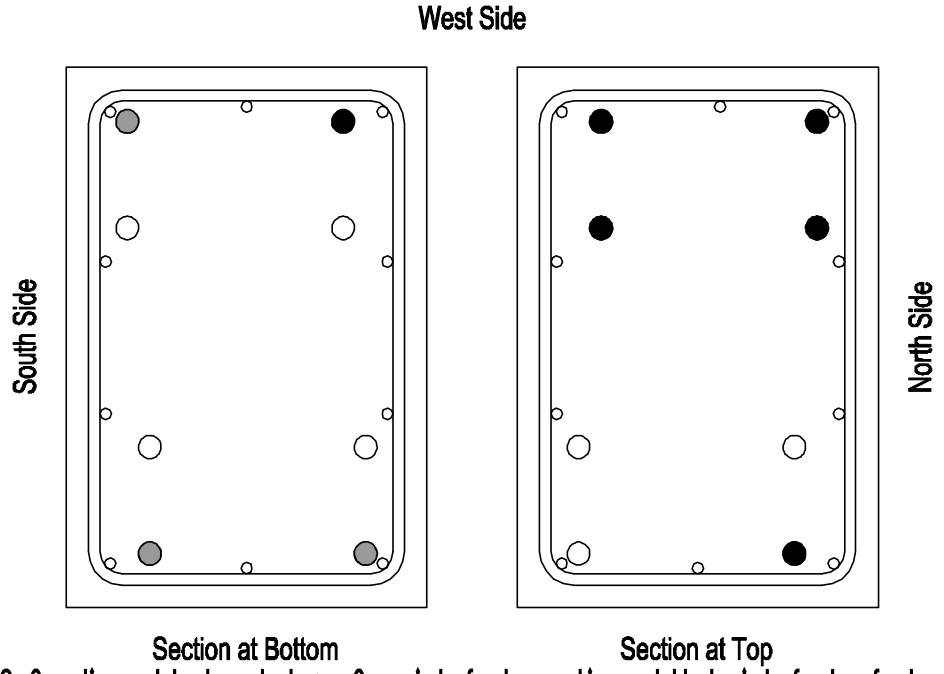

Figure 65 – Reinforcing bar fracture locations, D120-1.5

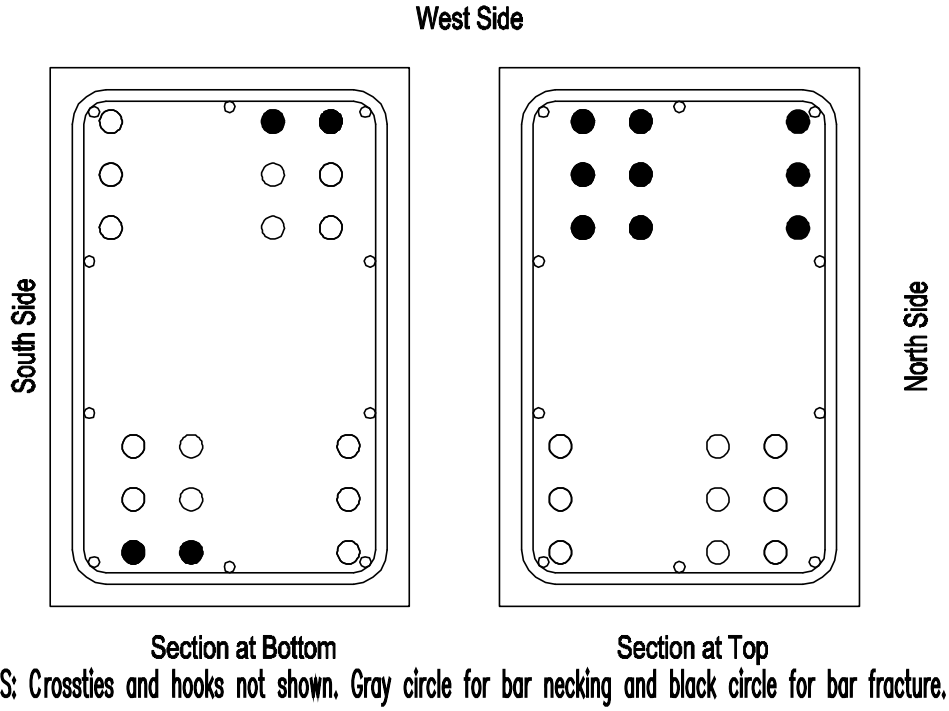

Figure 66 – Reinforcing bar fracture locations, D80-2.5

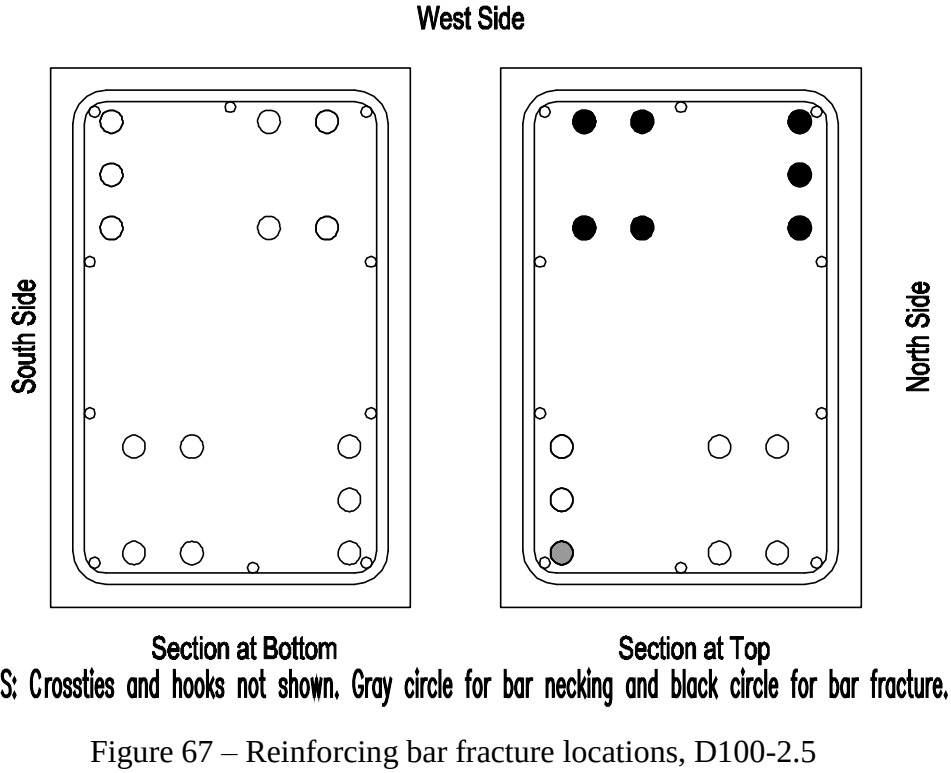

Figure 67 – Reinforcing bar fracture locations, D100-2.5

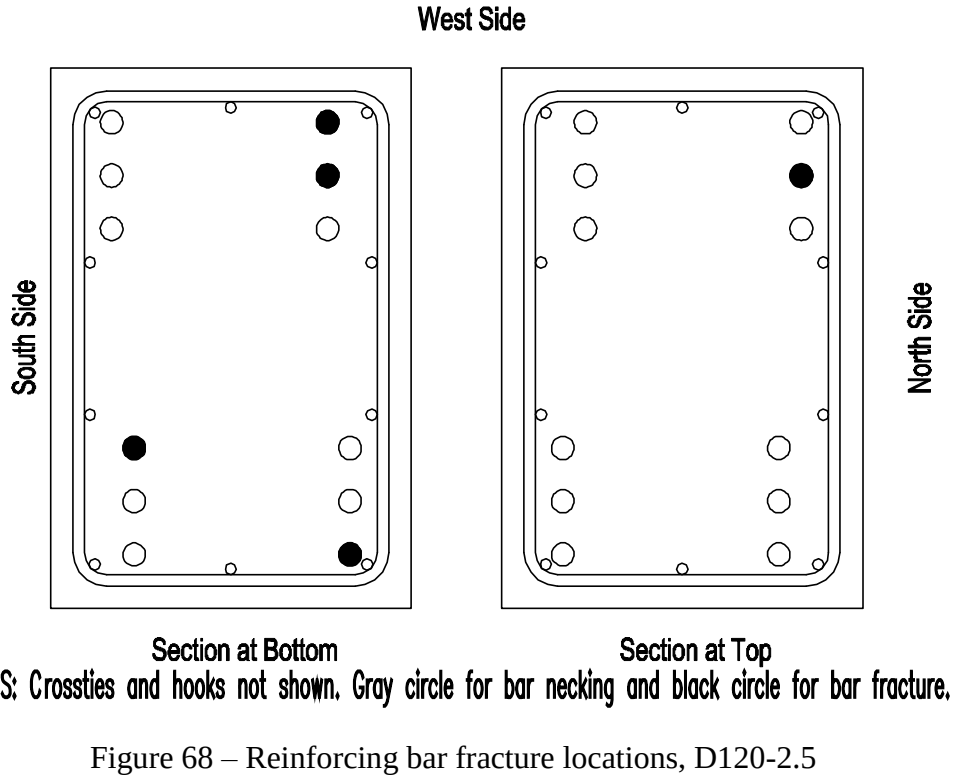

Figure 68 – Reinforcing bar fracture locations, D120-2.5

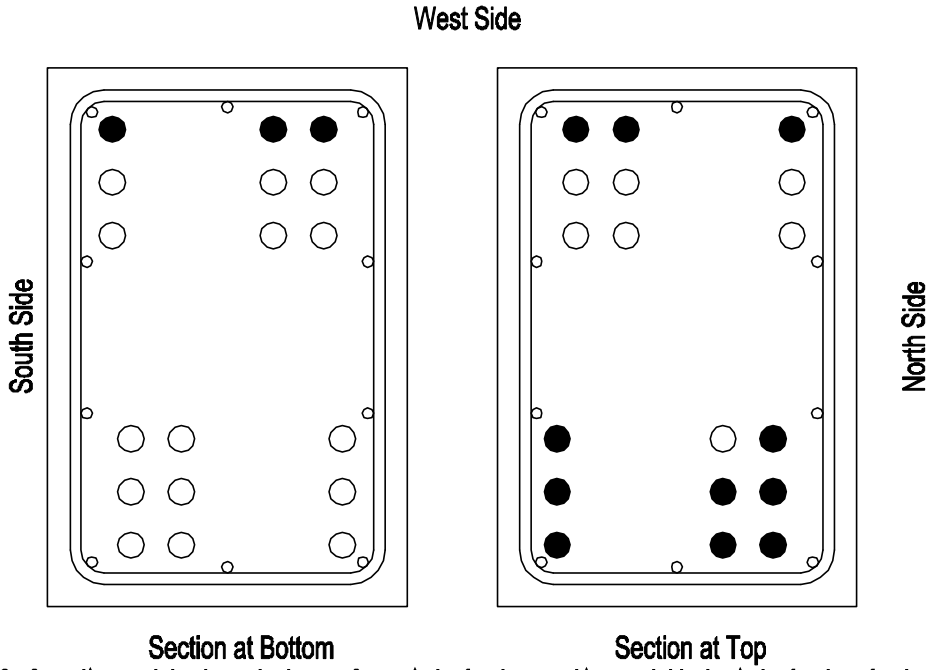

Figure 69 – Reinforcing bar fracture locations, D80-3.5

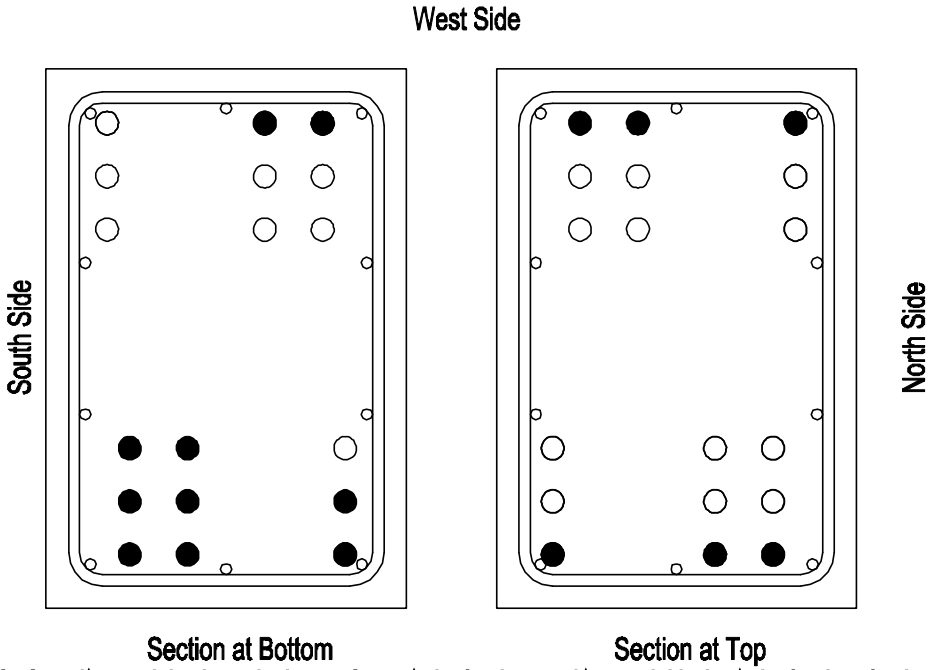

Figure 70 – Reinforcing bar fracture locations, D100-3.5

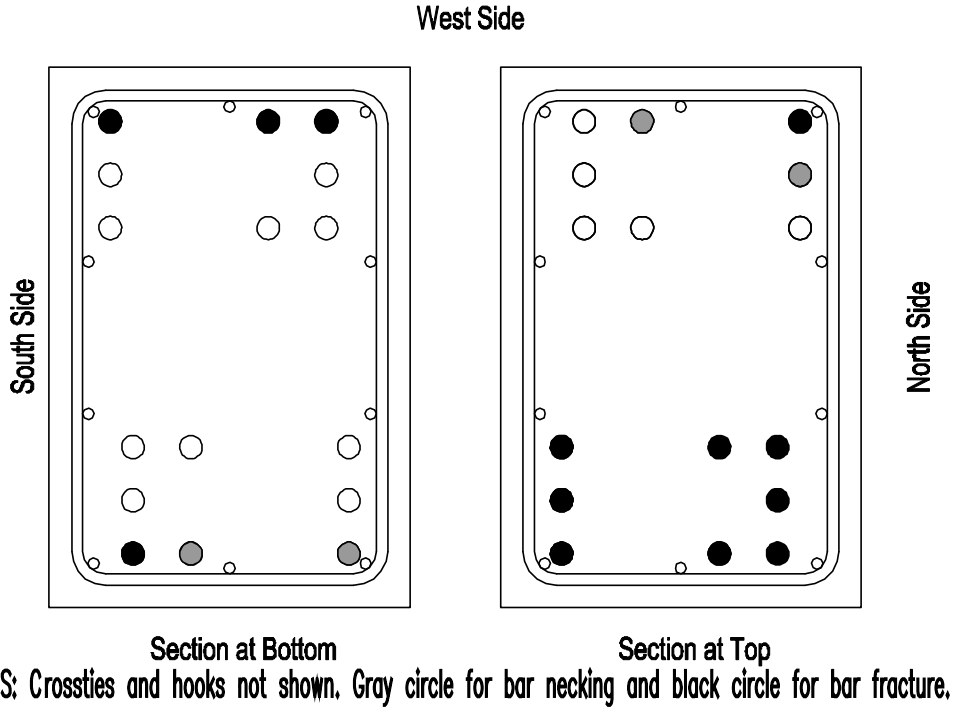

Figure 71 – Reinforcing bar fracture locations, D120-3.5

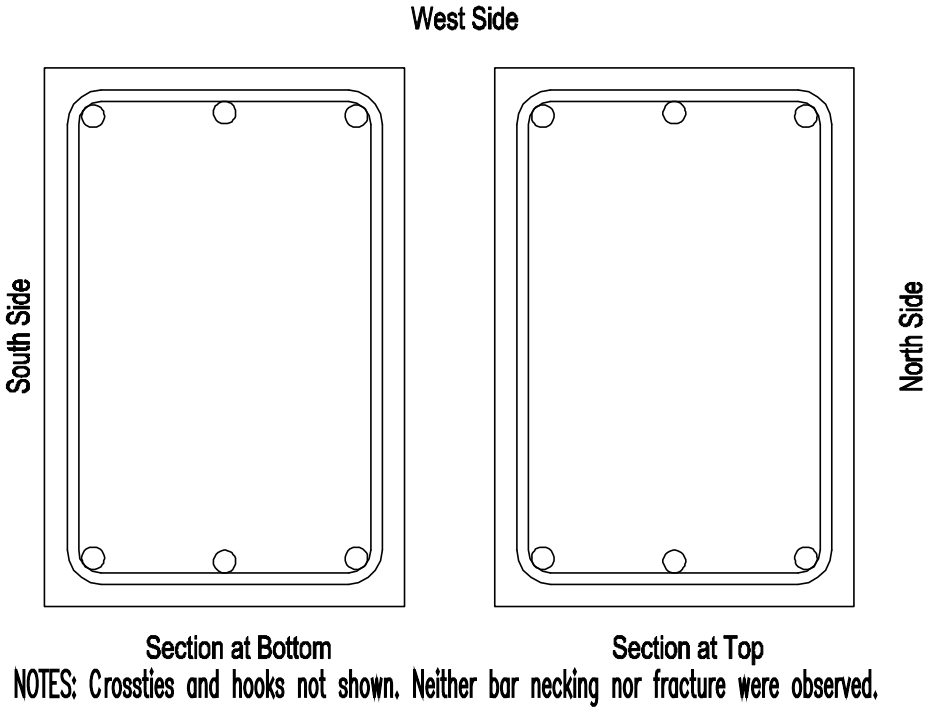

Figure 72 – Reinforcing bar fracture locations, P80-2.5

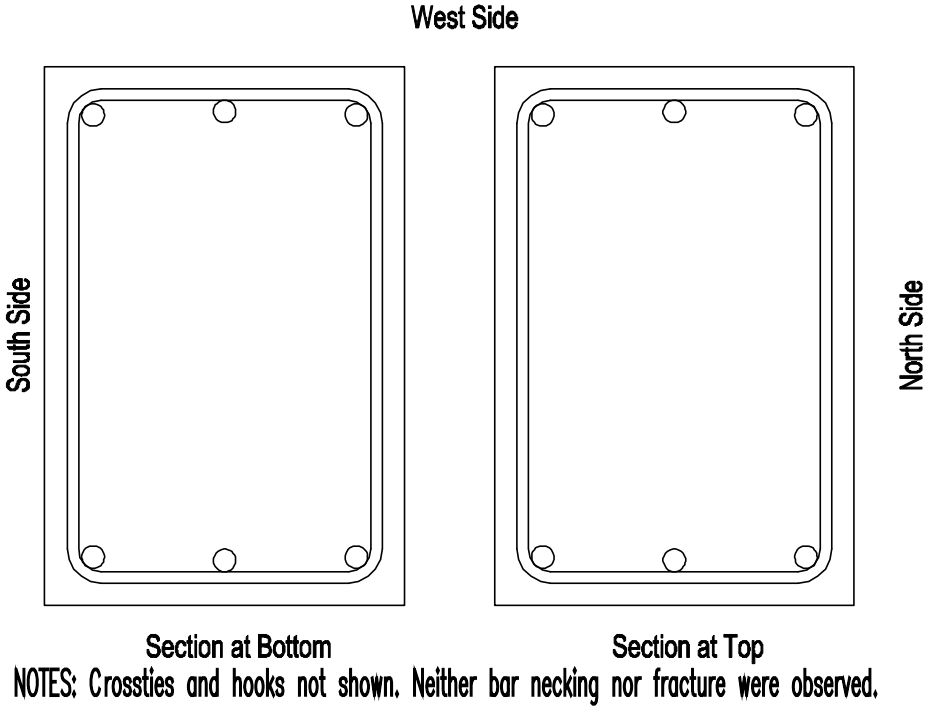

Figure 73 – Reinforcing bar fracture locations, P100-2.5

APPENDIX A: NOTATION

A_s = total area of primary longitudinal reinforcement along the top or bottom face of a coupling beam with parallel reinforcement layout, in.^{2}

A_{vd} = total area of reinforcement in each group of diagonal bars in a diagonally-reinforced coupling beam, in.^{2}

b_w = beam width, in.

c_c = clear cover of reinforcement, in.

CR = chord rotation of the coupling beam, corrected for sliding and relative rotation between the top and bottom block, rad

d = distance from extreme compression fiber to centroid of longitudinal tension reinforcement, in.

d_b = nominal diameter of the primary longitudinal reinforcing bar, in.

f_c' = specified compressive strength of concrete, psi

f_{cm} = measured average compressive strength of concrete, psi

f_{ct} = measured average splitting tensile strength of concrete, psi

f_t = measured peak stress or tensile strength of reinforcement, ksi

f_y = specified yield stress of longitudinal reinforcement, ksi

f_{ym} = measured yield stress of longitudinal reinforcement, ksi

f_{yt} = specified yield stress of transverse reinforcement, ksi

f_{ytm} = measured yield stress of transverse reinforcement, ksi

h = beam height, in.

ℓ_e = minimum straight embedment length to develop a tension stress of $1.25f_y$, in.

ℓ_n = length of clear span measured face-to-face of supports, in.

M_{nm} = calculated flexural strength corresponding to a stress of f_{ym} in the primary longitudinal reinforcement, in.-lb

M_{pr} = calculated flexural strength corresponding to a stress of $1.25f_y$ in the primary longitudinal reinforcement, in.-lb

n = total number of primary longitudinal reinforcing bars

For a D-type beam, number of bars in each group of diagonal bars

For a P-type beam, number of bars along the top or bottom face

s = spacing of transverse reinforcement, center-to-center, in.

v_e = calculated shear stress based on specified material properties, psi

for a D-type beam, $v_e = 2A_{vd}\, f_y \sin\alpha\, /(b_w\, h)$, psi

for a P-type beam, $v_e = (2M_{pr}/\ell_n)\, /(b_w\, d)$, psi

v_{max} = shear stress associated with V_{max}, psi

for a D-type beam, $v_{max} = V_{max}\, /(b_w\, h)$, psi

for a P-type beam, $v_{max} = V_{max}\, /(b_w\, d)$, psi

v_{nm} = shear stress associated with V_{nm}, psi

for a D-type beam, $v_{nm} = V_{nm}/(b_w\, h)$, psi

for a P-type beam, $v_{nm} = V_{nm}/(b_w\, d)$, psi

V = applied shear, kips

V_{max} = maximum applied shear, kips

V_{nm} = calculated shear strength based on measured material properties, kips

for a D-type beam, $V_{nm} = 2A_{vd}\, f_{ym} \sin\alpha$

for a P-type beam, $V_{nm} = 2M_{nm}/\ell_n$

α = angle of inclination of diagonal reinforcement relative to beam longitudinal axis, degrees

δ_{bot} = displacement of the bottom block top surface, in.

δ_{top} = displacement of the top block bottom surface, in.

ε_{sf} = fracture elongation of reinforcement, in./in.

ε_{su} = uniform elongation of reinforcement or strain corresponding to f_t, in./in.

θ_{bot} = rotation of the bottom block (in the loading plane), rad

θ_{top} = rotation of the top block (in the loading plane), rad

APPENDIX B: SELECTED PHOTOS OF SPECIMENS DURING CONSTRUCTION

Figure B.1 – Coupling beam reinforcement, D120-2.5

Figure B.2 – Coupling beam reinforcement, P100-2.5

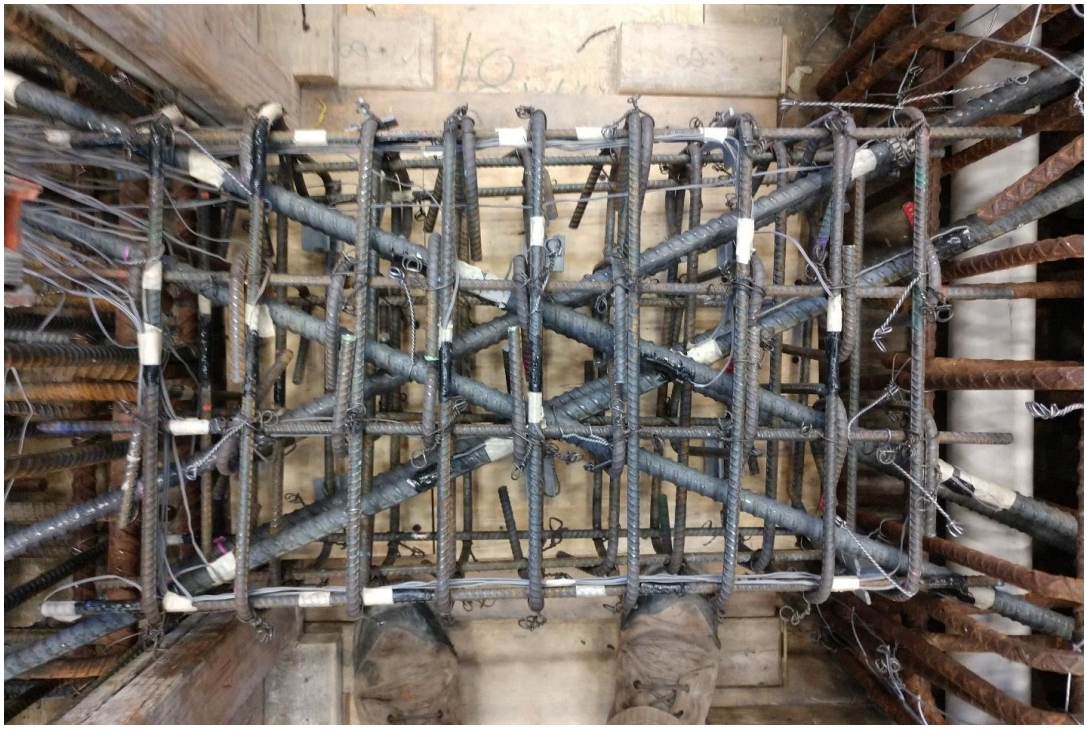

Figure B.3 – Coupling beam reinforcement, D120-1.5

Figure B.4 – Base block reinforcement, P80-2.5

Figure B.5 – Specimens prior to casting, D80-1.5, D100-1.5, and D120-1.5 (from left to right)

Figure B.6 – Specimens after formwork removal, D100-3.5, D80-3.5, P100-2.5, P80-2.5, D100-2.5, and D80-2.5 (from left to right)

APPENDIX C: SELECTED PHOTOS OF SPECIMENS DURING TESTING

Figure C.1 – D80-1.5 at
+2% chord rotation, second cycle

Figure C.2 – D80-1.5 at
–2% chord rotation, second cycle

Figure C.3 – D80-1.5 at
+4% chord rotation, second cycle

Figure C.4 – D80-1.5 at
–4% chord rotation, second cycle

Figure C.5 – D80-1.5 at
+6% chord rotation, second cycle

Figure C.6 – D80-1.5 at
–6% chord rotation, second cycle

Figure C.7 – D80-1.5 at
+8% chord rotation, first cycle

Figure C.8 – D80-1.5 at
–8% chord rotation, first cycle

Figure C.9 – D100-1.5 at
+2% chord rotation, second cycle

Figure C.10 – D100-1.5 at
–2% chord rotation, second cycle

Figure C.11 – D100-1.5 at
+4% chord rotation, second cycle

Figure C.12 – D100-1.5 at
–4% chord rotation, second cycle

Figure C.13 – D100-1.5 at
+6% chord rotation, second cycle

Figure C.14 – D100-1.5 at
–6% chord rotation, second cycle

Figure C.15 – D100-1.5 at
+8% chord rotation, first cycle

Figure C.16 – D120-1.5 at
+2% chord rotation, second cycle

Figure C.17 – D120-1.5 at
–2% chord rotation, second cycle

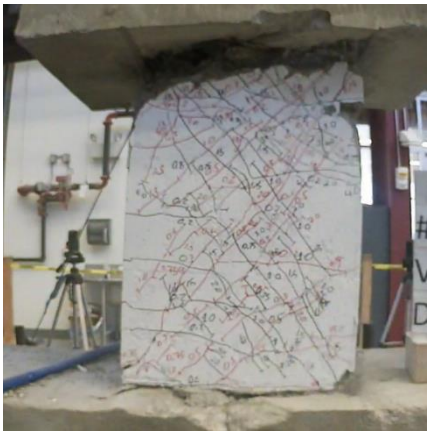

Figure C.18 – D120-1.5 at
+4% chord rotation, second cycle

Figure C.19 – D120-1.5 at
–4% chord rotation, second cycle

Figure C.20 – D120-1.5 at
+6% chord rotation, first cycle

Figure C.21 – D120-1.5 at
–6% chord rotation, first cycle

Figure C.22 – D80-2.5 at
+2% chord rotation, second cycle

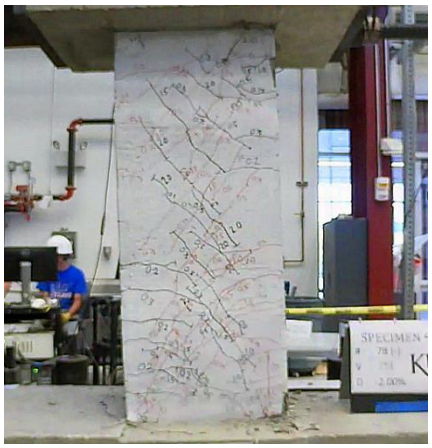

Figure C.23 – D80-2.5 at
–2% chord rotation, second cycle

Figure C.24 – D80-2.5 at
+4% chord rotation, second cycle

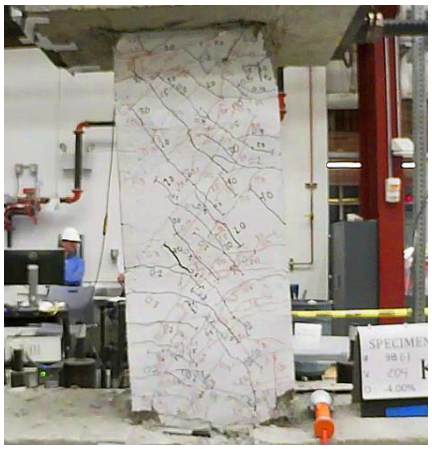

Figure C.25 – D80-2.5 at
–4% chord rotation, second cycle

Figure C.26 – D80-2.5 at
+6% chord rotation, second cycle

Figure C.27 – D80-2.5 at
–6% chord rotation, second cycle

Figure C.28 – D80-2.5 at
+8% chord rotation, second cycle

Figure C.29 – D80-2.5 at
–8% chord rotation, second cycle

Figure C.30 – D80-2.5 at
+10% chord rotation, first cycle

Figure C.31 – D80-2.5 at
–10% chord rotation, first cycle

Figure C.32 – D100-2.5
at +2% chord rotation, second cycle

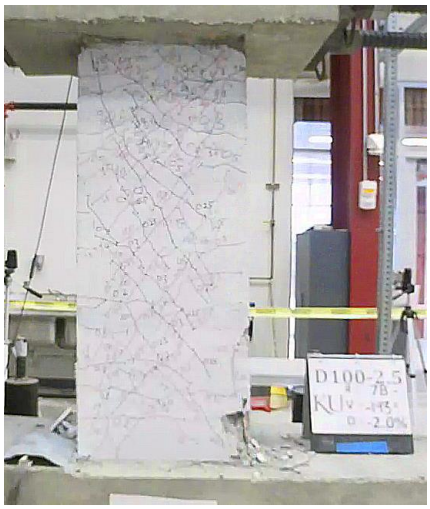

Figure C.33 – D100-2.5 at
–2% chord rotation, second cycle

Figure C.34 – D100-2.5 at
+4% chord rotation, second cycle

Figure C.35 – D100-2.5 at
–4% chord rotation, second cycle

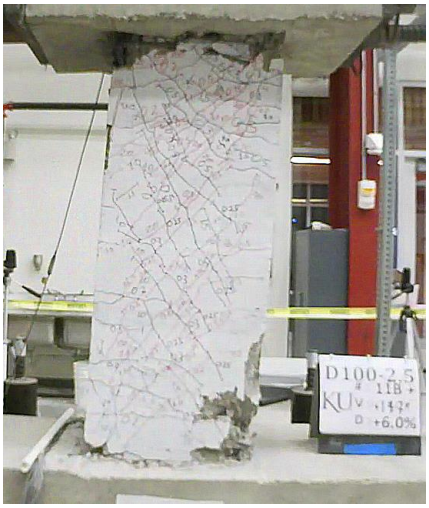

Figure C.36 – D100-2.5 at
+6% chord rotation, second cycle

Figure C.37 – D100-2.5 at
–6% chord rotation, second cycle

Figure C.38 – D100-2.5 at
+8% chord rotation, first cycle

Figure C.39 – D100-2.5 at
–8% chord rotation, first cycle

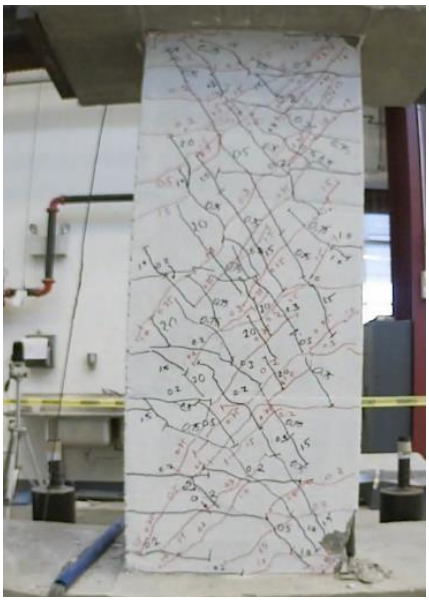

Figure C.40 – D120-2.5 at
+2% chord rotation, second cycle

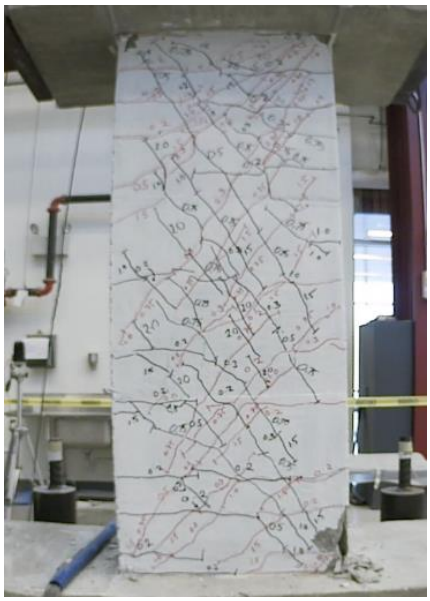

Figure C.41 – D120-2.5 at
–2% chord rotation, second cycle

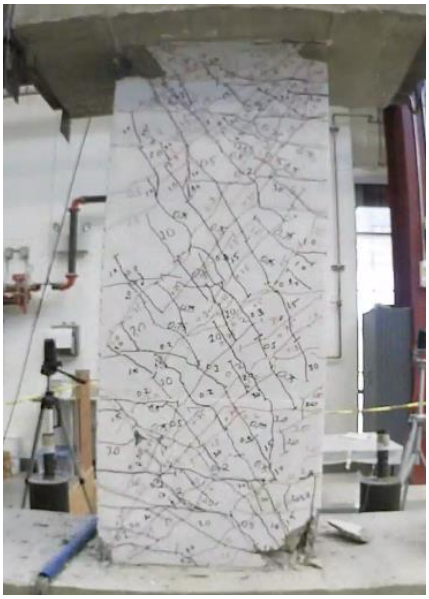

Figure C.42 – D120-2.5 at
+4% chord rotation, second cycle

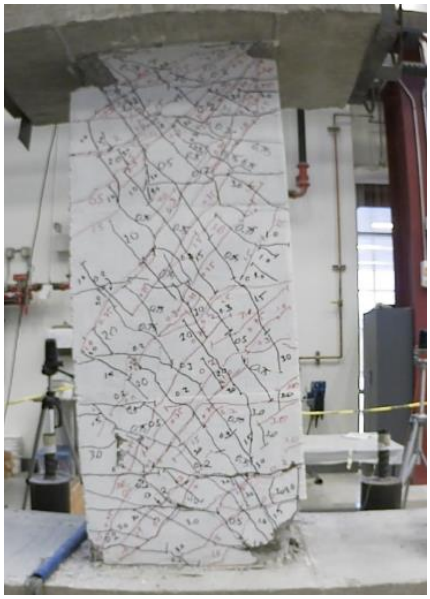

Figure C.43 – D120-2.5 at
–4% chord rotation, second cycle

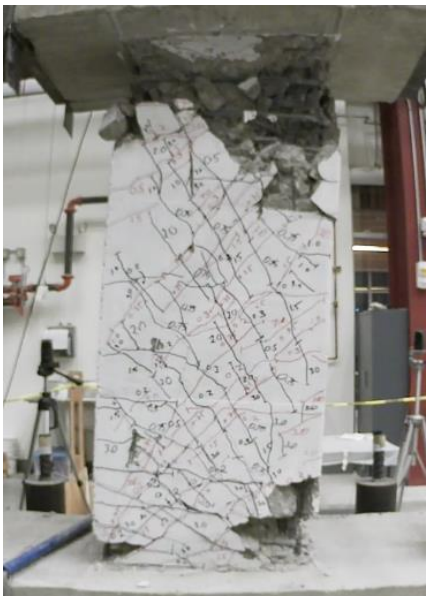

Figure C.44 – D120-2.5 at
+6% chord rotation, second cycle

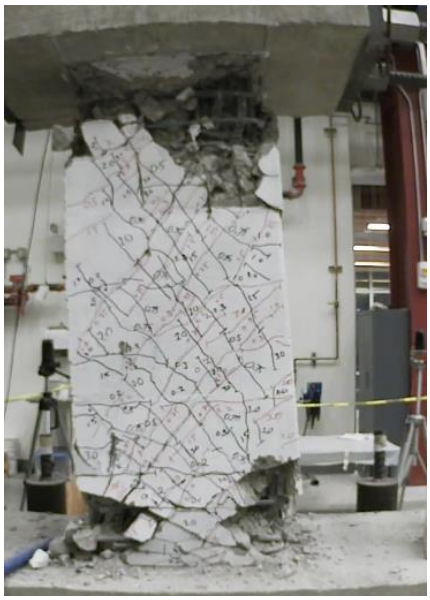

Figure C.45 – D120-2.5 at
–6% chord rotation, second cycle

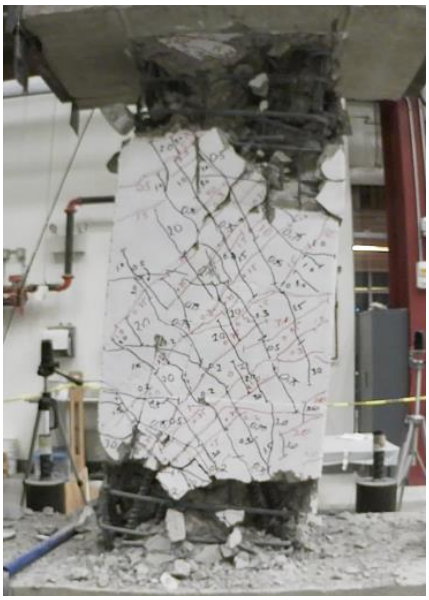

Figure C.46 – D120-2.5 at
+8% chord rotation, second cycle

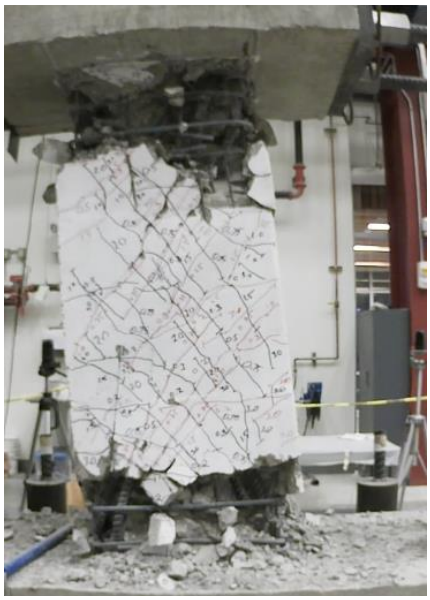

Figure C.47 – D120-2.5 at
–8% chord rotation, second cycle

Figure C.48 – D80-3.5 at
+2% chord rotation, second cycle

Figure C.49 – D80-3.5 at
–2% chord rotation, second cycle

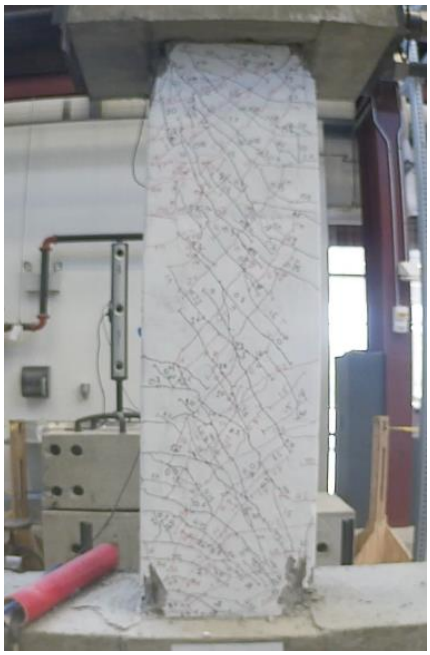

Figure C.50 – D80-3.5 at
+4% chord rotation, second cycle

Figure C.51 – D80-3.5 at
–4% chord rotation, second cycle

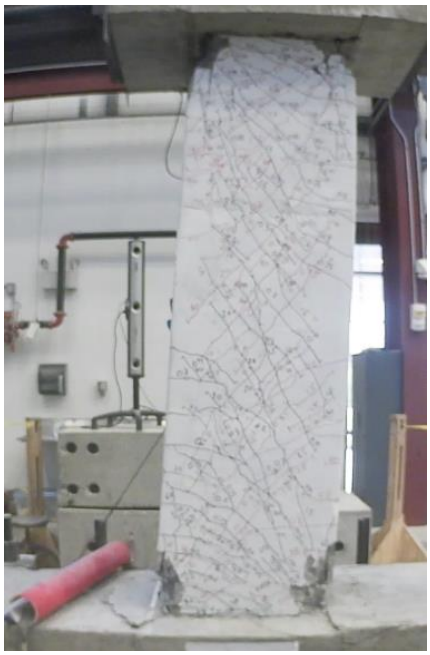

Figure C.52 – D80-3.5 at
+6% chord rotation, second cycle

Figure C.53 – D80-3.5 at
–6% chord rotation, second cycle

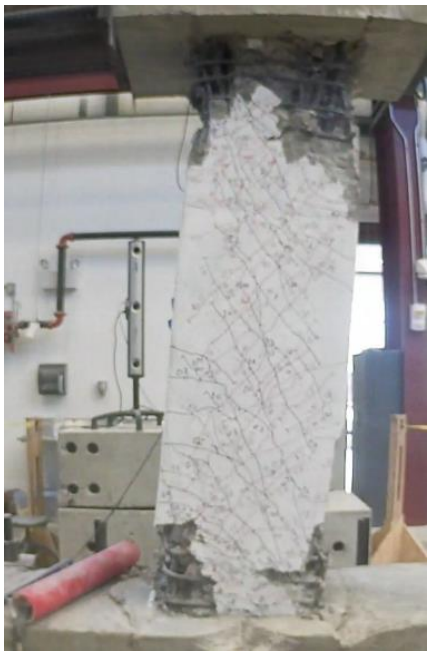

Figure C.54 – D80-3.5 at
+8% chord rotation, second cycle

Figure C.55 – D80-3.5 at
–8% chord rotation, second cycle

Figure C.56 – D80-3.5 at
+10% chord rotation, first cycle

Figure C.57 – D80-3.5 at
–10% chord rotation, first cycle

Figure C.58 – D100-3.5 at
+2% chord rotation, second cycle

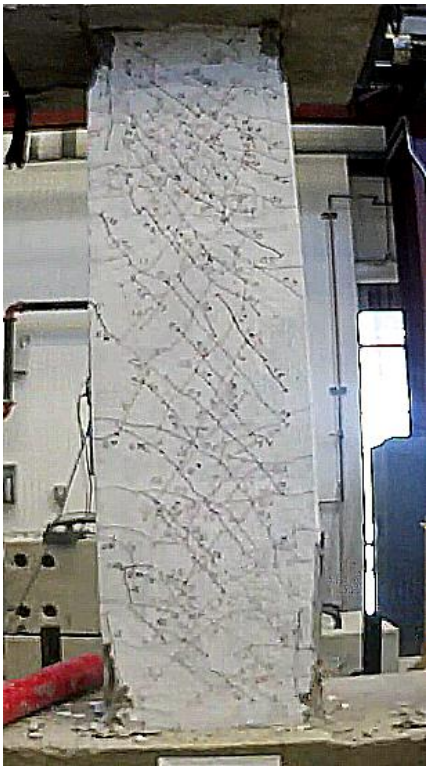

Figure C.59 – D100-3.5 at
–2% chord rotation, second cycle

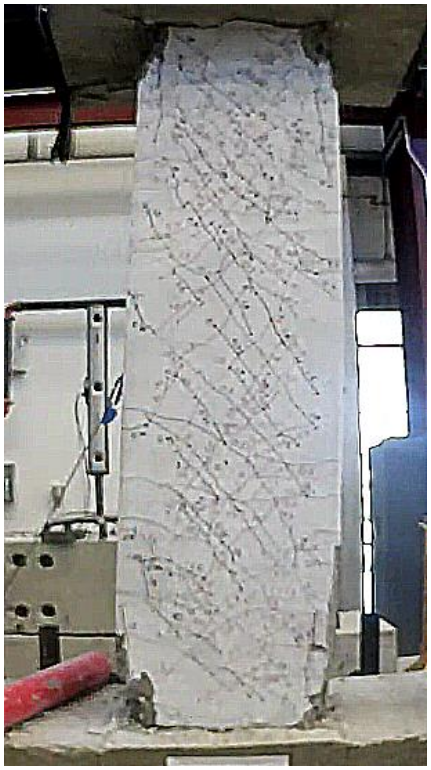

Figure C.60 – D100-3.5 at
+4% chord rotation, second cycle

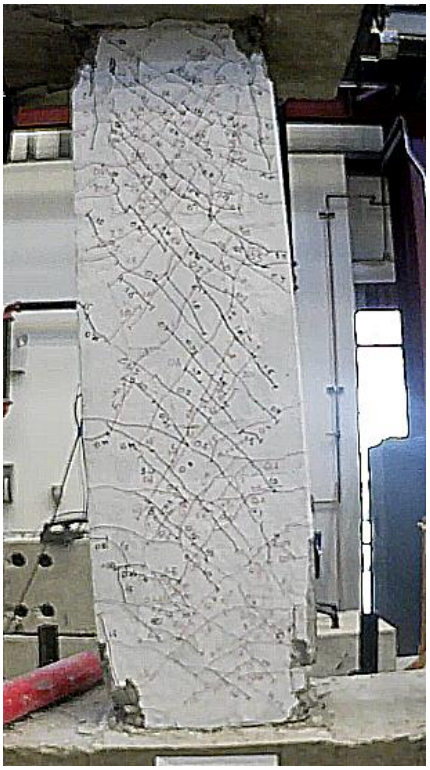

Figure C.61 – D100-3.5 at
–4% chord rotation, second cycle

Figure C.62 – D100-3.5 at
+6% chord rotation, second cycle

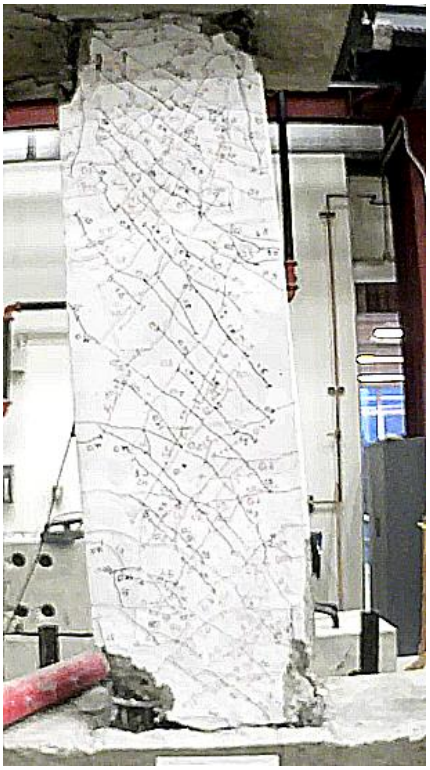

Figure C.63 – D100-3.5 at
–6% chord rotation, second cycle

Figure C.64 – D100-3.5 at
+8% chord rotation, second cycle

Figure C.65 – D100-3.5 at
–8% chord rotation, second cycle

Figure C.66 – D100-3.5 at
+10% chord rotation, first cycle

Figure C.67 – D100-3.5 at
–10% chord rotation, first cycle

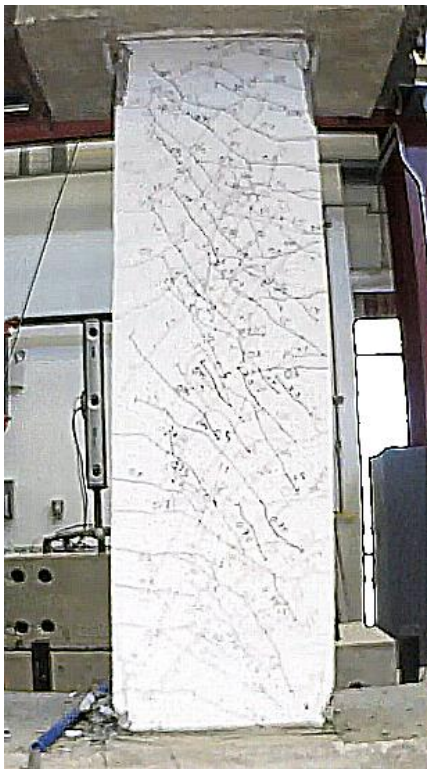

Figure C.68 – D120-3.5 at
+2% chord rotation, second cycle

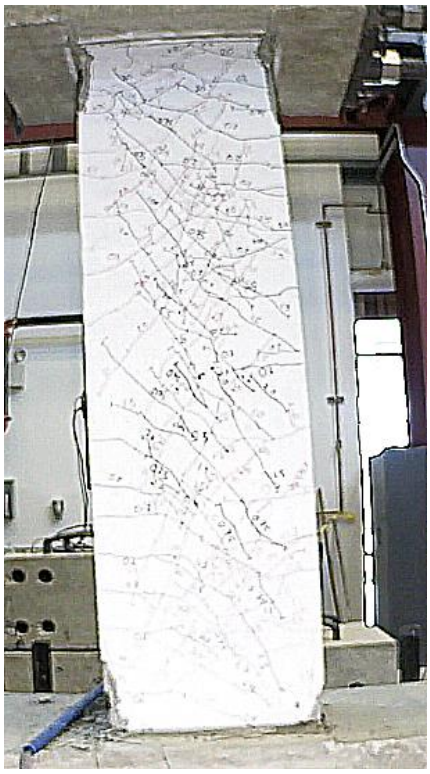

Figure C.69 – D120-3.5 at
–2% chord rotation, second cycle

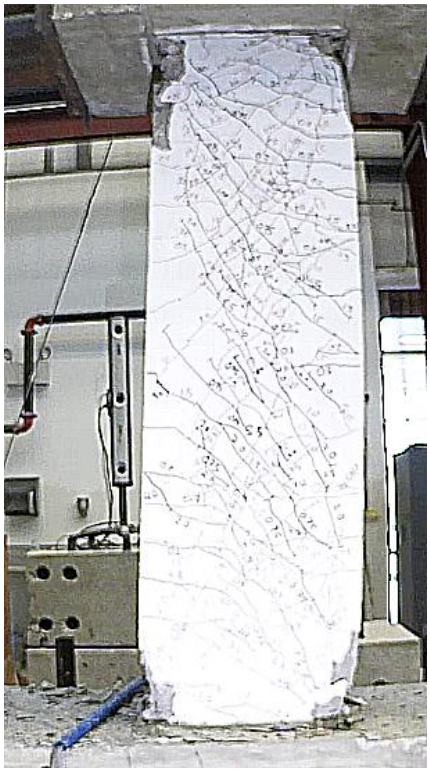

Figure C.70 – D120-3.5 at
+4% chord rotation, second cycle

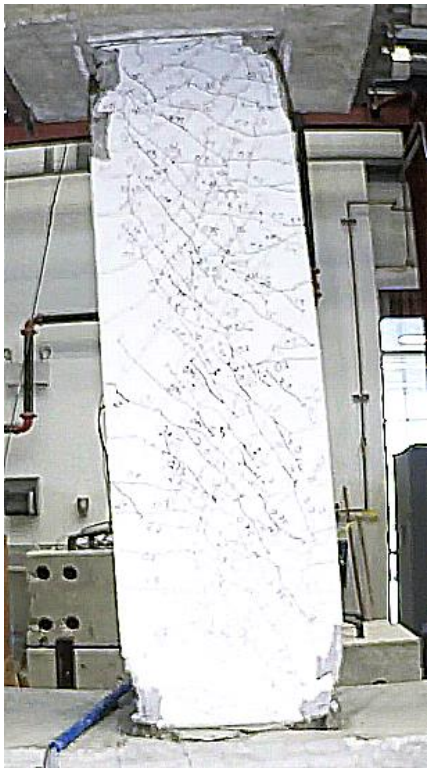

Figure C.71 – D120-3.5 at
–4% chord rotation, second cycle

Figure C.72 – D120-3.5 at
+6% chord rotation, second cycle

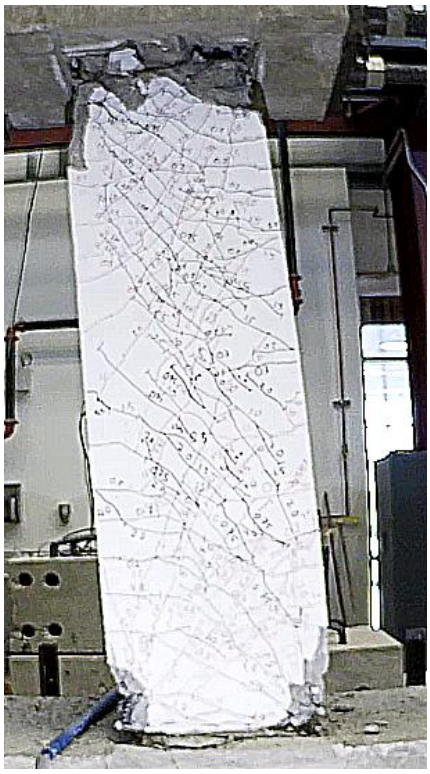

Figure C.73 – D120-3.5 at
–6% chord rotation, second cycle

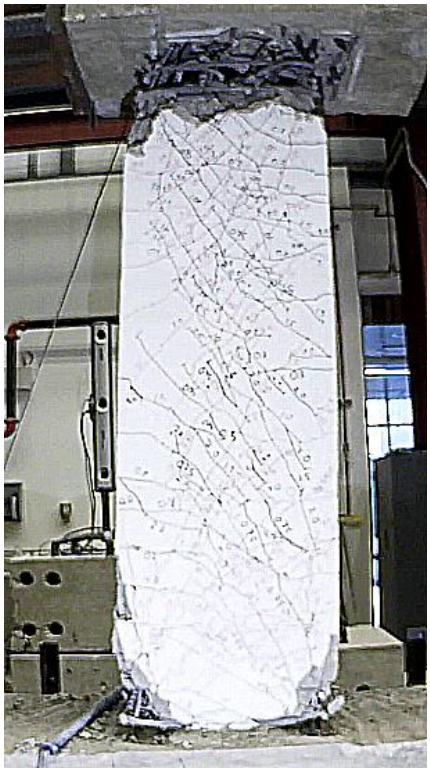

Figure C.74 – D120-3.5 at
+8% chord rotation, second cycle

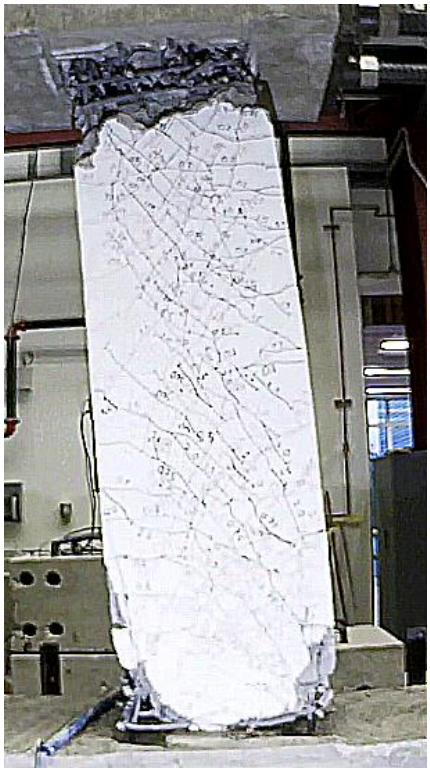

Figure C.75 – D120-3.5 at
–8% chord rotation, second cycle

Figure C.76 – P80-2.5 at
+2% chord rotation, second cycle

Figure C.77 – P80-2.5 at
–2% chord rotation, second cycle

Figure C.78 – P80-2.5 at
+4% chord rotation, second cycle

Figure C.79 – P80-2.5 at
–4% chord rotation, second cycle

Figure C.80 – P80-2.5 at
+6% chord rotation, second cycle

Figure C.81 – P80-2.5 at
–6% chord rotation, second cycle

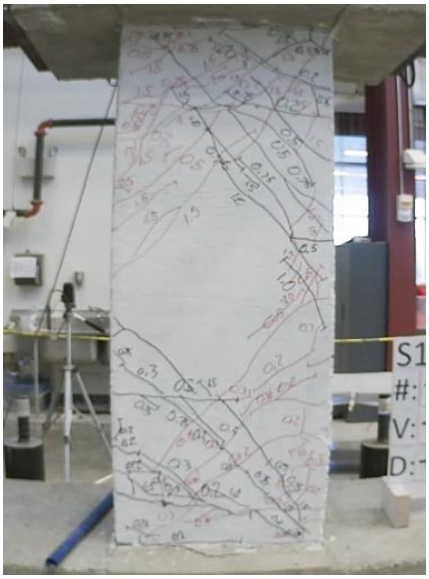

Figure C.82 – P100-2.5 at
+2% chord rotation, second cycle

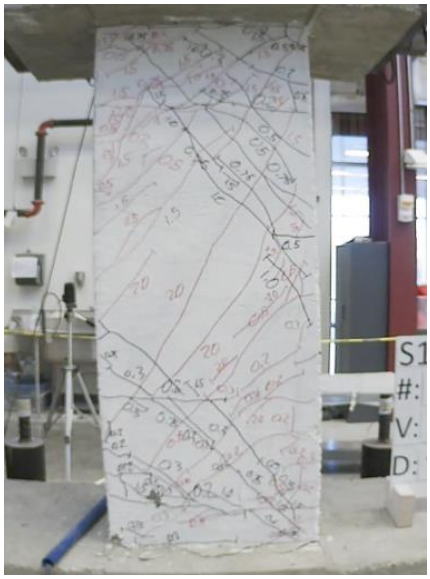

Figure C.83 – P100-2.5 at
–2% chord rotation, second cycle

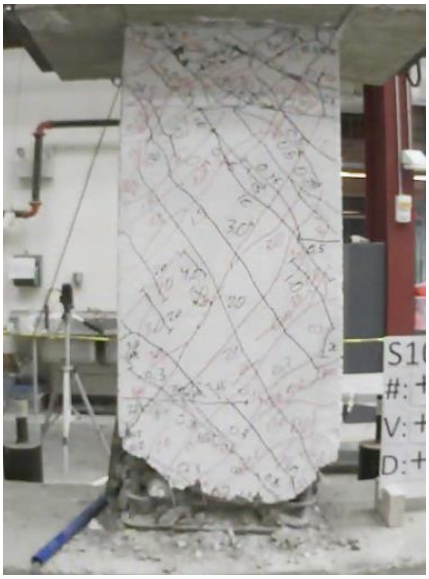

Figure C.84 – P100-2.5 at
+4% chord rotation, second cycle

Figure C.85 – P100-2.5 at
–4% chord rotation, second cycle

Figure C.86 – P100-2.5 at
+6% chord rotation, second cycle

Figure C.87 – P100-2.5 at
–6% chord rotation, second cycle